UNIVERSITÀ CATTOLICA DEL SACRO CUORE

Sede di Piacenza

Dottorato di ricerca per il Sistema Agro-alimentare

Ph.D. in Agro-Food System

Cycle XXXVIII

S.S.D. IIND-06/B, IIND-08/B, AGRI 02/A.

Multi-Criteria Optimization and Assessment of Agrivoltaic Systems

Coordinator:

Prof. Paolo Ajmone Marsan

Candidate:

Amirhossein Nik Zad

Matriculation n: 5214852

Academic Year 2024/2025

UNIVERSITÀ CATTOLICA DEL SACRO CUORE

Sede di Piacenza

Dottorato di ricerca per il Sistema Agro-alimentare

Ph.D. in Agro-Food System

Cycle XXXVIII

S.S.D. IIND-06/B, IIND-08/B, AGRI 02/A.

Multi-Criteria Optimization and Assessment of Agrivoltaic Systems

Coordinator:

Prof. Paolo Ajmone Marsan

Tutor:

Prof. Stefano Amaducci

Co-Tutor:

Prof. Pietro Elia Campana

Candidate:

Amirhossein Nik Zad

Matriculation n: 5214852

Academic Year 2024/2025

Abstract

Agrivoltaic (APV) systems enable simultaneous food and electricity production, addressing the conflict between renewable energy expansion and agricultural land preservation. This thesis investigates three interconnected research areas within the European context. The first study develops a techno-economic optimization framework for integrating bifacial APV systems (vertical, single-axis, and dual-axis tracking) with anaerobic digestion infrastructure for biomethane production, employing a multi-objective genetic algorithm coupled with the technique for order preference by similarity to ideal solution for a case study in Piacenza, Italy. The second study conducts life cycle assessment benchmarking of four bifacial APV configurations across diverse European climatic conditions. The third study performs cross-validation of commercial and in-house developed energy simulation platforms for advanced dual-axis bifacial APV systems operating under Full Tracking and Anti-Tracking modes against empirical field measurements. Collectively, these investigations provide integrated assessment tools spanning economic viability, environmental sustainability, and operational performance validation for sustainable APV deployment.

Keywords: Agrivoltaics, Photovoltaics, Anaerobic digestion, Biomethane, Optimization, Life cycle assessment, Cross-validation.

Contents

Nomenclature

Abbreviations and acronyms

AD	Anaerobic digestion
APV	Agrivoltaic
AT	Anti-tracking
BESS	Battery energy storage systems
$BioCH_4$	Biomethane
BOS	Balance of system
CAPEX	Capital expenditures
CGMPV	Conventional ground-mounted photovoltaic
CHP	Combined heat and power
CO_{2eq}	Carbon dioxide equivalent
COP	Coefficient of performance
COP_{real}	Effective coefficient of performance
CY	Crop yield
EOL	End-of-life
FL	Full light
FT	Full tracking
FU	Functional unit
GCR	Ground coverage ratio
GHG	Greenhouse gas
GHI	Global horizontal irradiance
GMPV	Ground-mounted photovoltaic
GWHP	Groundwater heat pump
ha	Hectare
ILUC	Indirect land use change
kW_{el}	Kilowatt electrical
kWh	Kilowatt-hour
kW_p	Kilowatt peak
kW_{th}	Kilowatt thermal
LCA	Life cycle assessment
LCC	Life cycle cost
LCI	Life cycle inventory
LCIA	Life cycle impact assessment
LCR	Life cycle revenue
LHV	Lower heating value

MAE	Mean absolute error
MAPE	Mean absolute percentage error
MCDA	Multi-criteria decision analysis
MOGA	Multi-objective genetic algorithm
MW_p	Megawatt peak
NPV	Net present value
ODP	Ozone depletion potential
OPEX	Operational expenditures
PV	Photovoltaic
R^2	Coefficient of determination
RH	Relative humidity
RMSE	Root mean square error
SOC	State of charge
SPEI	Standardized precipitation evapotranspiration index
STC	Standard test conditions
T_a	Air temperature
TMY	Typical meteorological year
TOPSIS	Technique for order preference by similarity to ideal solution
WACC	Weighted average cost of capital
Symbols and parameters	
A_{max}	Maximum available land area (m^2)
APV_t	Instantaneous APV energy conversion at time t
C_0	Initial cost of each equipment (€)
C_{cap}	Capital cost of components (€)
C_n	Nominal capacity of the battery (Ah)
$C_{O\&M}$	Operation and maintenance costs (€)
C_{PPG}	Costs of purchasing power from the national grid (€)
C_{rep}	Replacement cost (€)
d	Discount rate (%)
E_{GWHP}	Hourly electrical energy consumed by GWHP (kWh_{el})
elecLoadt	Instantaneous electrical load at time t
EP_{APV}	Effective APV penetration (%)
i	Inflation rate (%)
INT	Integer function
L_{comp}	Component lifetime
L_{proj}	Project lifetime

L_{rem}	Remaining lifetime of the component at project end
N_{Batt}	Number of batteries required
NNSD	Number of non-sunny days
N_{PVreq}	Total number of PV modules needed
OH_{BGCHP}	Daily operating hours of the biogas CHP
$P_{el,BiogasCHP}$	Electrical output of the biogas CHP (kW_{el})
$P_{th,Biogasboiler}$	Thermal output of the biogas boiler (kW_{th})
$P_{th,BiogasCHP}$	Thermal output of the biogas CHP unit (kW_{th})
$P_{PVmax,actual}$	Maximum output of each PV module (W)
PSH	Peak sun hours
$Q_{Biogasboiler}$	Required biogas input rate for boiler (Nm^3)
$Q_{BiogasCHP}$	Biogas availability for the CHP unit (Nm^3/day)
Q_{GWHP}	Hourly thermal energy produced by the GWHP (kWh_{th})
R_{sal}	Salvage value of components (€)
R_{SBG}	Revenue from selling BioCH4 (€)
R_{SPG}	Revenue from selling power (€)
T_{dig}	Digester operating temperature (°C)
TDL_{el}	Total daily electrical load (Wh)
T_{gw}	Groundwater temperature (°C)
V_n	Nominal voltage of the battery (V)
Greek symbols	
α	Land occupation factor
$\eta_{el,BiogasCHP}$	Electrical conversion efficiency of the biogas CHP (%)
η_{r-t}	Roundtrip efficiency of the battery (%)
$\eta_{th,BiogasCHP}$	Thermal conversion efficiency of the biogas CHP (%)
$\eta_{th,Biogasboiler}$	Biogas boiler efficiency (%)

Chapter 1

Introduction

1.1 Background and Context

The global imperative to decarbonize energy systems while simultaneously ensuring food security for a growing population presents one of the most consequential challenges of the twenty-first century. Agricultural land, which constitutes approximately 37% of the Earth's terrestrial surface, faces unprecedented competition from renewable energy infrastructure expansion, particularly utility-scale photovoltaic (PV) installations that typically require exclusive land occupation [1]. This land-use dichotomy has intensified concerns regarding the potential displacement of productive agricultural areas, threatening both rural economies and global food supply chains. Agrivoltaic (APV) systems have emerged as a transformative solution to this conflict, enabling the simultaneous production of food and solar electricity on the same land parcel through strategically elevated or spaced PV installations that permit continued agricultural operations beneath or between module arrays [2].

The technical evolution of APV systems has advanced considerably beyond early fixed-tilt configurations to encompass diverse architectural typologies, including vertical installations, single-axis trackers, and sophisticated dual-axis tracking systems capable of dynamic solar resource optimization [2]. Bifacial PV technology further enhances system performance by harvesting irradiance from both front and rear module surfaces, capitalizing on ground-reflected albedo to augment energy yields [3]. These technological advancements have positioned APV systems as compelling alternatives to conventional ground-mounted PV, offering enhanced land-use efficiency quantified through the land equivalent ratio and potential synergistic benefits for underlying crops, including reduced evapotranspiration, moderated thermal extremes, and protection against adverse weather events [4]. Within the European context, particularly Italy, the integration of renewable energy into agricultural systems assumes heightened significance given the sector's historical dependence on conventional energy sources and the concurrent policy impetus toward decarbonization under frameworks such as REPowerEU [5]. Italian agriculture has witnessed substantial growth in biogas production, positioning the nation among Europe's leading producers of upgraded biomethane [6]. However, the energy-intensive nature of biogas upgrading processes creates substantial auxiliary power demands, presenting opportunities for renewable hybridization strategies [7]. Concurrently, European climate objectives necessitate rigorous environmental accounting of emerging technologies through standardized life cycle assessment (LCA) methodologies to ensure that proposed solutions deliver genuine sustainability benefits rather than merely shifting environmental burdens across impact categories or geographical boundaries [8]. Importantly, the realisable potential of agrivoltaics is itself geographically differentiated; Abdalla et

al. [9] demonstrate through region-scale GIS-based suitability mapping that deployment potential varies substantially across territories as a function of land availability, climatic resources, and infrastructure constraints, underscoring the need to anchor performance assessments to location-specific conditions. Agrivoltaics is increasingly treated as an integrated system in which energy yield, crop environment, and sustainability outcomes are co-determined by the same design choices rather than being separable effects. Jamil and Pearce [10] synthesize recent evidence showing that APV performance should be interpreted through coupled mechanisms, because structural and operational decisions that shape electricity conversion can simultaneously influence microclimate, agricultural conditions, and resource-use pathways. This framing aligns with the thesis structure by supporting an integrated evaluation logic that combines techno-economic optimization, multi-category LCA, and performance modeling to identify trade-offs and avoid burden shifting. In addition to energy and environmental considerations, implementable APV layouts must preserve routine mechanized field operations, otherwise technically attractive configurations may be non-viable in practice. Bellone et al. [11] show that machinery access and maneuvering requirements can impose buffer zones and operational constraints that reduce effective cultivated area and field efficiency when APV layouts are not co-designed with farm logistics. This evidence strengthens the thesis interpretation of feasible design space by justifying why agricultural operability should be treated as a boundary condition when comparing typologies and drawing deployment-oriented conclusions.

1.2 Research gaps and scientific rationale

APV systems have experienced rapid growth, with global installed capacity expanding from 5 MW_p in 2012 to over 14 GW_p by 2021 driven by supportive policy frameworks in Germany (DIN-SPEC 91434), France (dedicated tenders), and Italy (€1.1B NRRP investment) [12]. Despite this commercial deployment and accompanying research expansion, three critical knowledge gaps impede the comprehensive understanding and optimal deployment of these technologies. These gaps span the domains of techno-economic optimization, environmental impact assessment, and energy simulation validation. Importantly, these domains are not independent: system design choices that determine techno-economic viability simultaneously define the material inventories and energy yields that underpin environmental impact assessment, while the reliability of both economic projections and environmental benchmarks depends on the accuracy of the simulation tools used to predict field performance. Addressing these gaps in an integrated manner is therefore essential for credible deployment guidance, and this interdependence motivates the thesis structure in which each chapter generates inputs or boundary conditions that inform the others. The real-world impact of agrivoltaics also depends on economic competitiveness relative to conventional ground-mounted PV systems,

meaning that favorable technical indicators alone do not guarantee deployment. Böhm et al. [13] demonstrate that the levelized cost of electricity for different APV configurations in Germany ranges from 4% to 148% above ground-mounted PV systems, with farmland preservation costs substantially exceeding agricultural returns to land, underscoring the need for rigorous techno-economic optimization to identify configurations that can narrow this cost gap. This provides an economic rationale for the thesis structure and motivates the integrated assessment of system viability alongside environmental and operational performance.

The first gap concerns the integration of APV systems with downstream agricultural processing infrastructure, specifically anaerobic digestion (AD) facilities for biomethane production, which remains largely unexplored. Existing literature has examined individual system components in isolation: Sieborg et al. [14] analyzed PV-driven biomethanation using a trickle bed reactor, Su et al. [15] evaluated PV-thermal technology for biogas upgrading, Álvaro et al. [16] assessed solar-AD hybridization for isolated livestock farms, and Temiz et al. [17] proposed an integrated APV-biogas energy system combining overhead fixed bifacial panels with biogas production in a single case study. However, these investigations are restricted to single APV configurations and single auxiliary heating strategies, and none provides an integrated optimization framework capable of simultaneously evaluating multiple APV typologies with diverse heating technologies for biomethanation applications [18]. Furthermore, systematic comparative analyses between grid-connected and off-grid APV-biogas configurations have not been conducted, limiting the capacity to identify economically optimal system designs that ensure complete energy coverage for AD operations. Because the economic ranking of configurations is sensitive to energy yield assumptions, closing this gap also requires reliable performance simulation, a need addressed by the third research line of this thesis.

The second gap relates to LCA research on APV systems, which exhibits substantial methodological heterogeneity and geographical limitations. The predominant focus on conventional fixed APV configurations with mono-facial modules has left advanced mounting structures and bifacial technologies comparatively understudied [19]. Ravilla et al. [20] conducted a combined techno-economic and LCA of APV designs, yet the analysis was limited to a single US location and did not include bifacial PV modules. Similarly, Sponagel et al. [21] explored the climate change mitigation potential of agrivoltaics through geodata-based LCA but confined the assessment to a single German region and one system typology. Critically, no prior investigation has comprehensively compared the environmental performance of vertical, interspace and overhead single-axis, and overhead dual-axis bifacial APV configurations within a unified methodological framework spanning diverse European climatic conditions. Additionally, detailed material inventories for vertical APV systems remain

unavailable in the public domain due to commercial confidentiality constraints, severely hampering research reproducibility and technology advancement [22]. The disproportionate emphasis on climate change impacts while neglecting ecosystem quality and resource depletion categories further constrains holistic sustainability evaluation [6]. Robust environmental benchmarking in turn depends on accurate energy yield predictions, which links this gap directly to the simulation validation challenge addressed in the third chapter.

The third gap pertains to the operational complexity of advanced dual-axis APV systems, particularly the implementation of anti-tracking (AT) strategies for agricultural light management, which lacks robust empirical validation under real-world conditions [23]. While Full Tracking (FT) mode, wherein panels orient perpendicular to solar radiation to maximize energy capture, has received considerable attention, the AT mode where panels align parallel to incident radiation to enhance crop illumination represents a paradigm unique to APV contexts with minimal scientific investigation [24]. Alam and Butt [25] demonstrated that module tracking strategies for agrivoltaics differ fundamentally from standard PV tracking due to the need to co-optimize energy capture and crop light transmission, yet their analysis relied on modeled rather than empirically validated outputs. Bruno et al. [3] proposed a digital twin approach for optimizing tracking in APV orchards, further illustrating the growing interest in dynamic tracking but also the reliance on simulation without systematic cross-platform validation against field measurements. Commercial simulation platforms predominantly lack native functionality for AT mode modeling and provide limited capability for advanced overhead bifacial dual-axis systems with critical parameters such as row pitch and installation height [26]. This validation gap between simulated predictions and actual field performance impedes reliable system design, performance guarantees, and broader commercial adoption. Resolving this gap provides retrospective confidence in the energy yield predictions on which the preceding chapters rely, given that commercial simulation platforms were used to generate the energy inputs for both the techno-economic optimization of the first chapter and the LCA of the second chapter, thereby closing the methodological loop that unifies the three research lines of this thesis.

1.3 Research questions

Addressing these interconnected knowledge gaps, this thesis poses three fundamental research questions that collectively advance the scientific understanding of APV system design, environmental performance, and operational validation.

The first research question asks what the optimal techno-economic configuration is for integrating bifacial APV systems with AD infrastructure for biomethane production, and how various APV

typologies combined with different supplementary energy sources perform under grid-connected and off-grid scenarios.

The second research question investigates how the environmental impacts of different bifacial APV configurations compare across diverse European climatic conditions, and which system designs offer optimal sustainability performance across multiple impact categories.

The third research question examines how accurately PV platforms predict the energy conversion performance of advanced overhead dual-axis bifacial APV systems operating under FT and AT modes when validated against real-world field measurements.

1.4 Thesis objectives and methodological approach

This thesis pursues three interconnected objectives corresponding to the identified research questions, each employing rigorous methodological frameworks appropriate to the investigative domain. The first objective develops a comprehensive techno-economic optimization framework for APV-powered biomethane production systems. This framework evaluates the integration of bifacial APV systems encompassing vertical, single-axis, and dual-axis tracking configurations with AD infrastructure, combined with supplementary energy sources including biogas boilers, combined heat and power units, groundwater heat pumps, battery energy storage systems, and grid electricity. The methodological approach employs a multi-objective genetic algorithm (MOGA) developed in MATLAB to generate portfolios of candidate solutions, subsequently ranked using the technique for order preference by similarity to ideal solution (TOPSIS). This represents, to current knowledge, the first combined application of MOGA and TOPSIS for APV-biomethanation system optimization. The analysis encompasses grid-connected scenarios, baseline configurations, and off-grid alternatives for a case study AD plant situated in Piacenza, Italy.

The second objective conducts comprehensive LCA benchmarking of four bifacial APV configurations, namely fixed vertical, interspace and overhead single-axis as well as overhead dual-axis, against conventional ground-mounted bifacial PV systems and country-specific electricity grid mixes. The assessment spans diverse European climatic conditions from Sweden to Italy, capturing latitudinal variation in solar resource availability and agricultural productivity. The methodology employs a hybrid LCA approach combining attributional assessment for PV components across ten environmental impact categories with consequential analysis for agricultural land-use change contributions. Monte Carlo analysis ensures statistical robustness of conclusions. Critically, this research provides the first publicly available detailed material inventory for vertical APV systems.

The third objective performs systematic cross-validation of energy simulation platforms for advanced overhead dual-axis bifacial APV systems operating under FT and AT modes. The methodology leverages empirical field data from a cutting-edge APV installation in Piacenza, Italy, encompassing measured meteorological parameters and energy output data. Cross-simulation analysis employs established commercial software tools, namely PVSOL, SISIFO, and System Advisor Model, alongside an in-house developed platform known as the UCSC platform, with error analysis quantifying prediction accuracy against measured performance.

1.5 Thesis structure

This thesis is structured as a compilation of three interrelated studies, each constituting a distinct chapter that addresses one of the research questions articulated above. Chapter 2 presents the techno-economic optimization framework for APV-powered biomethane production, detailing the MOGA-TOPSIS methodology and comparative scenario analyses. Chapter 3 reports the multi-LCA of bifacial APV configurations across European climates, providing environmental impact profiles and configuration-specific recommendations. Chapter 4 documents the cross-validation study of energy simulation platforms against empirical field measurements for FT and AT operational modes. Finally, Chapter 5 synthesizes the principal findings. Collectively, these investigations advance the scientific foundation for APV system development by providing integrated assessment tools spanning economic viability, environmental sustainability, and operational performance validation. The findings contribute actionable guidance for policymakers, system developers, and agricultural stakeholders seeking to implement APV technologies that genuinely reconcile renewable energy expansion with agricultural land preservation.

Chapter 2

Techno-economic optimization of agrivoltaic-powered anaerobic digestion plant for biomethane production

This chapter is based on:

Nik Zad, A.[1,*], Zainali, S.[2], Croci, M.[1], Guezgouz, M.[2], Impollonia, G.[1], Campana, P.E.[2] and Amaducci, S.[1] (2026). Techno-economic optimization of agrivoltaic-powered anaerobic digestion plant for biomethane production. Energy Conversion and Management, 348, 120791.

https://doi.org/10.1016/j.enconman.2025.120791

[1]*Department of Sustainable Crop Production, Università Cattolica del Sacro Cuore, Piacenza, Italy*

[2]*Department of Sustainable Energy Systems, Mälardalen University, Västerås, Sweden*

*Corresponding author

2.1 Abstract

Decarbonizing biomethane facilities demands integrated electricity-heat strategies respecting land constraints. This study presents the first optimization framework integrating bifacial agrivoltaic (APV) systems with anaerobic digestion (AD) plants for biomethane production, addressing a critical gap in renewable energy system design. A multi-objective genetic algorithm coupled with Technique for Order Preference by Similarity to Ideal Solution ranking methodology was developed to simultaneously optimize economic performance and land utilization across three distinct APV configurations including fixed vertical, 1-axis, and 2-axis tracking systems. The framework evaluates eight scenarios encompassing on-grid APV systems with various heating technologies (biogas boilers, groundwater heat pumps, and biogas combined heat and power units), alongside benchmark alternatives including standalone combined heat and power unit (baseline), grid-dependent systems (without APV), and off-grid APV configurations.

Results demonstrate that the on-grid 1-axis APV system integrated with groundwater heat pump achieves superior techno-economic performance, delivering a net present value of 2.88 M€, representing a 4.1-fold improvement over conventional combined heat and power baseline systems. This configuration maximizes biomethane sales by electrifying thermal demands, avoiding biogas combustion and capitalizing on favorable biomethane-to-electricity price ratios. Heat pump electrification strategies consistently outperform biogas-combustion strategies (boiler or combined heat and power) in net present value, achieving up to 8.7 times higher performance through strategic biogas preservation for upgrading within the primary scenarios. Comparative analysis confirms the superior techno-economic and spatial performance of optimized on-grid systems, with 9.17-11.23 M€ higher net present value and 17-20 times lower land occupation than off-grid alternatives. Sensitivity analysis confirms the consistent superiority of on-grid 1-axis APV systems paired with heat pumps, reflecting robust trade-offs between energy yield, cost, and land priorities. The developed framework offers a versatile approach for integrating renewable energy in agricultural systems, promoting a sustainable energy transition while maintaining agricultural productivity.

Keywords: Agrivoltaic, Photovoltaic, Optimization, Anaerobic digestion, Biogas, Biomethane.

2.2 Introduction

The incorporation of renewable energy systems into small-scale agricultural activities, defined as farms occupying up to two hectares [1], is essential for advancing sustainability, mitigating greenhouse gas (GHG) emissions, and enhancing rural energy accessibility [5]. Among renewable solutions, biomethane ($BioCH_4$) production via anaerobic digestion (AD) of organic substrates offers substantial environmental and economic benefits, serving both as a renewable energy source and an effective waste management strategy [6]. Upgraded $BioCH_4$ is highly versatile, as it can be integrated into existing gas infrastructure or utilized directly in combined heat and power (CHP) plants and biogas boilers to address diverse energy requirements.

Previous studies have evaluated several renewable integration frameworks designed to boost energy self-reliance and economic viability. Temiz et al. [17] explored an integrated energy system in Thailand that combined overhead fixed bifacial agrivoltaic (APV) systems, biogas production units, and community-scale energy infrastructure, fully addressing local electricity, biogas, heating, and cooling demands. Similarly, Bambokela et al. [27] validated the dependability of hybrid mini-grid solutions integrating ground-mounted photovoltaic (GMPV) systems and biogas facilities for rural communities in Sub-Saharan Africa, underscoring the necessity for ongoing assessment of economic impacts across different configurations.

Further research into advanced hybrid technologies has highlighted specific economic challenges and opportunities. For instance, Sieborg et al. [14] analyzed biomethanation driven by GMPV integrated with a trickle bed reactor, indicating notable economic constraints for technology scale-up compared to conventional biogas upgrading methods. Conversely, Su et al. [15] demonstrated the promising economic prospects, and efficiency gains achievable through combining concentrated photovoltaic thermal (CPVT) collectors with AD processes, reporting a short payback period of approximately 5.6 years alongside significant reductions in fossil fuel dependency. Recent investigations have confirmed the effectiveness of integrating solar hybrid systems with AD units. For instance, Álvaro et al. [16] highlighted that hybrid photovoltaic thermal (PV/T) collectors can successfully supply both the heat and electricity required for biogas production and upgrading on isolated livestock farms, thereby reducing GHG emissions and enhancing farm energy self-sufficiency. Another study [28] focused on CPVT systems, demonstrating that their integration into a biogas plant improved annual biomethane production by 1.7% and was economically feasible, achieving a positive net present value (NPV) and a payback period of around 10 years. Calise et al. [29] assessed concentrating solar power

(CSP) integrated with biogas facilities to satisfy both electrical and thermal energy demands, employing dynamic simulation using TRNSYS software. Their results indicated a substantial 45% reduction in grid electricity reliance and 126% savings in primary energy, coupled with a favorable payback period of six years, thus confirming the economic viability for transportation sector decarbonization. Additionally, Akarsu and Demir [30] conducted techno-economic and environmental analyses of biogas-based hybrid renewable systems for small livestock farms in rural Türkiye, concluding that a biogas-solar PV hybrid configuration integrated with the grid provided optimal performance, achieving a renewable energy fraction of nearly 90%. Their study emphasized the critical role of governmental incentives in ensuring the financial feasibility of such renewable hybrid systems.

In the context of Italian agriculture, biogas generation stands out as a pivotal opportunity [31], providing the dual advantages of diversifying farm revenue streams and reinforcing sustainable agricultural practices [32]. Historically, the sector expanded under supportive renewable energy policies, beginning with the 2008 All-Inclusive Feed-in Tariff for small-scale plants, followed by revised incentive schemes in 2012 and 2016 [5]. This growth has positioned Italy among Europe's leading producers of upgraded biogas [6]. Currently, legislative frameworks and incentives are steering the sector toward biomethane production via biogas upgrading technologies [33], aligning with support measures under the REPowerEU framework [5]. However, the upgrading process required to convert raw biogas into biomethane is characterized by high energy consumption, creating a significant demand for auxiliary power [7]. Consequently, improving the energy efficiency of these facilities has emerged as a critical operational challenge. To address this energy demand and decarbonize the production chain, hybridizing AD infrastructure with APV systems represents a compelling renewable energy solution. Contemporary APV configurations have evolved to include diverse module designs, mounting structures, and tracking mechanisms tailored to various agricultural environments [2]. However, despite these advancements, integrated solutions combining biogas and solar energy, particularly APV systems, remain unexplored. Such integrated systems offer significant potential to enhance overall sustainability and energy independence. Taramasso et al. [18] assessed four heat-power supply configurations for biomethane-producing AD plants in Italy, ranging from groundwater heat pumps (GWHP) powered by grid or GMPV electricity to CHP units supported by GWHPs or wood chip boilers. While combinations of GWHPs with PV generation proved economically attractive, achieving payback times of 4.2-4.8 years compared to 3.6-5.4 years for GWHPs powered by the grid, their analysis did not extend to the techno-economic optimization of APV systems.

Despite these advances, existing research has focused primarily on individual system components rather than integrated optimization frameworks that simultaneously evaluate multiple APV configurations with different heating technologies for biogas plants with a focus on $BioCH_4$ production. Additionally, systematic comparative analysis between on-grid and off-grid APV systems remains limited, particularly regarding the application of multi-objective optimization methods for APV-biogas integration strategies. The present research addresses these knowledge gaps by presenting a comprehensive optimization framework that evaluates the integration of biomethane production plant with various bifacial APV systems, which differ from conventional GMPV systems through greater pitch (row spacing) and elevated structures that allow continued farming. This study examines vertical and tracking (1-axis and 2-axis) APV configurations combined with supplementary energy sources, including biogas boilers, CHP units fueled by biogas, GWHPs, battery energy storage systems (BESS), and grid electricity. Methodologically, the framework explicitly accounts for key agronomic factors, such as row spacing, ground clearance, and tracker type, that influence both energy yield and land use in APV systems, thereby aligning energy-system design with crop management requirements.

The primary objective is to optimize grid-connected APV-biomethanation scenarios by applying the technique for order preference by similarity to ideal solution (TOPSIS) to results from a multi-objective genetic algorithm (MOGA) developed in MATLAB. To the best of current knowledge, there is no prior report of a combined and scenario-rich application in which a MOGA produces a portfolio of candidate solutions that is subsequently ranked using transparent multi criteria decision analysis (MCDA) with TOPSIS for the APV-biomethanation context. A techno-economic assessment is also conducted for alternative configurations, including biomethanation plant with a standalone biogas CHP unit (baseline), individual grid-based systems (without APVs), and off-grid APV systems, analyzed through analytical techno-economic evaluations to provide further insights. This analysis aims to establish the most economically viable configuration that ensures full coverage of the energy demands of an AD plant situated in Piacenza, Italy, over the project lifetime.

2.3 Materials and methods

This research explores energy strategies by integrating APV systems with a biogas plant producing an average of 125 Sm^3/h of $BioCH_4$. Considering APV limitations during night-time and unfavorable weather conditions, various scenarios are modeled to optimize energy performance and reliability. Each system component is sized according to the plant's electrical and thermal demands.

2.3.1 Description of the site and load profile

The mesophilic AD plant in Piacenza, Italy, operates at a constant temperature of 37°C and incorporates membrane technology for biogas upgrading. The process involves biogas production from organic waste in the AD plant, followed by upgrading biogas into $BioCH_4$. Table 2.1 reports the breakdown of feedstock materials in tons per hour.

Table 2.1 The breakdown of feedstock material mass and specific heat values for AD Plant in Piacenza **[34]**.

Feedstock material	Feedstock intake (ton/hour)	Specific heat of feedstock (kJ/kg·K)
Fresh Cattle Manure	1.14	3.7
Dairy Cattle Slurry	1.48	4.0
Corn Silage	0.46	3.0
Corn Stover Silage	0.42	3.2
Dilutants	1.25	4.18

Summing these categories results in a total hourly intake of 4.75 tons (41,610 tons per year), corresponding to a weighted average specific heat of approximately 3.81 kJ/kg.K. Based on site-specific data [34], the plant produces 6789 normal cubic meters (Nm^3) of biogas per day, which, given a methane content of 54.2%, corresponds to a daily $BioCH_4$ production of about 3680 Nm^3. A predominant fraction (75.95%) of the total biogas output is upgraded to $BioCH_4$, while the remaining 24.05% is fed into the CHP unit with a capacity of 150 kW_{el} (1633 Nm^3 biogas/day). Figure 2.1 illustrates the plant's annual electrical and heat demands at an hourly resolution.

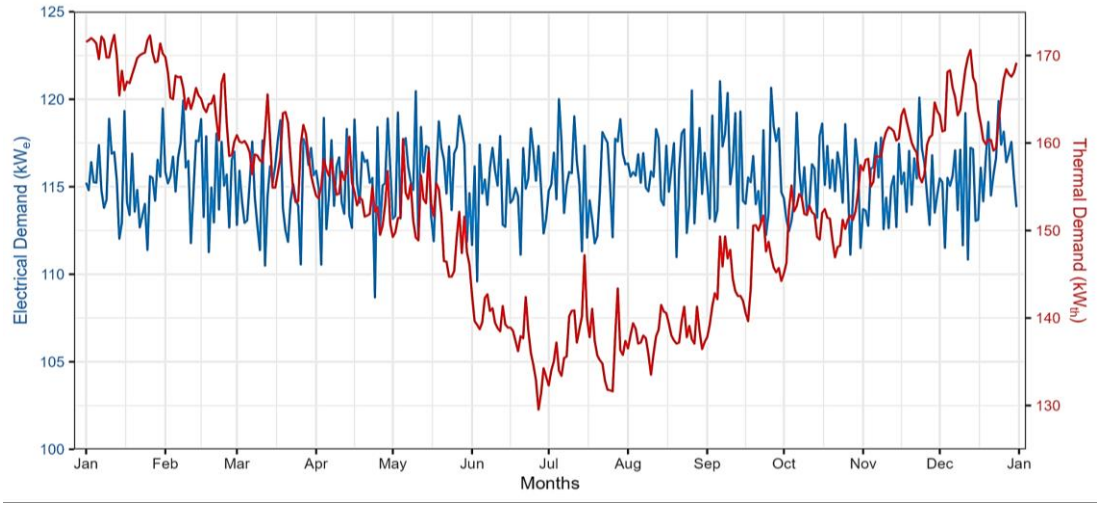

Figure 2.1 Hourly electrical and thermal demand of the AD plant in Piacenza (excluding heat producer's electricity demand) **[34]**.

The total annual electricity demand is 1011.8 MWh_{el}, with a peak requirement of 119 kW_{el}. This demand covers the entire biogas production process including biogas compression, upgrading, and auxiliary systems. In contrast, the plant's heat demand of 1340 MWh_{th} shows considerable seasonal fluctuations, peaking at 179 kW_{th} in wintertime (January) and reaching its lowest levels during the summer. A detailed breakdown of the plant energy requirements is given in Table 2.2.

Table 2.2 Breakdown of the AD plant electrical consumption in Piacenza **[34]**.

Component	Power Consumption (kW)
Cogeneration Unit	3.8
Biological Process	29.9
Upgrading System	56.2
Auxiliary Services	4.1
Booster System	25.0
Total	119

Note that electricity required by control electronics, motor starters, sensors, and cooling pumps associated with heat production units will be integrated into the overall electrical demand after system sizing.

2.3.2 Description of scenarios

This study evaluates eight scenarios designed to fully meet the thermal and electrical energy demands of the mesophilic AD plant in Piacenza. The analysis is structured around three primary on-grid APV scenarios (S1-S3), optimized using MOGA in MATLAB. These optimized scenarios are benchmarked against five alternative scenarios (S4-S8). Alternative scenarios assessed through analytical techno-economic evaluations, include a baseline case representing common industry practice (S4), two grid-dependent systems without APV integration (S5 and S6), and two fully off-grid APV systems designed for energy autonomy (S7 and S8). The terminology for these off-grid scenarios requires clarification. In the off-grid APV scenarios, the 'off-grid' designation applies exclusively to the electrical system. While the APV facility operates independently using battery storage, the biogas plant and upgrading unit maintain their connection to the gas grid for biomethane sales. These scenarios are representative of agricultural contexts where electrical grid interconnection is technically challenging or economically prohibitive, often due to remote siting. This configuration is contingent upon viable access to the gas grid or the feasible transport of biomethane via a virtual

pipeline (i.e., truck transport). The analytical modeling of benchmark scenarios provides comparative insights into economic viability, performance, and trade-offs between optimized APV systems and conventional alternatives. All APV configurations utilize bifacial PV modules in three distinct setups including fixed vertical, overhead 1-axis, and overhead 2-axis tracking systems. The key components and energy supply strategies for all eight scenarios are summarized in Table 2.3.

Table 2.3 Summary of Evaluated Energy System Scenarios.

Scenario	APV	BESS	Grid	CHP	GWHP	Boiler
S1	✓	-	✓	-	-	✓
S2	✓	-	✓	-	✓	-
S3	✓	-	✓	✓	-	-
S4	-	-	-	✓	-	-
S5	-	-	✓	-	✓	-
S6	-	-	✓	-	-	✓
S7	✓	✓	-	-	-	✓
S8	✓	✓	-	-	✓	-

A comprehensive schematic showing all the technological components and their potential interconnections, including heat, electricity, and biogas streams, is presented in Figure 2.2.

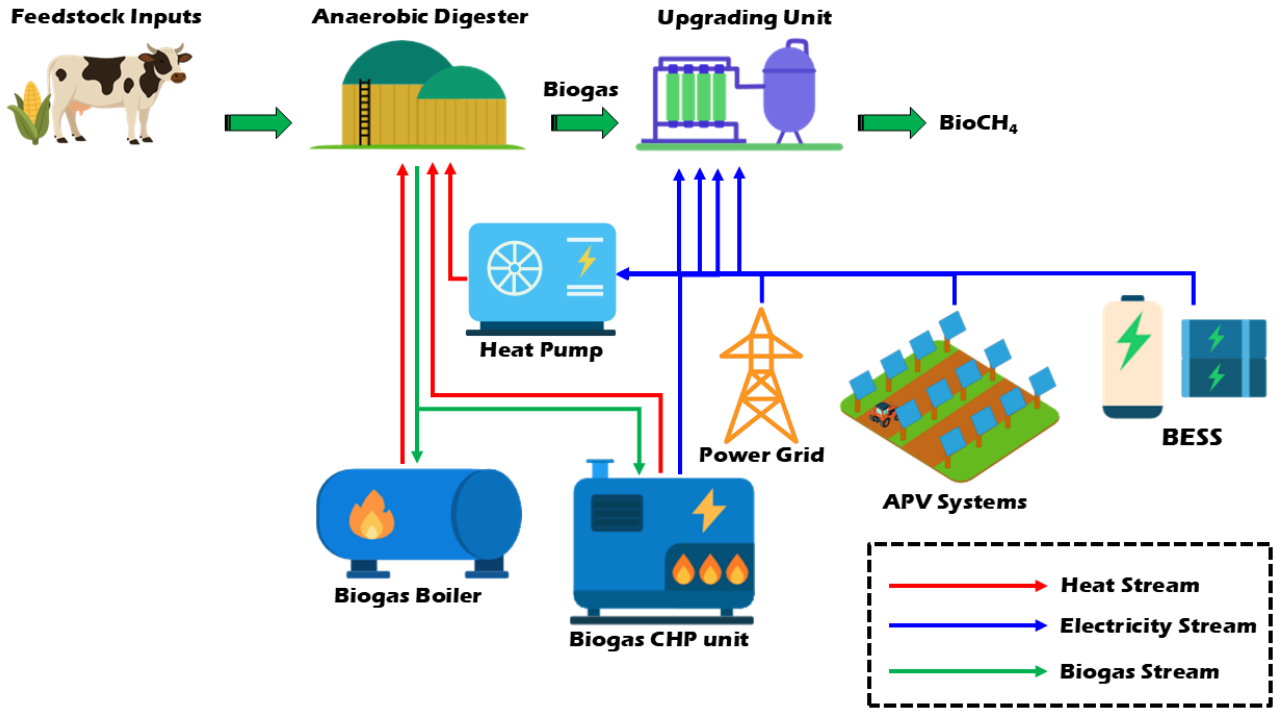

Figure 2.2 Schematic of all involved equipment under investigation in this study.

2.3.3 Heat and electricity supply

The study adopts a heat load-following strategy, whereby heat producers are sized to fully meet the thermal demand of the AD plant, ensuring stable digester operation. If an oversized heat producer is identified after sizing (probably due to the market availability), it is assumed that a system controller is implemented to modulate the heat producer's thermal output to exactly match hourly thermal demands, thus preventing excess heat production. Subsequent sections focus on the sizing criteria, selection process, biogas consumption (if applicable) and electrical energy requirements of the heat producers.

2.3.3.1 Biogas boiler

Biogas boilers burn biogas to generate thermal energy for uses like heating, drying, or preheating digesters. They offer environmental benefits from renewable fuel use but require careful design due to biogas variability and have higher initial costs than conventional boilers. In this study, the biogas boiler is sized based on the peak heat demand observed in January, measured at 179 kW_{th}. The lower heating value of biogas (LHV_{Biogas}) is assumed to be 5.5 kWh/Nm^3, with the biogas boiler's efficiency ($\eta_{th,Biogasboiler}$) estimated at 85% [35]. Given these parameters, the required biogas input rate can be calculated using Eq. 2.1 [35]:

$$P_{th,Biogasboiler}=Q_{Biogasboiler}\times LHV_{Biogas}\times \eta_{th,Biogasboiler} \quad \text{Eq. 2.1}$$

Where, $P_{th,Biogasboiler}$ represents the thermal output of the biogas boiler (kW_{th}), and $Q_{Biogasboiler}$ represents the required biogas input rate (Nm^3). Given that both the boiler efficiency and the LHV of biogas are predefined, the hourly biogas input rate is derived using Eq. 2.1. Finding a biogas boiler that precisely matches the peak thermal load (179 kW_{th} in January) poses challenges in the current market. As a result, the ATTSU RL-300 biogas boiler [36] with a maximum thermal output of 228 kW_{th} and 85% efficiency was identified as a suitable option for this study. Since the selected biogas boiler has a higher thermal capacity than the actual peak demand, a system controller is assumed to regulate the boiler's biogas input rate. By adjusting the biogas flow rate according to hourly thermal demand, the boiler generates only the necessary heat, avoiding energy wastage despite its oversized nominal capacity.

The boiler's electrical demand mainly arises from its auxiliary components, such as pumps, fans, and control systems. By examining the catalogues, this consumption is estimated to be 1-2% of the biogas boiler's thermal output, depending on the size of the boilers [36]. In this study, a conservative estimate of 1.5% has been assumed. This auxiliary demand is covered within each scenario according to the respective energy supply configuration described in Section 2.3.2.

2.3.3.2 Heat pump

A heat pump is an energy-efficient system that transfers heat from external sources to meet heating demands. In this study, groundwater heat pumps (GWHPs) have been selected due to their stable groundwater temperatures year-round, enabling higher efficiency, particularly during colder months when heating demand peaks [18]. Compared to air-source heat pumps (ASHPs), GWHPs have higher initial installation costs associated with drilling and groundwater access; however, their superior efficiency results in lower operational costs, substantial long-term savings, and environmental benefits such as reduced GHG emissions, lower electricity usage, and minimal noise pollution [37]. Considering the peak heat demand and market availability, the Viessmann Vitocal 350 [38], with a maximum capacity of 181 kW_{th}, was selected as the most suitable option, closely matching the peak thermal requirement. Nevertheless, to ensure precise hourly heat delivery, the controller is assumed to modulate electrical input to the heat pump according to real-time heat requirements. Thus, the heat pump operates efficiently at varying partial loads, aligned exactly with the plant's hourly thermal demand. The hourly electrical power required for operating the GWHP is determined using Eq. 2.2 [18]:

$$E_{GWHP} = \frac{Q_{GWHP}}{COP_{real}} \qquad \text{Eq. 2.2}$$

In this expression, E_{GWHP} denotes the hourly electrical energy consumed by GWHP (kWh_{el}). Q_{GWHP} refers to the hourly thermal energy generated by the heat pump in kWh_{th}, which is set to exactly match the hourly heating requirement based on the heat load-following approach. The effective coefficient of performance (COP_{real}), a dimensionless indicator of the heat pump's efficiency in converting electricity into thermal energy, corresponds to 50% of the theoretical COP obtained from the reversed Carnot cycle, as expressed in Eq. 2.3 [23,24]:

$$COP_{real}=1/2\times COP_{Carnot} = 1/2\times \left(\frac{273.15 + T_{dig}}{T_{dig} - T_{gw}}\right) \quad \text{Eq. 2.3}$$

Where, the digester temperature (T_{dig}) is maintained at 37 °C and the groundwater temperature (T_{gw}) is set at 10 °C throughout the year, resulting in a calculated COP of 5.74. The COP directly determines the heat pump's electrical energy consumption through Eq. 2.2. With a calculated COP of 5.74, GWHP converts each kWh of electrical input into 5.74 kWh of thermal output. This electrical consumption is integrated into the plant's total electricity demand, which is then supplied by the configurations presented in Section 2.3.2.

2.3.3.3 Biogas combined heat and power unit

A biogas CHP unit converts biogas into electricity and heat simultaneously. Eq. 2.4 is utilized to calculate the rated heat capacity of biogas CHP unit [41]:

$$P_{th,BiogasCHP}=\frac{Q_{BiogasCHP}\times LHV_{Biogas}\times \eta_{th,BiogasCHP}}{OH_{BiogasCHP}} \quad \text{Eq. 2.4}$$

Where, $P_{th,BiogasCHP}$ (kW_{th}) represents the thermal output of the biogas CHP unit. $Q_{BiogasCHP}$, the biogas availability, is calculated as 24.05% of biogas production as described in Section 2.3.1, and $OH_{BiogasCHP}$ refers to the daily operating hours. These parameters were obtained through on-site assessments of the proposed biogas plant, as detailed in the Table 2.4.

Table 2.4 The technical specifications of biogas plant in Piacenza **[34]**.

Parameters	Unit	Specification
Q_{BGCHP}	Nm^3/day	1633
OH_{BGCHP}	hour	24
LHV_{Biogas}	kWh/Nm^3	5.5
Biogas density	Kg/Nm^3	1.28

The thermal conversion efficiency of the biogas CHP unit, denoted as $\eta_{th,BiogasCHP}$, is assumed to be 50%, for a small-scale biogas plant [42]. Eq. 2.5 is utilized to calculate the rated electrical capacity of biogas CHP unit [41]:

$$P_{el,BiogasCHP} = \frac{Q_{BiogasCHP} \times LHV_{Biogas} \times \eta_{el,BiogasCHP}}{OH_{BiogasCHP}} \quad \text{Eq. 2.5}$$

Where, $P_{el,BiogasCHP}$ (kW_{el}) represents the electrical output of the biogas CHP unit. The electrical conversion efficiency of the biogas CHP unit, denoted as $\eta_{el,BiogasCHP}$ is assumed to be 33%, for a small-scale biogas plant [26]. Based on Eq. 2.4 and 2.5, the thermal and electrical outputs of the biogas CHP unit are 187.12 kW_{th} and 123.49 kW_{el}, respectively, both of which fall within the range of the peak thermal and electrical demands. However, due to market availability, a biogas CHP unit with specifications closely matching the actual energy demand and efficiency requirements was selected, as shown in Table 2.5 [43].

Table 2.5 The technical specifications of TEDOM CENTO-T150 biogas CHP selected in this study **[43]**.

Parameter	Unit	Specification
Max. electrical output @LHV5.5	kW	127.9
Max. heat output @LHV5.5	kW	195.7
Max. electrical consumption	kW	3.84
Max. electrical efficiency	%	34.2
Max. thermal efficiency	%	52.3
Max. overall efficiency	%	86.5

The selected biogas CHP unit has slightly higher heat capacity compared to the peak thermal load (179 kW_{th}). Consequently, a system controller is deployed to adjust biogas consumption hourly, ensuring the thermal output strictly corresponded to the actual thermal demand, preventing excess heat generation and reducing unnecessary biogas consumption. Using Eq. 2.4, the hourly biogas consumption of the CHP unit is calculated by equating its thermal output at each hour to the hourly thermal demand (heat load-following approach), divided by the product of the biogas LHV and the CHP's thermal efficiency. Once the hourly biogas input rates are determined through this procedure, the corresponding electrical output is calculated at each hour using Eq. 2.5. This component requires a continuous supply of electrical power to operate its auxiliary systems, including control electronics, sensors, and cooling pumps. This auxiliary consumption is assumed 3% of the unit's electrical output [42]. Figure 2.3 illustrates the plant's annual hourly thermal and electrical demands, including electricity consumed by heat generation units, as well as the hourly biogas consumption by the boiler and CHP units.

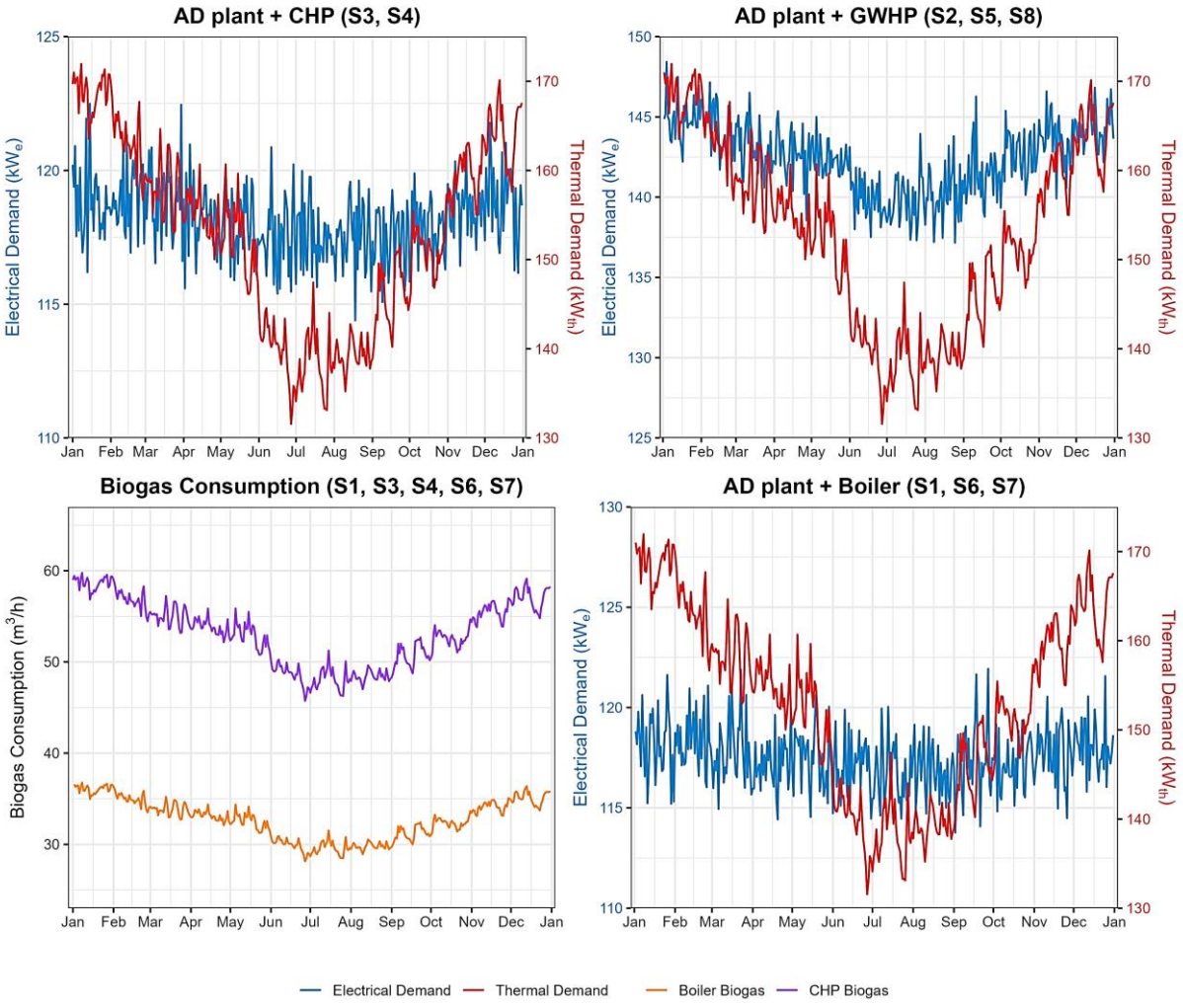

Figure 2.3 Annual hourly profiles of AD plant energy demands and consumption in Piacenza. The electrical and thermal demand profiles are shown for systems using CHP unit (top-left), GWHP (top-right), and biogas boiler (bottom-right). The bottom-left panel details the hourly biogas consumption rates for the boiler and CHP unit scenarios.

The total annual electricity demand of the AD plant varies depending on the heating technology employed, as detailed in Figure 2.3. When incorporating a GWHP (top-right panel), the plant's annual electricity demand is highest at 1246 MWh_{el}, with a peak power requirement of 158 kW_{el}. In contrast, utilizing a CHP unit (top-left panel) results in an annual electricity demand of 1035 MWh_{el}, with a peak of 131 kW_{el}. Notably, the CHP unit generates 871 MWh_{el} annually when operated with the system controller. Employing a boiler system (bottom-right panel) leads to the lowest electricity demand at 1029 MWh_{el}, with a peak of 130 kW_{el}. Regardless of the heating technology employed, the plant's total annual heat demand remains constant at 1340 MWh_{th}, consistent with the findings reported in [18], with a peak thermal demand of 179 kW_{th}. Concerning biogas use (bottom-left panel),

the CHP unit uses a significantly higher volume, totaling 465,665 Nm^3 annually, compared to the boiler system, which consumes 286,521 Nm^3 per year.

2.3.4 On-grid agrivoltaic systems modeling

In this study, Agri-OptiCE® framework is employed to simulate and evaluate the hourly electricity production from three distinct APV system configurations. Agri-OptiCE® is an integrated simulation environment tailored to APV applications, extending a previously validated model [28,29] to account for a broader set of design variables and performance indicators. The framework integrates a solar irradiance and shading model that accounts for geometric layout and orientation, and a detailed PV performance model for bifacial modules. The resulting irradiance is converted to DC power using five parameter single-diode model with parameter extraction via the Newton-Raphson method, and subsequently to AC power through an inverter model, with losses such as mismatch also considered. These components simulate energy output based on irradiance conditions (including rear-side PV module's contributions), angle-of-incidence (AOI) effects, and temperature-dependent module efficiency. The simulation results have previously shown good agreement with field measurements and outputs from commercial software tools, providing confidence in the accuracy of this model [46]. The modeling framework employed for the simulations is outlined in the flowchart shown in Figure 2.4, which is adapted from the procedure presented in [45].

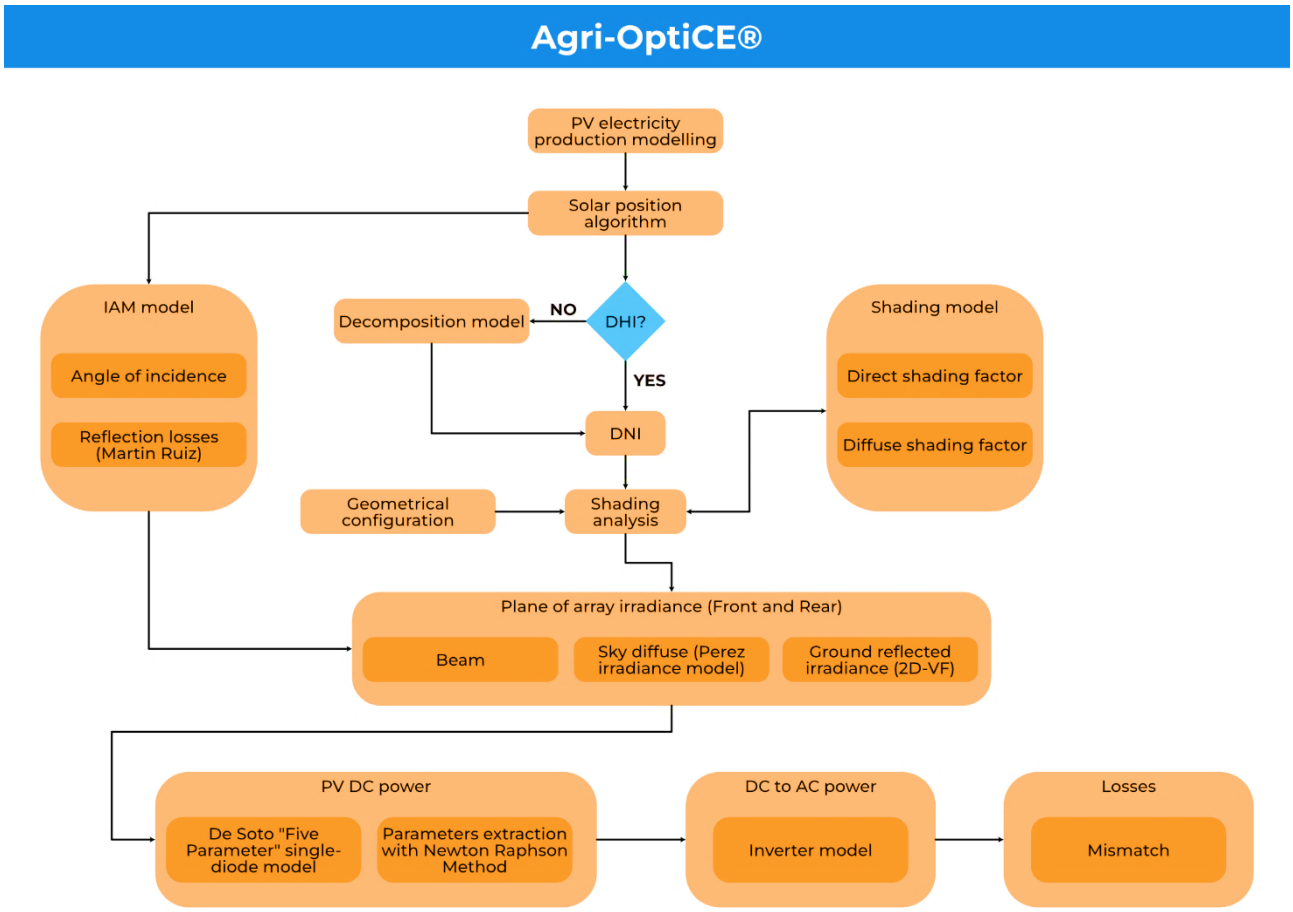

Figure 2.4 Flowchart of the Agri-OptiCE® framework used in the simulation process **[45]**.

Comparative assessment across APV typologies is sensitive to geometric assumptions, shading representation, and climate-driven boundary conditions, which makes transparent reporting of the modeling pipeline essential. Maity and Kumarasamy [47] reinforce this methodological point by proposing an integrated modeling workflow beyond the most commonly studied temperate contexts and by showing that configuration choice, including bifacial-oriented layouts such as vertical arrangements, can materially influence predicted performance under distinct irradiance patterns. This supports the thesis modeling approach by emphasizing that comparative conclusions should be tied to explicitly stated assumptions and parameterization, particularly when results are compared at hourly resolution.

In this study, three APV system configurations are simulated. The system setups and input parameters used in the model are detailed in Table 2.6.

Table 2.6 Input data for simulation of energy output from different types of APV systems.

Parameters	**Specifications**
Location	Piacenza, 44.9744° N, 9.8924° E
Tracker max/min rotation angle	+55°/-55°
Height at rotation axis for 1-axis and 2-axis	5 m
Clearance for Vertical mounting system	0.7 m
Axis azimuth angle for 1-axis and 2-axis	South (0°)
Axis azimuth angle for Vertical	East (-90°)
PV array layout	6-Landscape (2-axis), 1-Portrait (1-axis), 2-Landscape (Vertical)
PV module	Trina solar, TSM-DEG21C-20
PV module nominal capacity	660 W_p
Efficiency	21.28%
Bifaciality factor	75%
Nominal operation module temperature	43°C (±2°C)
Temperature co-efficient for P_{max}	- 0.34%/°C
Number of cells	132 (66×2)
PV module dimension	2384mm×1303mm×35mm
Albedo factor	0.25
Pitch between PV strings for 2-axis system	15m
Module-to-module row spacing for 2-axis system	3.5m
Pitch between PV strings for 1-axis system	6m
Module-to-module row spacing for 1-axis system	1 cm
Pitch between PV strings for vertical system	8m
Module-to-module row spacing for vertical system	1 cm

A distinct pitch between PV strings was evaluated for each APV system configuration, starting from a minimum allowable spacing for agricultural activities, as outlined in [48]. While reduced pitch can improve land use efficiency, it was only considered when it did not obstruct agricultural machinery or introduce excessive PV self-shading. This approach ensures a careful balance between agricultural operability and energy performance. In practice, APV systems are also influenced by ground reflectance (albedo factor) from crops, but this aspect is beyond the scope of the present study. The hourly climate data used in the simulations were sourced from a nearby virtual weather station for the year 2019 [49], as illustrated in Figure 2.5.

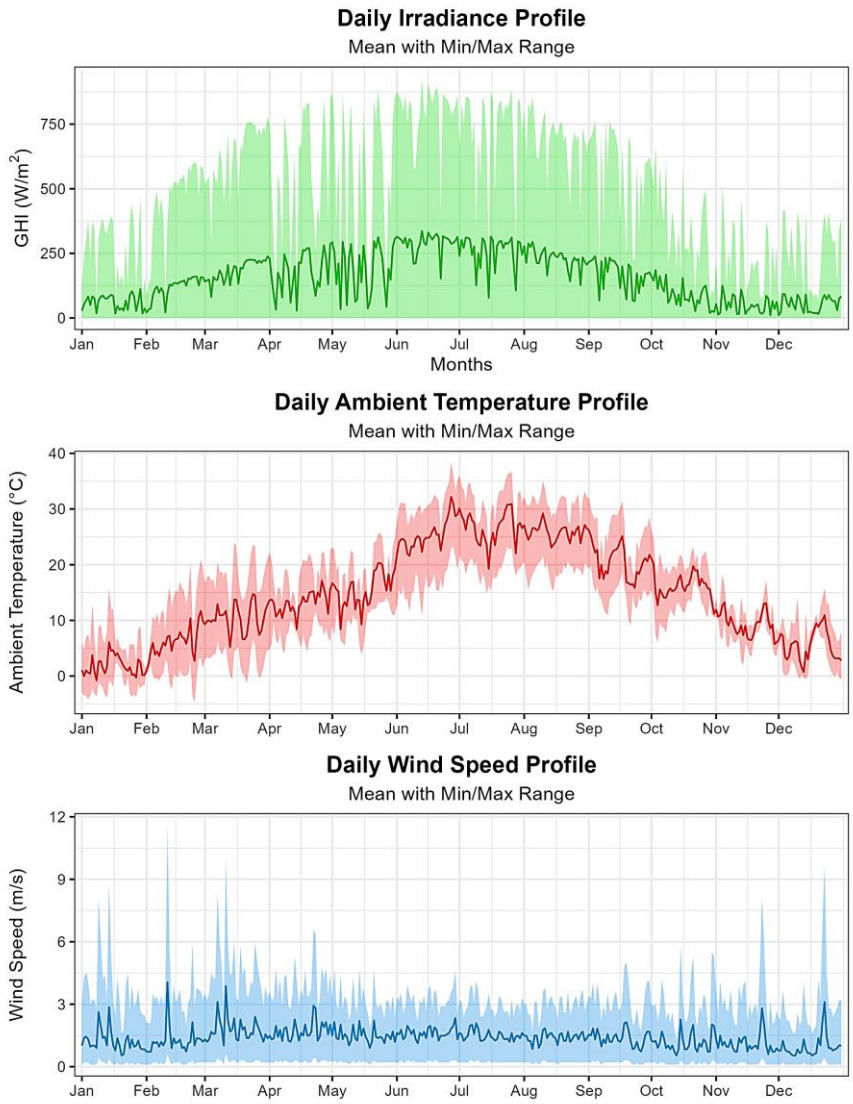

Figure 2.5 Hourly Climatic Profile of Piacenza in 2019 **[49]**.

In this year, the selected location recorded an annual global horizontal irradiance of 1370 kWh/m², an average temperature of 14.7 °C, and an average wind speed of 1.4 m/s. To reflect operational conditions, the simulations also include the characteristics of an on-grid inverter, as outlined in Table 2.7.

Table 2.7 Specifications of the selected solar inverter.

Parameters	**Specifications**
Max. Efficiency (%)	98.6
Euro. Efficiency (%)	98.3
AC output	Triple-phase
Grid frequency range (Hz)	50/60
Grid voltage range (V)	230/270-480

2.3.4.1 Optimization problem

This section formulates the integrated on-grid optimization problem for S1−S3 as a multi-objective problem. As described earlier, the entire heat demand of the AD plant is assumed to be fully met by the heat producers through the adoption of a heat-load-following approach. In the case of the CHP unit (Scenario 3), although the use of a system controller that regulates the biogas input based on hourly thermal demand ensures that all heat requirements are met, it also influences the unit's electricity production. Specifically, while the CHP operates at full load during winter due to high heat demand, it functions at partial capacity in summer when heat demand is significantly lower. As the system controller reduces the biogas input to match the reduced thermal needs, this also results in lower biogas input for electricity generation, thereby contributing to power deficits during those periods. Therefore, the optimization identifies the optimal combination of APV system type and capacity, along with the necessary contribution from the power grid, to fully meet the plant's electrical demand in the most cost-effective manner. The difference between the hourly electricity needs and the sum of the hourly electricity produced by the CHP and APV indicates the amount of electricity that needs to be drawn from the grid or the surplus electricity that can be injected into the grid. This value is crucial for the economic evaluation.

The objectives of the optimization are to maximize NPV, and to minimize the land occupation of the APV systems. NPV represents the difference between the present value of total project revenues and total project costs over the system lifetime, accounting for inflation and discount rates, as detailed in the economic modeling section. The decision variables include the type of APV system, represented as an integer variable that selects among vertical, 1-axis, and 2-axis configurations, and the installed capacity of the APV system in kilowatt-peak.

The problem is subject to two principal constraints that ensure realistic and sustainable operation. The first is a land-use constraint, stipulating that the product of installed capacity and the specific land area per kW_p (configuration-dependent) must not exceed 2 hectares (20,000 m^2). This upper limit is consistent with the definition of small-scale agricultural holdings (≤2 ha) [1] adopted in this study, thereby aligning the system design with the intended application context. This constraint enforces the efficient use of available space. The second constraint concerns renewable energy penetration. In the boiler and heat pump scenarios, the effective APV penetration (EP_{APV}), defined as the proportion of the electrical load supplied by the APV system, must be at least 20% to ensure a meaningful contribution from on-site renewables. In the CHP case (S3), the residual demand not met by the CHP

unit is covered by APV and the grid, with the grid share limited to 50%. The thresholds of 20% and 50% were adopted as pragmatic lower bounds. The 20% requirement secures a tangible role for APV in hybrid systems, while the 50% limit maintains on-site generation from CHP and APV as the dominant supply source without creating unrealistic operating constraints. This design choice ensures the feasibility of the optimization process while maintaining consistency with the study's focus on renewable energy integration. Finally, all annual costs and revenues are aggregated over the lifetime. The objective functions, constraints and decision variables are presented in the following subheadings.

2.3.4.2 Objective functions

The multi-objective optimization problem is formulated to minimize the objective vector (x), which is defined as:

$$\min J(x) = [f_1(x), f_2(x)] \quad \text{Eq. 2.6}$$

The individual objective functions, representing the economic and land-use performance criteria, are detailed below.

1. Economic Performance (f_1): The first objective is to maximize the project's financial return. This is achieved by minimizing the negative NPV, ensuring the selection of the most economically viable solution:

$$f_1(x) = -\,NPV \quad \text{Eq. 2.7}$$

2. Land Occupation (f_2): The second objective is to minimize the land footprint of the APV installation. This is calculated as the product of the APV system's installed capacity and a technology-dependent land occupation factor:

$$f_2(x) = x_2 \times \alpha \quad \text{Eq. 2.8}$$

Here, x_2 represents the APV capacity in kW_p, and α is the specific land occupation factor (m^2/kW_p). Following [48], the value of α is influenced by the APV system type, pitch, and PV module layout. In this study, $\alpha = 19.5\ m^2/kW_p$ is adopted for fixed vertical APV with 8m pitch, $\alpha = 14.4\ m^2/kW_p$ for 1-axis tracking with 6m pitch, and $\alpha = 20.95\ m^2/kW_p$ for 2-axis tracking with 15m pitch (values aligned with Table 2.6).

2.3.4.3 Constraints

The optimization is governed by the following constraints:

1. Land Area Constraint: The total land area occupied by the APV system cannot exceed the maximum available agricultural land, A_{max}. This physical limitation is expressed as:

$$c_1(x)=(x_2\times\alpha)-A_{max}\leq 0 \quad \text{Eq. 2.9}$$

Where, A_{max} is defined as 20,000 m^2.

2. On-site Generation Constraint: A minimum threshold for on-site electricity conversion must be met. The formulation of this constraint, $\mathbf{c_2(x)}$, varies depending on the heating system configuration. For boiler and GWHP scenarios, it is assumed that at least 20% of the annual electrical load must be satisfied by on-site APV electricity conversion. The constraint is formulated to ensure the energy conversion fraction meets this requirement:

$$c_2(x)=0.2-EP_{APV}\leq 0 \quad \text{Eq. 2.10}$$

Where, EP_{APV} over an 8760-hour period is calculated through Eq. 2.11:

$$EP_{APV}=\frac{\sum_{t=1}^{8760}\min(APV_t, elecLoad_t)}{\sum_{t=1}^{8760} elecLoad_t} \quad \text{Eq. 2.11}$$

In the equation above, APV_t is the instantaneous energy conversion by the APV system at hour t, and $elecLoad_t$ is the electrical load at hour t. For the CHP scenario, since the CHP unit already contributes to on-site generation, this constraint is modified to limit the grid dependency of the residual load. The fraction of the total load supplied by the grid, F_{grid}, must not exceed 50%:

$$c_2(x)=F_{grid}-0.5\leq 0 \quad \text{Eq. 2.12}$$

Where, F_{grid} denotes the ratio of net electricity imported from the grid to the total electrical load, as defined in Eq. 2.13:

$$F_{grid}=\frac{\sum_{t=1}^{8760}\max\left(elecLoad_t\text{-}APV_t,\ 0\right)}{\sum_{t=1}^{8760}elecLoad_t} \quad \text{Eq. 2.13}$$

2.3.4.4 Decision variables

The optimization process is guided by the decision vector x, which includes one discrete and one continuous variable:

$$x=\begin{bmatrix}x_1\\x_2\end{bmatrix} \quad \text{Eq. 2.14}$$

Where, x_1 is APV system type. A discrete integer variable representing the technology choice: $x_1 \in [1, 2, 3]$, corresponding to vertical, 1-axis, and 2-axis systems, respectively. The APV system capacity, x_2, is a continuous variable representing the installed capacity of the APV system in kW_p. The search space is bounded as follows: $x_2 \in [1,1400]$. The upper bound is constrained by the maximum available land area (A_{max}) and the most land-intensive APV configuration (2-axis).

2.3.4.5 Optimization framework

The optimization framework in MATLAB loads scenario-specific MAT files containing hourly time series of electrical load, thermal demand, biogas consumption, and CHP electricity generation. This hourly input enables reliable modeling of energy flows, supports effective system sizing, and captures variability in operating conditions relevant for grid interaction [33, 34]. Following data acquisition, simulation settings are defined by establishing a simulation period (8760 h) and setting decision variables. The next phase involves configuring the genetic algorithm (GA) with parameters including population size, generation count, mutation, and crossover rates. The GA solver is then executed using the described multi-objective functions. Within these functions, APV power output is obtained by loading kWh/kW_p profiles from Agri-OptiCE® and scaling them by candidate capacity. Scenario-specific calculations determine capital and operational expenditures (CAPEX, OPEX) as well as revenue streams. To evaluate long-term financial viability, the model applies discounted cash-flow factor that convert all future costs and revenues into present-value terms. This approach simultaneously accounts for inflation and the time value of money, ensuring that all monetary flows are consistently expressed in real terms suitable for NPV calculation. This evaluation framework supports the multi-objective optimization by integrating both technical performance and economic outcomes, providing a robust basis for comparing competing configurations and identifying the most cost-effective and revenue-enhancing design. The system economics are aggregated through these

evaluations, culminating in a composite objective vector. Finally, a post-processing step employs TOPSIS ranking and candidate evaluation functions, which are discussed in the next section, to identify the optimal design candidate, which is then visualized through detailed metrics, specifically NPV and APV land occupation. Figure 2.6 presents a detailed flowchart that illustrates the optimization process.

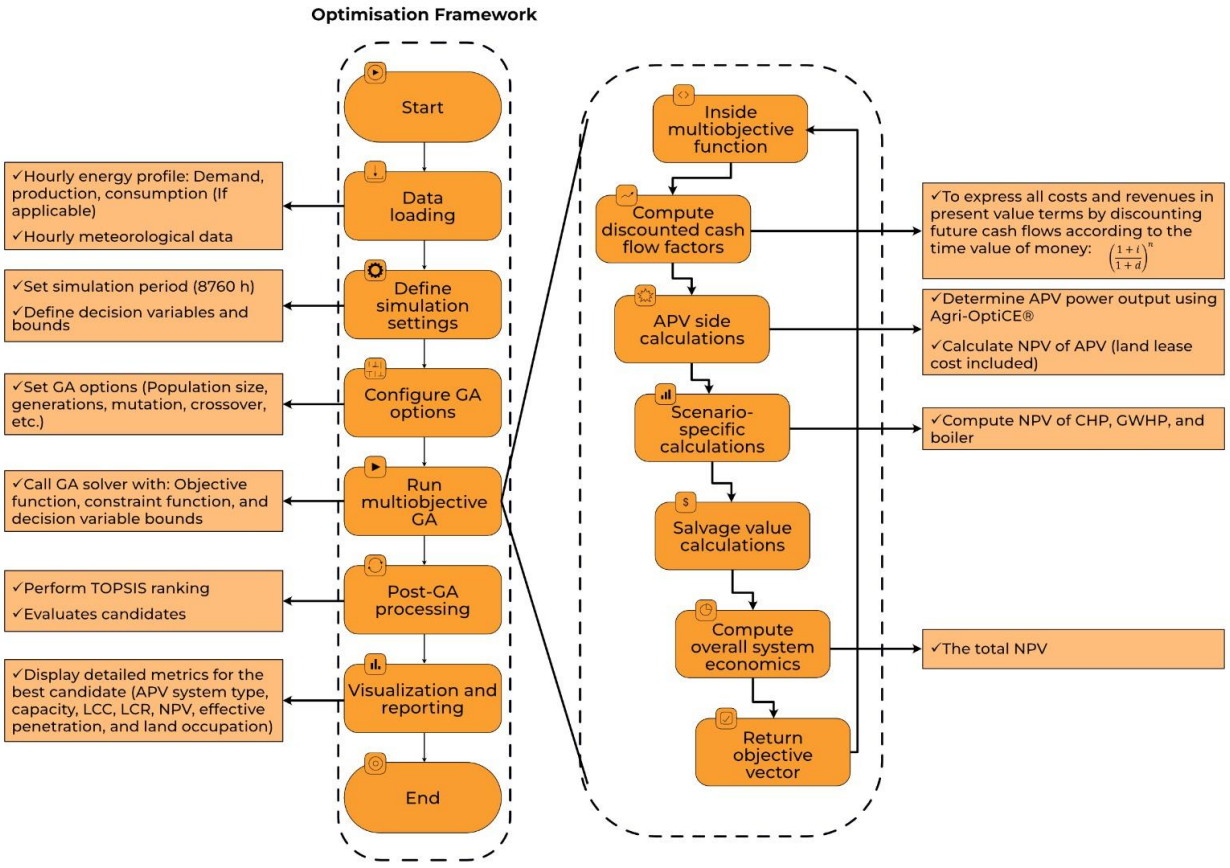

Figure 2.6 Detailed flowchart explicitly illustrating the entire optimization process.

2.3.4.6 Procedure for TOPSIS-Based Candidate Selection

To assess and rank the most suitable configurations for primary scenarios, we adopted MCDA framework based on results from a multi-objective optimization process. Among the available MCDA techniques, we selected TOPSIS for its capability to handle compensatory criteria and its widespread application in energy and environmental decision-making contexts [35, 36]. TOPSIS is based on the idea that the optimal scenario should simultaneously show the shortest distance from a hypothetical positive ideal solution (PIS) and the greatest distance from a negative ideal solution (NIS), both

defined by performance across a set of key performance indicators (KPIs). Note that neither the PIS nor the NIS corresponds to an actual configuration; rather, they are theoretical constructs representing the best and worst observed performance values across all considered KPIs [54]. The method was applied by first constructing a decision matrix, where rows represented candidate configurations and columns corresponded to the two selected KPIs: NPV, to be maximized, and APV land occupation, to be minimized. To eliminate dimensional inconsistencies and ensure comparability, all KPI values were normalized using Min-Max scaling, transforming them to a common 0-1 range. A weighted-normalized matrix was then obtained by assigning a weight to each KPI according to its relative importance. In the primary analysis, equal weights (0.5 each) were assigned to the mentioned KPIs to maintain neutrality, avoiding subjective bias given the absence of specific stakeholder preferences or policy directives. For each configuration, the Euclidean distance to the PIS (D_i^+) and to the NIS (D_i^-) was calculated, and these two measures were synthesized into a similarity index (C_i) as follows:

$$C_i = \frac{D_i^-}{D_i^+ + D_i^-} \qquad \text{Eq. 2.15}$$

This index, ranging from 0 to 1, expresses the relative closeness of each configuration to the ideal solution. Higher C_i values indicate a better overall performance, representing a more favorable balance between maximizing NPV and minimizing APV land use. Configurations were then ranked in descending order according to their C_i scores.

To assess the robustness of the ranking, a sensitivity analysis was performed by varying the NPV weight (0.25, 0.50, and 0.75), while complementarily adjusting the weight of APV land occupation. This analysis illustrates how the rankings change under different stakeholder priorities, providing decision-makers with a broader understanding of the trade-offs and stability of each configuration. The analysis was implemented using the Scikit-Criteria python module [55], ensuring transparency and reproducibility.

2.3.5 Off-grid agrivoltaic systems modeling

In this section, three different off-grid bifacial APV systems (vertical, 1-axis, and 2-axis) are simulated using PVSOL® software [56], a comprehensive tool for designing, simulating, and analysing PV systems. PVSOL supports various off-grid PV configurations equipped with bifacial PV modules and enables performance modeling based on custom meteorological data and component specifications. To ensure consistency with the on-grid APV scenarios, all off-grid APV configurations were modeled using the same software assumptions (Table 2.6) and hourly

meteorological data (Figure 2.5). However, it is important to clarify the complementary roles of the simulation tools employed in this study. While Agri-OptiCE® provides APV performance baselines and crop-energy interaction modeling, it is not designed for off-grid applications. Commercial PV software such as PVSOL and PVsyst can simulate off-grid system performance effectively, but they do not inherently perform optimal component sizing based on detailed techno-economic constraints or load profiles. Typically, dedicated optimization tools such as HOMER Pro are required for techno-economic optimization; however, HOMER Pro directly lacks comprehensive support for bifacial PV modules, specific definitions of module height, pitch between PV strings, and the integration of custom hourly meteorological data. Additionally, PVsyst does not support the bifacial 2-axis configurations. Consequently, PVSOL was selected as the most suitable software since it supports all necessary configurations and custom data inputs. Nevertheless, component sizing, specifically the number of PV modules and battery banks, cannot be automatically sized within PVSOL. To overcome this limitation, a mathematical modeling was employed to accurately calculate the required number of PV modules and batteries. To determine the total required quantity of PV modules within the software, the following equation is employed [57]:

$$N_{PV,req} = \frac{TDL_{el} \times 1000}{PSH \times P_{PVmax,actual}} \quad \text{Eq. 2.16}$$

Where, $N_{PV,req}$ represents the total number of PV modules needed, TDL_{el} is the total daily electrical load (Wh), $P_{PVmax,actual}$ represents the maximum output of each PV module (W), factoring in system losses collectively referred to as the derating factor. This includes losses due to temperature, soiling, cabling, shading, module aging, and inefficiencies in batteries and inverters. The derating factor typically ranges from 0.7 to 0.8, with an average value of 0.75 assumed in this study [58]. PSH denotes the peak sun hours, representing the period during which solar irradiation totals 1 kWh/m^2 on the PV module surface. For the specified location, the PSH values are calculated using PVSOL software.

In the off-grid scenarios, an annual capacity shortage of 0% is set as a constraint, ensuring that the systems fully meet the entire electrical demand without interruption. This conservative approach is adopted to appropriately size the stand-alone APV capacity by explicitly considering the worst-case scenario of minimal solar availability. While this method may result in relatively large system sizes, it is essential to ensure uninterrupted operation under all seasonal and solar conditions. The off-grid inverter, essential for converting DC power from batteries to AC, was sized using PVSOL software.

The chosen model has an efficiency comparable to that of the on-grid inverter, ensuring fairness in the performance comparison. Technical specifications are given in Table 2.8.

Table 2.8 Specifications of the selected solar MPPT off-grid inverter.

Parameters	Specifications
Max. Efficiency (%)	98
Euro. Efficiency (%)	97
AC output	Triple-phase
Grid frequency range (Hz)	50/60
Grid voltage range (V)	230/180-265
Battery voltage range (V)	12/24/36/48 V Auto Select

The battery banks ensure system reliability by storing energy to meet electricity demand during periods of low solar availability, such as cloudy conditions and nighttime. Surplus solar energy is stored in multiple battery units. The optimal number of batteries is determined using Eq. 2.17 [59]:

$$N_{Batt}=\frac{TDL_{el}\times NNSD}{C_n\times V_n\times \eta_{r\text{-}t}\times(1-\frac{SOC_{min}}{100})} \quad \text{Eq. 2.17}$$

Where, N_{batt} represents the number of batteries, TDL_{el} is the total daily electrical load (Wh), and NNSD refers to the number of non-sunny days per month (system autonomy days), assumed to be 3 [59]. C_n is the nominal capacity of a single storage unit (Ah), $\eta_{r\text{-}t}$ is the roundtrip efficiency (%), and V_n denotes the nominal voltage of a single storage unit (V). The minimum state of charge (SOC_{min}) is set at 20%. The battery specifications selected by the software [60] are provided in Table 2.9.

Table 2.9 The technical specifications of Huawei Luna 2000-15 BESS selected in this study **[60]**.

Parameters	Specifications
Technology	Lithium-ion phosphate, LFP
Nominal voltage (V)	48
Capacity (Ah)	300
Round-trip efficiency (%)	90

It should also be noted that the dispatch of battery charging and discharging cycles, based on hourly load demands and solar irradiance variations, is performed by PVSOL. Key outputs from PVSOL

simulations include total annual energy stored in batteries, annual surplus electricity generated, optimal off-grid inverter size, and missing energy (unmet load percentage). The calculation of APV land occupation follows the same approach as that employed for on-grid APV scenarios.

2.3.6 Economic modeling

The economic analysis for each scenario is performed by calculating the life cycle cost (LCC), life cycle revenue (LCR), and NPV. The NPV is defined as the difference between LCR and LCC, expressed in present value terms. A higher NPV indicates greater economic viability of the project. LCC represents the total expenses incurred over the lifetime of each component, discounted to present value by accounting for the time value of money. This includes the costs associated with initial investment, operation and maintenance costs (O&M), replacement costs, and the cost of purchasing electricity from the power grid. The LCC is calculated using the following equation [20]:

$$LCC=C_{cap}+C_{rep}+C_{O\&M}+C_{PPG} \quad \text{Eq. 2.18}$$

Where, C_{cap} denotes the capital cost of each component along with its installation costs (€), which is calculated using Eq. 2.19:

$$C_{cap}=C_{APV\ system}+C_{AD\ plant}+C_{Upgrading\ unit}+C_{battery\ packages}+C_{CHP\ unit}+C_{Biogas\ boiler}+C_{Heat\ pump} \quad \text{Eq. 2.19}$$

C_{rep} includes the replacement cost of equipment at the end of its lifetime (€) and is calculated using Eq. 2.20 [61]:

$$C_{rep}=\sum_{n=1}^{N} C_0 \times \left(\frac{1+i}{1+d}\right)^n \quad \text{Eq. 2.20}$$

Where, C_0 is the initial cost of each equipment (€), i represents the inflation rate, d the discount rate, n the year of equipment replacement, and N the total project lifetime.

$C_{O\&M}$ (€) represents the total annualized costs, including operations and maintenance of all system components, feedstock, and land lease for the APV systems, and is calculated as follows [20]:

$$C_{O\&M}=\sum_{n=1}^{N} C_{O\&M,\,i} \times \left(\frac{1+i}{1+d}\right)^n \quad \text{Eq. 2.21}$$

Where, $C_{O\&M,\,i}$ represents the first-year operation and maintenance cost (€), and n denotes the number of year. It is assumed that all biogas fuel for the biogas boiler and CHP unit is supplied by the on-site biogas plant, eliminating the need for fuel price considerations.

C_{PPG} represents the costs associated with purchasing power from the national grid (€) over the project's lifetime, as indicated in Eq. 2.22 [20]:

$$C_{PPG}=\sum_{n=1}^{N}(\text{Annual electricity export}\times\text{unit price})\times\left(\frac{1+i}{1+d}\right)^{n} \quad \text{Eq. 2.22}$$

LCR represents the total revenue generated over the project's lifetime from the sale of $BioCH_4$ to the gas grid, salvage value, and surplus electricity exported to the power grid. As given in [20], LCR is calculated using Eq. 2.23:

$$LCR=R_{sal}+R_{SPG}+R_{SBG} \quad \text{Eq. 2.23}$$

The salvage value refers to the estimated residual value of a system component at the end of its useful life. According to [62], the salvage value is calculated using Eq. 2.24:

$$R_{sal}=C_{rep}\times\frac{L_{rem}}{L_{comp}}=\sum C_{rep}\times\frac{L_{comp}-(L_{proj}-(L_{comp}\times\mathrm{INT}(\frac{L_{proj}}{L_{comp}})))}{L_{comp}} \quad \text{Eq. 2.24}$$

Where, R_{sal} refers to the salvage cost of all components (€), calculated based on linear depreciation, where the salvage value is proportional to the component's remaining life. L_{rem} indicates the remaining operational life of the component when the project ends, while L_{comp} represents the component's lifetime (years), and L_{proj} is the project lifetime, assumed to be 20 years. INT is a function that returns the integer value of a real number.

R_{SPG} and R_{SBG} represent the incomes from selling power back to the grid (€), and selling $BioCH_4$ produced to the gas grid (€) over the project's lifetime as indicated in Eq. 2.25:

$$\begin{aligned} R_{SPG}&=\sum_{n=1}^{N}(\text{Annual electricity export}\times\text{unit price})\times\left(\frac{1+i}{1+d}\right)^{n} \\ R_{SBG}&=\sum_{n=1}^{N}(\text{Annual } BioCH_4 \text{ export}\times\text{unit price})\times\left(\frac{1+i}{1+d}\right)^{n} \end{aligned} \quad \text{Eq. 2.25}$$

Finally, the NPV is calculated using Eq. 2.26, applying the definition established in the Section 2.3.4.1:

$$NPV = LCR - LCC \quad \text{Eq. 2.26}$$

In this study, the electricity purchase price from the grid and the feed-in tariff for grid injection in Italy were set at 0.20 €/kWh and 0.06 €/kWh, respectively [63]. To calculate the income from $BioCH_4$ sales, the annual biogas consumed by the biogas boiler and biogas CHP is subtracted from the total yearly biogas produced in the biogas plant. The remaining biogas, considering a methane content of 54.2%, is then upgraded to $BioCH_4$ before being injected into the gas grid for sale. The revenue from $BioCH_4$ sales is 1.1 €/Nm^3 [34]. Additionally, an average inflation rate of 2% and a discount rate of 6% were applied, reflecting the economic conditions in Italy [64]. The lifespans assumed in this study were 20 years for the PV modules, heat pump, biogas boiler, AD plant, and biogas upgrading unit [18]; 10 years for solar batteries [63]; 7 years (60K operating hours) for the biogas CHP unit; and 15 years for the solar inverter [65]. Components with lifetimes matching the project duration exhibit zero salvage value, while decommissioning costs are omitted under the assumption that these counterbalancing factors offset at project end. The CAPEX and OPEX associated with on-grid and off-grid APV components, heating systems, the AD plant, upgrading unit, feedstock, and land lease are detailed in Table 2.10.

Table 2.10 The CAPEX and OPEX assumed in this study [17,18,31,48,49].

Components	**CAPEX (€)**	**OPEX (€)**
Overhead Bifacial 2-axis APV (6L layout)		0.025 × CAPEX
PV module	349/kW_p	
Inverters	77/kW_p	
Electric BOS	282/kW_p	
Supporting structure	340/kW_p	
Installation and work	373/kW_p	
Professionals and fees	61/kW_p	
Total	1482/kW_p	
Overhead Bifacial 1-axis APV (1P layout)		0.025 × CAPEX
PV module	305/kW_p	
Inverters	65/kW_p	
Electric BOS	100/kW_p	
Supporting structure	316/kW_p	
Installation and work	354/kW_p	
Professionals and fees	77/kW_p	
Total	1217/kW_p	
Bifacial Vertical APV (2L layout)		0.015 × CAPEX
PV module	291/kW_p	
Inverters	58/kW_p	
Electric BOS	153/kW_p	
Supporting structure	160/kW_p	
Installation and work	267/kW_p	
Professionals and fees	72/kW_p	
Total	1001/kW_p	
Lithium-ion phosphate battery	223/kWh	0.045 × CAPEX
Biogas CHP unit	2600/kW_{el}	6.5€/hour
Biogas boiler	270/kW_{th}	0.063 × CAPEX
Groundwater Heat pump	$(2485 \times P_{th}^{0.6034}) + C_{wells}$	0.01 × CAPEX + 3€/MWh_{th}
Geothermal wells investment cost (C_{wells})	50000	-
Land lease cost	-	3000€/ha/year
AD plant (125 Sm^3_{BioCH4}/h)	6,000,000	0.03 × CAPEX
Upgrading unit	1,300,000	0.02 × CAPEX
Feedstock	-	300,000€/year

2.4 Results and discussion

This section presents the techno-economic results in three parts. It reports performance within the primary on-grid scenarios, examines economic drivers and sensitivities, and benchmarks outcomes against alternative configurations.

2.4.1 Primary scenarios

This subsection synthesizes scenario-level outcomes, clarifying the joint influence of on-grid APV configuration and heating technology on system performance. The principal drivers of the leading configuration are identified, and recurrent trade-offs across scenarios are highlighted.

2.4.1.1 Scenario-Specific Performance Characteristics

The multi-objective optimization analysis was conducted for three on-grid energy integration scenarios to determine the optimal APV system configuration under varying energy demand profiles. Table 2.11 summarizes the techno-economic parameters of the evaluated scenarios, ranked by TOPSIS scores with equal weights assigned to all KPIs.

Table 2.11 Main results across on-grid APV scenarios, ranked by TOPSIS scores.

Scenario	APV System Type	APV Capacity (kW_p)	EP_{APV} (%)	Land Occupation (m^2)	LCR (M€)	LCC (M€)	NPV (M€)	TOPSIS score
S2	1-axis	173	22.46	2489	20.22	17.34	2.88	91.51
S2	2-axis	127	20.05	2665	20.22	17.40	2.82	89.76
S2	Vertical	208	19.92	4055	20.23	17.42	2.81	83.31
S1	1-axis	151	23.74	2181	17.83	16.75	1.08	56.39
S1	2-axis	104	19.93	2185	17.81	16.80	1.01	55.43
S1	Vertical	171	19.91	3343	17.82	16.82	1.00	52.43
S3	1-axis	112	7.94	1607	16.55	16.20	0.35	50.01
S3	2-axis	87	7.96	1815	16.53	16.19	0.34	49.56
S3	Vertical	113	7.95	2208	16.49	16.16	0.33	48.72

The results reveal substantial differences in economic and spatial performance among the tested configurations, offering critical insights for technology selection and investment prioritization. Scenario 2 (S2) demonstrates the most favorable economic performance, achieving the highest NPV range across all APV systems. The 1-axis APV system emerges as the most optimal configuration, delivering 173 kW_p of installed capacity with 22.46% effective APV penetration (EP_{APV}) while maintaining the highest TOPSIS score of 91.51. This superior performance is driven by its ability to achieve significant energy yield gains compared to vertical configurations, without incurring the high CAPEX penalties associated with 2-axis systems. In S2, the use of GWHP for digester heating

eliminates direct biogas consumption for thermal supply, allowing a greater proportion of biogas to be upgraded to biomethane and sold to the gas grid. The economic advantage of heat pump electrification in S2 arises from two main factors. The high COP of 5.74 minimizes the electricity required for thermal production, and the preserved biogas maximizes the sales of high-value biomethane. This strategy reduces the opportunity cost associated with combustion-based options such as biogas CHP or boilers, where a significant share of biogas is diverted from upgrading to heat generation. The economic advantage of this approach is reinforced by the Italian market price differential between biomethane sales and electricity purchases from the national grid, reported to range from approximately 3.5 times in [18] to 5.5 times in the present study. Consequently, preserving biogas for upgrading yields a disproportionately greater impact on LCR, which is the primary contributor to NPV in the present analysis. Comparable results were reported in [18], where PV-powered GWHP systems achieved shorter payback periods and higher net revenues than CHP or boiler configurations under similar boundary conditions, thereby confirming the economic advantage observed for S2 in this study. Scenario 1 (S1) ranks second in overall performance, with NPV values ranging from 1 to 1.08 M€. The biogas boiler integration strategy shows moderate economic performance compared to GWHP integration (S2), primarily due to the opportunity cost of biogas consumption. While the biogas boiler itself has lower capital costs (€61,560 vs €107,229 for GWHP) and lower yearly O&M costs (€3,879 vs €5,090), its consumption of 11.6% of total annual biogas production reduces the biomethane available for sale to the gas grid, resulting in 13% lower LCR from biomethane sales compared to S2. Similar to S2, the 1-axis tracking system again demonstrates superior performance among the APV typologies in this scenario, achieving a 151 kW_p capacity and 23.74% of EP_{APV}, although its TOPSIS score (56.39) remains markedly lower than that of S2 (91.51). Scenario 3 (S3) yields the lowest economic returns, with NPVs clustered between 0.33 and 0.35 M€. The biogas CHP integration, while theoretically offering high efficiency through cogeneration, demonstrates limited economic advantages due to its consumption of 18.8% of total annual biogas production, the highest among all scenarios. This substantial biogas consumption significantly reduces the biomethane available for profitable gas grid sales, resulting in the lowest overall economic performance despite the CHP's cogeneration benefits.

2.4.1.2 Technology-Specific Trade-offs

The comparative analysis across APV system types (Table 2.11) reveals consistent performance hierarchies within each scenario. 1-axis tracking systems consistently outperform both 2-axis and fixed vertical configurations in terms of TOPSIS scores, demonstrating an optimal balance between

energy yield, capital investment, and operational complexity. 2-axis tracking systems show intermediate performance, with higher energy yields partially offset by increased CAPEX and OPEX. The capacity reductions observed across scenarios (127 kW_p in S2, 104 kW_p in S1, 87 kW_p in S3) reflect the optimization algorithm's preference for cost-effectiveness over maximum energy capture under the given economic constraints. Fixed vertical APV systems exhibit the lowest economic performance among the configurations examined. The present results indicate that they do not confer a land occupation benefit; rather, they require greater land area while delivering lower energy yields compared to tracking systems.

2.4.1.3 Economic Analysis

The LCC analysis (Table 2.11) reveals distinct patterns across all on-grid APV scenarios. In S2, LCC values remain relatively stable across technologies, ranging only from 17.34 to 17.42 M€. This narrow spread indicates that total system costs in this scenario are only marginally affected by the APV configuration, meaning that economic performance is relatively insensitive to technology choice. By contrast, S3 shows the lowest LCC range (16.16-16.20 M€), which reflects reduced APV capacity requirements rather than inherent cost efficiency. The LCR patterns mirror the NPV trends, with S2 achieving the highest values (20.22-20.23 M€), followed by S1 (17.81-17.83 M€) and S3 (16.49-16.55 M€). This revenue hierarchy correlates directly with the EP_{APV} rates, highlighting the role of renewable energy integration in overall economic performance. Results indicating the economic advantage of 1-axis APV systems align with a broad body of literature conducted under diverse climatic conditions and methodological frameworks. For example, in the United States, a national techno-economic assessment reported 1-axis APV system outperforming static layouts [20]. In Belgium, a head-to-head field comparison of vertical, fixed-elevated, and 1-axis designs found the 1-axis APV setup delivered the lowest levelized cost of electricity (LCOE) [65]. In the Italian context, Agostini et al. [19] found that 1-axis APV systems outperformed both fixed-tilt and 2-axis designs in cost-effectiveness, as the additional energy yield from 2-axis did not compensate for its higher CAPEX and OPEX. Bellone et al. [48], in an Italy-wide simulation of various APV configurations across five sites including Piacenza, applied an MCDA integrating energy conversion per hectare and CAPEX. Their results ranked the 1-axis configuration highest in TOPSIS score, followed by 2- axis and vertical systems, thereby corroborating the superior economic and technical viability of 1-axis APV systems under comparable constraints. A cross-country Monte Carlo analysis encompassing Sweden, Denmark, Germany, and Italy confirmed that 1-axis APV systems are the most profitable configuration, achieving approximately 20-30 % lower LCOE and shorter payback periods compared

with vertical and elevated designs [66]. Multi-objective water-energy-food (WEF) nexus optimizations likewise consistently identify the 1-axis APV configuration as the most robust solution, balancing energy yield, crop performance, and irrigation water demand under diverse policy scenarios [67]. Additional Belgian field evidence further substantiates the technical and economic advantages of 1-axis APV systems, attributable to their higher energy conversion and more favorable LCOE [24].

2.4.1.4 Sensitivity Analysis

The sensitivity analysis examining the impact of NPV weight variations on TOPSIS scores reveals critical insights into the robustness of decision-making frameworks and the relative importance of economic versus technical criteria in APV systems optimization. The analysis systematically varies the NPV weight (ω) from 0 to 1 while maintaining proportional adjustments to APV land occupation weights, providing a comprehensive assessment of decision stability across different priority structures. Figure 2.7 presents the TOPSIS scores for primary scenarios (S1-S3), illustrating the trade-off between land occupation and NPV across all APV configurations including vertical (1), 1-axis tracking (2), and 2-axis tracking (3), under NPV weightings of 0.25, 0.5, and 0.75.

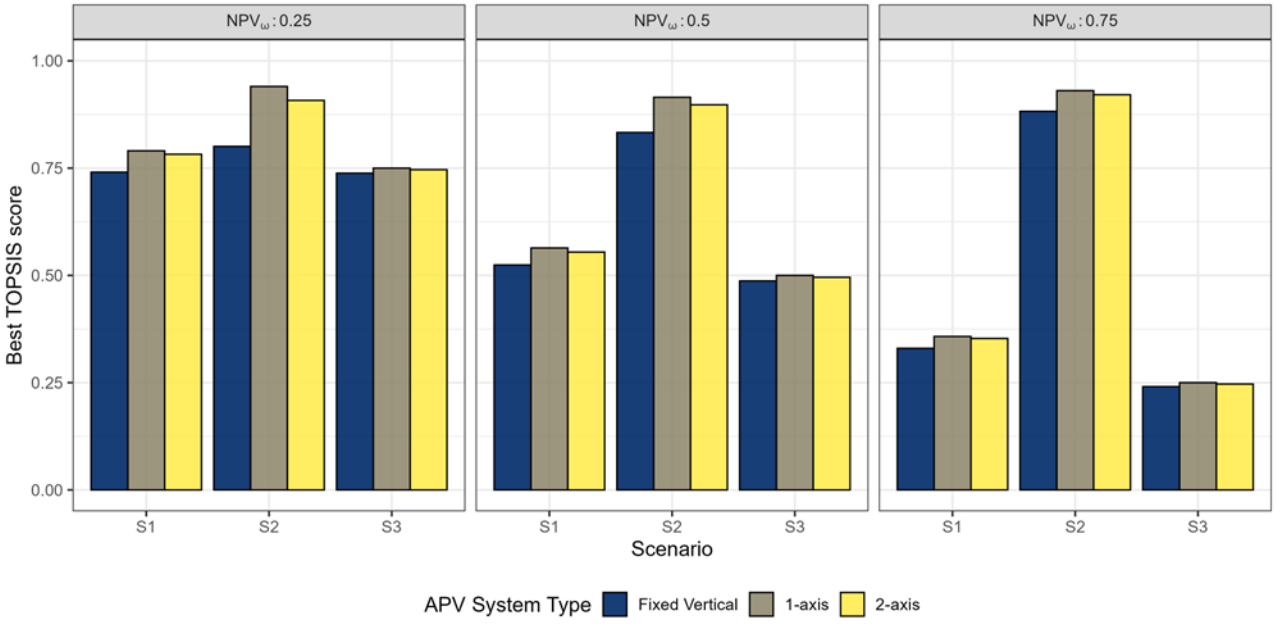

Figure 2.7 Sensitivity analysis of TOPSIS scores to NPV weight variations (0.25, 0.5, and 0.75) across primary scenarios.

Notably, S2 (GWHP configuration) consistently ranks highest in TOPSIS scores across all weightings, driven mainly by its superior NPV compared with S1 (biogas boiler configuration) and S3 (CHP configuration). This indicates that the higher NPV in S2 dominates the decision space and

cannot be offset by land occupation trade-offs in the other scenarios. This effect is particularly evident in S3, where TOPSIS scores remain consistently below 51 across all weightings, indicating that even its relatively compact land footprint cannot compensate for the economic penalties associated with high biogas consumption for CHP operation. Regarding the APV system types, 1-axis tracking systems tend to require less land while delivering the highest NPVs, explaining why the multi-objective optimization often converges on these configurations. In contrast, vertical APV systems generally require more land to achieve comparable NPVs, due to their lower specific energy yields. Importantly, the TOPSIS analysis reveals that increasing the weight on NPV (from $\omega = 0.25$ to $\omega = 0.75$) progressively enhances the relative performance advantage of S2. This indicates that economic prioritization tends to amplify the superiority of configurations that maximize biomethane sales revenue. Conversely, when more weight is placed on land occupation ($\omega = 0.25$), the performance differentials between scenarios narrows slightly, though S2 retains its dominant position, highlighting both the robustness of the GWHP-based strategy and the sensitivity of optimal rankings to decision-maker preferences regarding spatial versus economic objectives.

2.4.2 Alternative scenarios

Five alternative scenarios (S4-S8) were evaluated through analytical techno-economic evaluation to benchmark their performance against the optimized on-grid APV cases for further insights. These include a baseline CHP only system (S4), two grid-based options (S5 and S6), and two off-grid APV systems (S7 and S8). All configurations were designed to meet the complete electrical and thermal demands of the AD plant. Off-grid scenarios utilize a biogas boiler in S7 and a GWHP unit in S8. System sizing for two off-grid APV systems was determined using a mathematical modeling framework (as previously described in the Section 2.3.5) and operational performance was simulated in PVSOL. Key results for these two scenarios are presented in Table 2.12.

Table 2.12 Sizing and Performance Comparison of Off-grid APV Systems for S7 and S8.

Description	**APV system type in S7**			**APV system type in S8**		
	Vertical	**1-axis**	**2-axis**	**Vertical**	**1-axis**	**2-axis**
Total PV modules	4155	3908	2878	5537	5207	3835
Total Capacity (MW_p)	2.74	2.58	1.9	3.65	3.43	2.53
Off-grid Inverter Size (MW_p)	2.4	2.26	1.67	3.21	3	2.21
Total Batteries		851 for S7			1130 for S8	
Total energy stored in batteries (MWh)		11.03			14.64	
Unmet load (%)	<2	<1	<1	<3	<2	<2
	Pitch 8m	Pitch 6m	Pitch 15m	Pitch 8m	Pitch 6m	Pitch 15m
Land occupation (ha)	5.35	3.72	3.98	7.13	4.95	5.3
Annual surplus electricity (MWh)	2265	2709	2058	3135	3681	2724

Results indicate that the 2-axis APV system, due to advanced tracking technology, requires up to 26.35% fewer PV modules, total capacity, and inverter size compared to the 1-axis system in both scenarios. Conversely, the vertical APV system, due to its fixed orientation without tracking, necessitates the highest number of PV modules to sufficiently charge the batteries. Despite using more PV modules, the vertical system generates less surplus electricity than the 1-axis system, though still more than the 2-axis system. This variation arises from differences in system capacities and technological efficiencies. Across all evaluated metrics, S8 consistently presents higher values compared to S7, primarily due to the significantly greater electrical demand of the GWHP relative to the biogas boiler. Consequently, S8 demands substantially more PV modules, increased battery capacity (1130 compared to 851 batteries), and greater total battery storage capacity (14.64 MWh versus 11.03 MWh). These substantial quantities of PV modules and batteries stem from the fact that, in the sizing procedure for the off-grid APV systems, a 0% annual capacity shortage constraint was imposed to guarantee uninterrupted fulfillment of the total electrical demand. The resulting unmet load remains very low across all configurations (below 3% in all cases) demonstrating that the adopted sizing approach effectively meets the target reliability criteria. The 1-axis and 2-axis systems achieve the lowest shortfalls, reflecting their higher conversion efficiency and better alignment of generation with demand profiles. The slightly higher unmet load of the vertical systems, despite their greater installed capacity, is attributable to reduced production during low-sun periods when battery discharge is insufficient to fully meet instantaneous loads. In terms of land occupation, the vertical APV system requires the largest area, attributable to its higher PV module count and installation requirements. The 1-axis system remains the most space-efficient due to its smaller pitch. The 2-axis system, despite employing larger pitch spacing, occupies less land area than the vertical configuration due to fewer required PV modules, enabled by its advanced tracking capability. This makes the 2-axis system ideal for minimizing land use at greater pitches, whereas the 1-axis system is preferable for tighter spatial configurations. Nevertheless, considerations such as installation and maintenance costs should also influence final system selection.

In the grid-based alternatives, the Italian national power grid fully supplies the annual electrical demand. As indicated in Figure 2.3, the AD plant integrated with a GWHP (S5) has a total annual electricity demand of 1246 MWh_{el}, whereas using a biogas boiler (S6) reduces this demand to 1029 MWh_{el}. Regardless of the heating technology implemented, the plant's total annual heat demand remains constant at 1340 MWh_{th}.

In the baseline scenario (S4), CHP operation without complementary generation sources imposes constraints on energy output control. Implementing a system controller in this particular scenario is

not feasible because the CHP unit operates independently. Adjusting the CHP's power input to align its thermal output with monthly heat demands would consequently alter its electrical output. Since there is no additional electrical generator in this scenario, employing a controller is impractical. As a result, the selected biogas CHP unit generates electrical and thermal outputs exceeding the actual plant demands, resulting in an excess of 44 MWh_{el} electricity and 554 MWh_{th} heat annually. In this study, excess electricity is assumed to be exported to the power grid to generate revenue, while excess heat, due to the absence of control system, is considered wasted. In line with current policy frameworks, which prioritize upgrading biogas to $BioCH_4$ for grid injection or transport applications over heat production [68], stakeholders are incentivised to minimize on-site biogas use. This can involve replacing CHP units or biogas boilers with heat pumps, or combining them with APV systems. Finally, Table 2.13 presents the economic evaluation of all alternative scenarios over the project's lifetime, ranked by NPV as a benchmark for economic performance.

Table 2.13 Summary of the economic evaluation results for the alternative scenarios.

Scenario	Configuration	APV System Type	LCR (M€)	LCC (M€)	NPV (M€)
S5	Power grid + GWHP	None	20.22	17.81	2.41
S6	Power grid + biogas boiler	None	17.88	17.16	0.72
S4 (baseline)	Biogas CHP	None	16.48	15.78	0.70
S7	Off-grid APV + biogas boiler	Vertical	19.20	25.47	-6.27
	Off-grid APV + biogas boiler	2-axis	19.19	25.87	-6.68
	Off-grid APV + biogas boiler	1-axis	19.21	26.30	-7.09
S8	Off-grid APV + GWHP	Vertical	21.97	29.19	-7.22
	Off-grid APV + GWHP	2-axis	21.96	29.73	-7.77
	Off-grid APV + GWHP	1-axis	21.98	30.31	-8.33

The economic evaluation of the alternative scenarios reveals substantial performance disparities, clearly distinguishing the viability of grid-connected versus off-grid configurations. The results, summarized in Table 2.13, indicate that all off-grid APV systems (S7 and S8) are economically unfeasible under the current financial assumptions, yielding significantly negative NPV ranging from -6.27 M€ to -8.33 M€. This outcome is driven by a combination of the extremely high LCC associated with these systems (ranging from 25.47 M€ to 30.31 M€) and the inability to generate revenue from surplus electricity. The high LCC reflects the extensive capital investment required for large-scale APV arrays and battery storage systems sized to guarantee complete energy autonomy. Furthermore, a substantial amount of electricity conversion by off-grid APV systems is wasted as it cannot be sold to the grid, representing a significant loss of potential revenue. In terms of land-use intensity, off-grid systems occupy substantially more land than their optimized on-grid counterparts across all APV

typologies, typically ranging from 17 to 20 times higher. The greatest land occupation occurs in the vertical configuration, where the off-grid system (S8) requires 7.13 ha compared with 0.41 ha in its optimized on-grid counterpart, confirming the superior land-use efficiency of optimized on-grid APV systems. Comparing the two off-grid approaches, the scenarios utilizing a GWHP (S8) result in lower NPV than those with a biogas boiler (S7). This is because the higher electrical demand of the GWHP necessitates an even larger and more costly APV and battery installation, further inflating the LCC and exacerbating the economic deficit. S8 also exhibits lower spatial efficiency than S7 due to its larger installed capacity and consequently greater land requirement. In sharp contrast, the grid-based scenarios demonstrate positive economic returns. S5 (Power grid + GWHP) emerges as the most profitable alternative, achieving a robust NPV of 2.41 M€. Its strong performance is attributed to a high LCR of 20.22 M€, generated by upgrading and selling the entire volume of biogas as biomethane. This configuration avoids the prohibitive costs of energy storage while maximizing the primary revenue stream. S6 (Power grid + biogas boiler) is the second most profitable among the grid-based options, with an NPV of 0.72 M€, as it diverts 11.6% of the total biogas production for thermal energy, thereby lowering its LCR compared to S5. Finally, the baseline scenario, S4 (Biogas CHP unit), ranks as the third-most viable alternative with an NPV of 0.70 M€. Despite having the lowest LCC (15.78 M€), its profitability is constrained because the on-site consumption of 18.8% of the total biogas reduces potential biomethane sales revenues.

Crucially, a comparative analysis establishes that the optimal primary scenario identified through multi-objective optimization (S2: 1-axis APV system paired with GWHP) remains the most financially advantageous solution overall. With an NPV of 2.88 M€ (from Table 2.11), the S2 configuration outperforms the best alternative scenario (S5) by approximately 20%. Both S2 and S5 leverage the GWHP to maximize biomethane revenue, resulting in identical LCR. However, the superiority of S2 stems from its lower LCC (17.34 M€ vs. 17.81 M€ for S5). This cost advantage is achieved because the integrated APV system in S2 reduces the reliance on purchasing electricity from the grid over the project's lifetime. However, when viewed through the lens of energy sustainability and resilience, other primary scenarios (S1 and S3) present notable advantages over S5, despite their lower NPV. S5 relies entirely on the national grid for its electricity supply, whereas S1 and S3 incorporate significant shares of on-site renewable generation, with effective APV penetrations of over 20%. The case for S3 is particularly compelling from a sustainability standpoint; although it has a lower APV penetration (7.9%), approximately 84.1% of its total electrical demand is met by the biogas CHP unit. Consequently, only about 8% of its electricity is drawn from the grid, compared to 100% in S5. This highlights a critical trade-off between pure economic optimization and the

promotion of decentralized, renewable energy systems. This analysis confirms that the synergistic integration of an on-site APV system, as achieved in the optimized scenarios, yields a more profitable outcome than any of the evaluated fixed-alternative configurations, while also offering pathways to enhanced energy sustainability.

2.4.3 Study limitations and future directions

As a first attempt to integrate APV systems with biomethanation in a unified techno-economic optimization framework, this study presents several limitations that offer opportunities for future research development. The scope is deliberately constrained to techno-economic optimization of integrated APV-biomethanation systems, focusing exclusively on electrical energy output without agricultural yield modeling. While agrivoltaic terminology is employed due to the agricultural land context, the primary contribution lies in energy system optimization rather than agronomic analysis. Future research should integrate detailed crop yield models to quantify food-energy trade-offs within the water-energy-food nexus framework.

Energy yields are simulated using fixed derating factors, module temperature coefficients, and representative meteorological inputs. Single-year weather files and constant albedo parameters may under-represent interannual variability, seasonal surface changes, and degradation effects, which can influence hourly matching and annual energy conversion. Multi-year ensembles, dynamic albedo modeling for bifacial PV modules, and explicit degradation trajectories would narrow these uncertainties and propagate more faithfully to economic indicators.

Economic conclusions depend on price and policy parameters. CAPEX and OPEX, grid tariffs/feed-in conditions, biomethane market prices, land lease cost, and discount/inflation rates are treated as fixed parameters within each scenario. Because these drivers are volatile and policy-contingent, a stochastic cash-flow analysis (e.g., Monte Carlo on prices/incentives) would better characterise risk to LCOE, NPV, and payback and identify thresholds at which the preferred configuration changes.

Sizing and operational assumptions also affect performance. Off-grid designs are dimensioned to achieve zero annual capacity shortage, which ensures reliability but is conservative and capital-intensive. Allowing a small loss-of-load (LOL) probability, co-optimising battery/inverter ratings with demand response, or integrating thermal storage could materially reduce required PV and storage. Likewise, fixed pitch and simplified supervisory control may not capture the attainable benefits of advanced tracking and dispatch; variable-pitch optimization and enhanced control policies could further improve both economics and land use. Additionally, the analysis assumes mesophilic digestion at 37°C, though thermophilic operation (50-60°C) would increase thermal demand, potentially favouring biogas combustion over heat pump electrification due to reduced heat pump

efficiency at higher temperature lifts. Equipment selection was based on capacity matching and market availability rather than comprehensive market surveys, which may not fully represent efficiency ranges or cost structures across broader market conditions. Future studies could incorporate multiple manufacturer options or equipment sensitivity analysis to assess robustness across diverse market scenarios. The present analysis emphasizes cost, performance, and land occupation. A parallel LCA has recently quantified the environmental burdens of these configurations, highlighting that material-intensive systems like 2-axis APV systems incur higher carbon footprints despite their energy gains; while 1-axis APV configurations offer superior environmental performance, achieving the lowest GHG emissions due to optimized material efficiency [69]. Future research should strictly link these techno-economic models to LCA and crop models to enable comprehensive MCDA that balances financial returns with environmental sustainability and resource efficiency.

2.5 Conclusion

This study presents the first optimization framework integrating bifacial APV systems with an AD plant for biomethane production, employing MOGA coupled with the TOPSIS methodology to identify optimal energy configurations. Key findings demonstrate that the optimized on-grid APV configuration combining 1-axis tracking paired with GWHP (S2) achieves superior economic performance with an NPV of 2.88 M€, outperforming the conventional CHP baseline by 4.1 times. The economic advantage arises from strategic thermal-demand electrification, avoiding biogas combustion to maximize high-value biomethane sales, achieving up to 8.7 times higher NPV compared with combustion-based strategies within the primary scenarios. The 1-axis tracking systems consistently provided the most balanced trade-off between energy yield and cost-effectiveness across all configurations. Comparative analysis shows that off-grid APV systems incur substantially higher LCC (25.5-30.31 M€) than LCR (19.2-22 M€), leading to negative NPVs, while optimized on-grid systems maintain balanced revenues and costs, resulting in positive economic outcomes and 17 to 20 times lower land occupation across all APV typologies. These results underscore the critical role of grid connection in ensuring sustainable profitability and spatial efficiency. Electrifying anaerobic-digestion thermal loads via APV-powered heat pumps emerges as a robust decarbonization strategy that enhances biomethane-plant profitability. The consistent superiority of 1-axis tracking systems indicates technological maturity suitable for standardization and large-scale deployment, emphasizing the importance of site-specific, integrated optimization to maximize hybrid renewable-energy potential while maintaining efficient dual land use.

Chapter 3

Life cycle assessment of various agrivoltaics systems across Europe

This chapter is based on:

Nik Zad, A.[1,*], Agostini, A.[2], Impollonia, G.[1], Zainali, S.[3], Croci, M.[1], Colauzzi, M.[1], Campana, P.E.[3] and Amaducci, S.[1] (2025). Life cycle assessment of various agrivoltaic systems across Europe. Sustainable Production and Consumption, 60, pp.260-280.

https://doi.org/10.1016/j.spc.2025.10.003

[1]*Department of Sustainable Crop Production, Università Cattolica del Sacro Cuore, Piacenza, Italy*

[2]*ENEA-Italian National Agency for New Technologies, Energy and the Environment, Rome, Italy*

[3]*Department of Sustainable Energy Systems, Mälardalen University, Västerås, Sweden*

*Corresponding author

3.1 Abstract

The deployment of conventional ground-mounted photovoltaic (CGMPV) systems on farmland creates intense land-use competition with agriculture. Agrivoltaic (APVs) systems present a promising solution, yet the environmental viability of different designs remains insufficiently understood, hindering their strategic deployment. This study addresses this gap by presenting the first life cycle assessment (LCA) benchmarking four bifacial APV systems, including fixed vertical, interspace, overhead single-axis, and overhead dual-axis systems with varying pitch spacings. These systems are compared against a bifacial CGMPV system (baseline scenario) and national electricity grid mixes, country-specific combinations of fossil, nuclear, and renewable sources, across north to south of Europe. A combined LCA method is applied, with attributional LCA evaluating PV components from cradle-to-end-of-use across ten impact categories, and a consequential approach addressing agricultural land-use change contributions to climate change category. Results demonstrate that APV systems significantly outperform national electricity grids across nine impact categories, achieving 8-111 times lower environmental impacts. The interspace single-axis system emerged as the most optimal configuration with the lowest greenhouse gases (GHG) emissions (11-20 g CO_{2eq}/kWh), 57% lower particulate matter, 48% lower acidification, and 27% lower eutrophication versus other APVs. The overhead dual-axis system showed the highest impacts (16-29 g CO_{2eq}/kWh), driven primarily by steel consumption in mounting structures. Monte Carlo Analysis confirmed that performance rankings are statistically robust. All APV systems showed 3.5-9.6 times higher mineral resource consumption than electricity grid mixes, highlighting a critical trade-off for sustainable resource management. These findings demonstrate that while APV systems can synergize food-energy systems with superior performance in most environmental categories, mineral resource intensity remains challenging, with material-efficient configurations essential for minimizing trade-offs.

Keywords: Agrivoltaic, Photovoltaic, Life Cycle Assessment, Environmental Impacts, Monte Carlo Analysis, Climate Change

3.2 Introduction

Agrivoltaic systems (APVs) enable simultaneous food and electricity production on the same land, offering improved land-use efficiency and renewable energy conversion while contributing to climate change mitigation. Unlike conventional single-use agricultural systems, which dedicate land exclusively to crop production without renewable energy integration, APVs represent a paradigm shift toward multifunctional land management [56, 57]. However, this dual-use promise involves environmental trade-offs, including increased material consumption for mounting structures (particularly steel and aluminium), potential soil quality impacts from heterogeneous shading patterns, and altered water distribution affecting crop growth [58, 59]. Life cycle assessment (LCA) provides essential quantification of these environmental impacts, guiding sustainable APV development. Despite growing research interest, current literature predominantly examines conventional fixed APV configurations with mono-facial photovoltaic (PV) modules, reflecting their commercial maturity and widespread deployment [50, 60, 61]. Advanced mounting structures and bifacial module technologies remain comparatively understudied, as illustrated in Figure. 3.1, which shows the temporal distribution of LCA studies categorized by APV typologies and PV module types (Scopus database, 2014-2025, search terms: "LCA" AND ("agrivoltaics" OR "agro-photovoltaic" OR "agri-photovoltaic")).

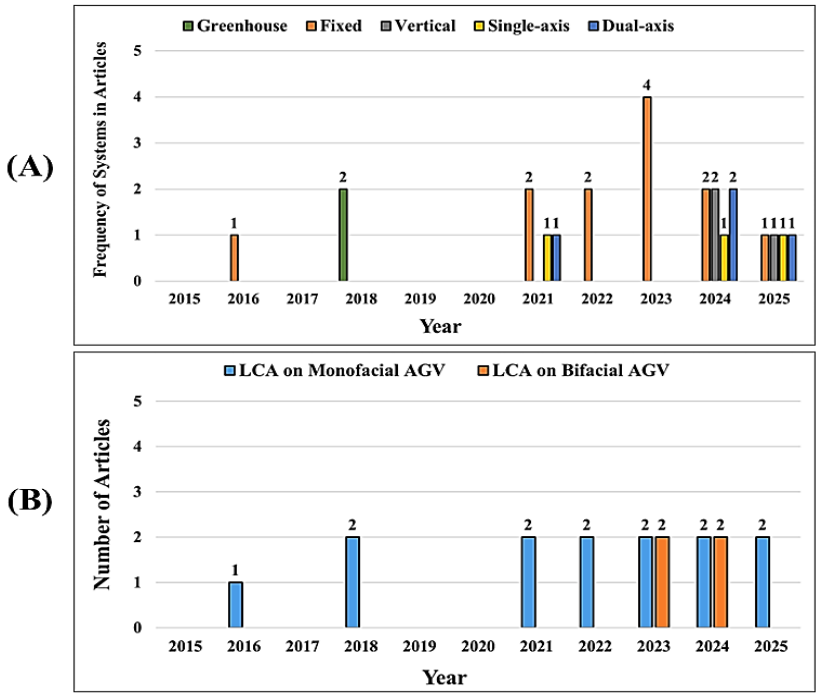

Figure 3.1 Temporal trends in LCA studies on APV systems. (A) Frequency of LCA articles categorized by APV system typologies. (B) Distribution of LCA studies based on PV module types in APVs.

3.2.1 Methodological approaches in APV life cycle assessment

LCA methodologies for APV systems demonstrate considerable heterogeneity in functional unit (FU) selection, system boundaries, and impact assessment methods. FUs range from energy-based metrics (kWh_{el}), agricultural outputs (kg), land area (hectares), to economic indicators (revenue per hectare), each influencing result interpretation and comparability. System boundary definitions vary from cradle-to-gate assessments focusing on production phases to comprehensive cradle-to-grave analyses incorporating end-of-life (EOL) scenarios, though the latter remain uncommon, with most studies adopting cradle-to-end-of-use boundaries due to data limitations [8]. The allocation methodology for co-products significantly affects results. Leon and Ishihara [76] introduced a novel "solar allocation" method for greenhouse APV systems, demonstrating that system expansion yielded 0.83-0.95 kg CO_{2eq}/kg tomatoes, while economic allocation produced 0.98-1.10 kg CO_{2eq}/kg, representing approximately 15% variation based solely on methodological choice. This methodological sensitivity underscores the importance of transparent reporting and sensitivity analysis in APV LCA studies.

3.2.2 Climate change mitigation performance

Regional-scale APVs deployment demonstrates substantial greenhouse gas (GHG) reduction potential. Implementation across 1-5% of agricultural land in Baden-Württemberg, Germany, achieves annual reductions of 1.2-5.9 Mt CO_{2eq}, with the upper range surpassing the region's entire agricultural sector emissions of ~4.4 Mt CO_{2eq} [21]. System-specific performance varies considerably, with vertical bifacial configurations achieving 31-63% lower climate change impacts compared to conventional agriculture combined with Austrian grid electricity (dominated by hydro and wind), while overhead fixed systems show a 36-70% reduction in freshwater eutrophication and a 50-75% reduction in fossil resource scarcity [22]. Greenhouse-integrated APV systems exhibit particularly strong mitigation potential. Integration with mushroom cultivation (*Panus giganteus*) reduces climate change impacts by 60% (achieving 0.074-0.088 kg CO_{2eq}/kg product) compared to conventional production, while simultaneously decreasing freshwater eutrophication by 47% and fossil depletion by 46% [77]. Similarly, tomato greenhouse systems with organic PV achieved 12% emission reduction through optimized solar allocation methodology [78].

3.2.3 Material efficiency and system design optimization

Environmental performance correlates strongly with mounting structure design and material selection. Vertical bifacial APV systems consistently outperform overhead fixed configurations in a

research study conducted in Austria, achieving lower environmental impacts across nine categories due to reduced steel and aluminium requirements, using glass-glass modules further enhances this advantage [22]. Comparative assessments of APV configurations in the United States revealed that APVs outperformed PV-only systems, achieving 15-55% lower impacts per revenue dollar, with dual-axis tracking demonstrating optimal performance despite higher upfront costs [20]. Balance-of-system (BOS) components represent critical environmental hotspots. Steel mounting structures, zinc coatings, inverters, and copper cabling collectively contribute approximately to 80% of non-module impacts across most APV configurations [44, 61]. In Italy, tracking APVs achieved similar climate performance (~19-20 g CO_{2eq}/MJ) to ground-mounted PV (~22 g), substantially outperforming biogas (113-209 g) and grid electricity (~167 g), though the study notably excluded crop-side impacts and EOL considerations [19].

3.2.4 Agricultural integration synergies

Integration strategies with different agricultural systems yield diverse sustainability outcomes. Livestock-integrated APVs demonstrate exceptional performance, with rabbit grazing systems achieving a 69.3% reduction in GHG emissions and an 82.9% decrease in fossil energy demand compared to spatially separated operations, primarily due to the elimination of feed production and transport [79]. Sheep grazing configurations reduce emissions by 3.9% compared to separated systems and achieve 280-894% reduction versus grid electricity, with land-use efficiency doubling relative to separate operations [80]. Novel applications including data center integration with pasture-based APV in ecologically fragile regions demonstrate potential for over 3 Mt/year GHG reduction while restoring >1140 ha degraded land [81]. Crop-based systems exhibit variable performance correlating with shade tolerance. Consequential LCA of organic four-crop rotation in Germany showed environmental improvements in 15 of 16 categories, with particularly significant reductions in climate change (572.9 t CO_{2eq}/ha), freshwater eutrophication (524 kg P_{eq}/ha), and fossil resource use (6745 GJ/ha), though mineral resource use increased (+3.1 kg Sb_{eq}/ha) due to PV infrastructure [74]. Dynamic grape-voltaic models in India achieved up to 100% elimination of groundwater by fully substituting irrigation needs with harvested rainwater, leading to substantial water savings (12-100% reduction depending on the state), land savings of 1.984 ha/MW_p, and low carbon footprints (0.074-0.088 kg CO_{2eq}/kg grapes) through blockchain-enabled resource sharing [82]. APV structures can generate fine-scale heterogeneity in near-surface conditions, which is important because crop response and water dynamics may vary within the same installation depending on geometry and local

meteorology. Synthesis of current knowledge Table 3.1 synthesizes key LCA studies, revealing methodological diversity and highlighting critical knowledge gaps requiring investigation.

Table 3.1 Comparative analysis of LCA studies on APV systems.

Authors	Year	Country	APV type	Study focus	Functional Unit	System boundary	Main findings	Limitations
Agostini et al. [19]	2021	Italy	Elevated fixed, single-axis, and dual-axis	LCA of APV vs. roof/ground mounted PV, wind, biogas, fossil, Italian grid mix	1 MJ of electricity delivered to the grid	Cradle-to-gate (PV). Indirect Land Use Change (ILUC) factors included for biogas and ground-mounted PV.	APV tracking systems achieved ~19-20 g CO_{2eq}/MJ, comparable to ground PV (~22 g) and much lower than Italian grid (~167 g) or biogas (113-209 g). Similar performance to PV in acidification and eutrophication; much better than bioenergy and fossil fuels.	(1) EOL excluded (assumed negligible or covered by EU WEEE). (2) Crops under APV excluded from system boundary (only energy side modelled). (3) Inventory dependent on manufacturer. (4) Results site-specific to Italy.
Wagner et al. [74]	2023	Germany	Overhead fixed	Consequential LCA assessing environmental impacts of shifting from 1 ha of single-use agriculture to APV system (four-crop organic rotation)	Fresh matter (Celery bulb, potato tuber), dry matter (Wheat grain, clover grass), MWh (electricity)	Consequential LCA (crops), Cradle-to-end-of-use (PV)	Installation of APV reduced environmental impacts in 15 of 16 categories, notably climate change (572.9 t CO_{2eq}/ha), freshwater eutrophication (524 kg $P_{eq.}$/ha), and fossil resource use (6745 GJ/ha), mainly due to substitution of coal- and gas-based electricity. Only resource use, minerals & metals increased (+3.1 kg $Sb_{eq.}$/ha) due to PV and BOS material demand.	(1) Results highly dependent on assumptions about marginal electricity mix, which will evolve (renewables expected to reach 80-100% by 2030-2035). (2) Lack of tracking APV systems. (3) Excludes biodiversity and ecosystem service impacts. (4) Results site-specific to a APV pilot in Germany. (5) EOL of PV not included.

Table 3.1 (*continued*)

Authors	Year	Country	APV type	Study focus	Functional Unit	System boundary	Main findings	Limitations
Busch and Wydra [75]	2023	Germany	Overhead fixed	Attributional LCA comparing APV potato-electricity co-production with separate PV + potato production and with potato + German grid electricity	14,402,942 kWh electricity (30 years) + 9,236 dt potatoes (30 years)	Cradle-to-gate (crop and PV)	APV scenario reduced GHG emissions by 72% compared to potato + German grid electricity. Ground-mounted PV + potato had the lowest impacts in 12 of 17 categories due to reduced steel consumption. In land use, APV performed best (33% lower than grid scenario). PV modules and steel mounting identified as hotspots.	(1) Only fixed APV system. (2) Only conventional potato cultivation considered (organic not modelled). (3) Inventory partly based on assumptions and pilot system data. (4) Crop rotation and variability in yields not included. (5) EOL of PV not included.
Kiehbadroudinezhad et al. [8]	2025	Global (review)	Multiple APV case studies synthesized	Critical review of LCA methodologies and results for renewable energy systems in agriculture, including agrivoltaics	Varied across reviewed studies: mass-based (kg crop), area-based (m2, ha), energy-based (kWh, MJ), economic (USD/ha)	Varied: cradle-to-gate, cradle-to-grave, gate-to-gate; both attributional and consequential frameworks	Review highlights that APV reduce GHG emissions vs. conventional farming + grid electricity (e.g., −69% for rabbits, −12% for tomatoes, up to −5.5 Mt CO2eq for Baden-Württemberg land scenarios).	(1) Many studies remain limited to GWP and fossil energy demand, neglecting toxicity, eutrophication, water use, and biodiversity. (2) EOL of PV/BOS frequently excluded. (3) Inventories often incomplete, especially for mounting structures. (4) Functional unit choices inconsistent, leading to non-comparable results. (5) Few studies integrate social LCA.
Leon and Ishihara [76]	2018	Japan	Tomato greenhouse with organic photovoltaics (OPV) integrated on roof and walls	Evaluation of allocation methods for Life Cyle CO2 emissions	1 kg tomatoes (crop FU); 1 ha land area (land FU	Cradle-to-gate (crop), Module production to use phase (PV)	Life Cycle CO2 emissions for tomatoes were lowest under system expansion (0.83-0.95 kg CO2/kg), followed by solar allocation (0.86-0.96), and highest under economic allocation (0.98-1.10). Total emissions reduced by 12% in PV-powered greenhouse compared to conventional greenhouse.	(1) Results sensitive to OPV embodied emissions and short lifetimes. (2) Case-specific to Kyoto experimental greenhouse, limiting generalization. (3) EOL of PV not included.

Table 3.1 (*continued*)

Authors	Year	Country	APV type	Study focus	Functional Unit	System boundary	Main findings	Limitations
Sponagel et al. [21]	2024	Germany	Vertical, interspace single-axis	Assessment of the climate impacts of large-scale APV deployment in Germany using an integrated land-use and life-cycle modeling framework	Regional GHG mitigation potential under AVS deployment scenarios (no single FU defined)	Scenario-based consequential LCA elements (land-use model combined with LCA)	Deployment of AVS on 1-5% of agricultural land could reduce GHG emissions by 1.2-5.9 Mt CO2eq, mainly through substitution of fossil-based grid electricity	(1) Limited to climate change; other environmental categories (e.g., eutrophication) not addressed. (2) Lack of material inventories of APV configurations. (3) EOL of PV not included.
Krexner et al. [22]	2024	Austria	Vertical, overhead stilted (suspended structure)	Compares the environmental impacts of stilted and vertical bifacial APV plants against mono-use scenarios (agriculture or PV only) in Austria	Mixed FU via system expansion: provision of 1 kWh electricity combined with a basket of agricultural crops (sugar beet, wheat, soybean)	Cradle-to-farm gate	Vertical APV had consistently lower environmental impacts than S-APV across nine impact categories, due to lower steel and aluminium demand. Both AVS reduced impacts (31-63% in climate change; 36-70% in freshwater eutrophication; 50-75% in fossil resource scarcity) compared to agriculture + Austrian average electricity. PV modules and steel substructures identified as main hotspots.	(1) Focus limited to nine midpoint impact categories; (2) EOL and recycling of PV modules and structures not included; (3) Inventory data for mounting structures partly based on assumptions and secondary sources.
Cheng et al. [77]	2024	China	Greenhouse mushroom farming with rooftop PV integration	Assessing the environmental effects of mushroom farming with and without a fixed APV system.	1 kg fresh weight of P. giganteus	Cradle-to-gate	PV integration reduced most environmental impacts by 4-60%, including 60% lower climate change (CO2eq.), 47% lower freshwater eutrophication, and 46% lower fossil depletion.	(1) Respiration-related CO2 emissions from mushrooms not fully integrated into CC management. (2) Other APV system types were not investigated. (3) High sensitivity to substrate composition; data site-specific to Hainan. (4) EOL of PV not included.

Table 3.1 (*continued*)

Authors	Year	Country	APV type	Study focus	Functional Unit	System boundary	Main findings	Limitations
Ravilla et al.[20]	2024	United States	Static full-density (FD), static half-density (HD), single-axis tracking, and dual-axis tracking	Techno-economic and environmental LCA of APV compared to PV-only and crop-only systems	Life-cycle revenue per hectare of land ($/ha) (monetary-based FU encompassing electricity, crops, and water use)	Cradle-to-farm-gate (crop), Cradle-to-end-of-use (PV)	All APV designs outperformed PV-only in both cost/revenue ratio and environmental impacts. APS had ~15-55% lower impacts per $ revenue than PV-only. Dual-axis tracking achieved the best performance; FD showed higher costs and impacts. Electricity generation dominated ~80% of impacts; BOS (steel, zinc, inverters, copper) identified as hotspots.	(1) Analysis limited to one crop (romaine lettuce). (2) Results sensitive to discount and inflation rates, electricity price, and crop price assumptions. (3) Geographic scope limited to South Dakota. (4) EOL of PV not included.
Handler and Pearce [80]	2022	United States	Conventional ground-mounted PV with integrated sheep grazing (dual-use)	Attributional LCA of sheep-based APV compared to separate sheep grazing and electricity supply (PV-only or grid mix)	216,429-317,727 MWh electricity + 376,800 kg sheep meat	Cradle-to-gate (PV + sheep inputs)	Sheep-based APV systems reduced GHG emissions by 3.9% compared to conventional PV + sheep and by 280-894% compared to grid + sheep, depending on grid mix. Land use efficiency doubled relative to separate PV and sheep systems.	(1) Only GWP and ecotoxicity assessed. (2) Sheep productivity assumed constant; pasture-shading effects not fully modelled. (3) Results sensitive to regional electricity mix. (4) EOL excluded.
Zhang et al. [81]	2023	China	Fixed APV (pasture-based)	Development of a symbiosis model to enhance energy efficiency, reduce GHG emissions, and promote ecological restoration in fragile regions	N/A	Cradle-to-gate (PV), IPCC Tier 1 carbon stock factors (ecological restoration)	APV system saved 10,965 tCO_{2eq}/year vs coal. Nationally, APV system could cut 0.8-3.25 Mt CO_{2eq} annually and restore >1140 ha degraded land.	(1) Not a full ISO LCA; multimethod framework lacks integration across categories. (2) EOL of PV excluded. (3) Annual-average modelling ignores hourly variability of DC loads and PV generation. (4) Limited soil and biomass data reduce accuracy of carbon stock estimates.

Table 3.1 (*continued*)

Authors	Year	Country	APV type	Study focus	Functional Unit	System boundary	Main findings	Limitations
Kumar and Chopra [82]	2023	India	Overhead fixed	Integrated techno-economic assessment and LCA of grape-voltaic farms under a shared circular business model (grape farmer + PV operator)	1 MW PV installation (electricity) and 1 kg grapes (crop)	Gate-to-gate (crop), Cradle-to-gate (PV)	12-100% reduction in groundwater dependency due to rainwater harvesting. Land-use mitigation ~1.984 ha/MW. National average GWP: 0.074-0.088 kg CO_{2eq}/kg grapes.	(1) Model assumptions for blockchain and rainwater harvesting not yet validated at commercial scale. (2) Revenues and GWP results highly sensitive to grape prices, PPA tariffs, and local yields. (3) Location-specific, with variation across 12 states. (4) EOL of PV not included.
Ravi et al. [83]	2016	India	Conceptual colocation of PV farms with Aloe vera cultivation (dual land use in arid zones)	Exploratory LCA and techno-economic analysis of solar-aloe systems vs stand-alone PV or aloe	No single ISO FU; results expressed per m^3 water used, per hectare land, and per kg aloe gel	Cradle-to-grave (mono-facial PV), Cradle-to-gate (Aloe vera gel)	Colocation achieved higher returns per m^3 water than PV or aloe alone. Weekly PV cleaning water (~20 m^3/ha) sufficient to sustain aloe under panels.	(1) Hypothetical analysis, not field-tested. (2) Aloe vera only crop modelled. (3) Broader impact categories (toxicity, eutrophication) excluded.
Junedi et al. [84]	2022	Malaysia	Fixed APV	Systematic review of 76 studies (2010-2021) on environmental (GHG, EPBT) and economic (LCOE) performance of PV systems	1 kWh electricity + land-equivalent ratio (LER) for APV	Cradle-to-grave (mono-facial PV)	APV systems showed GHG emissions ~0.02 kg CO_2/kWh, close to GMPV (~0.01-0.05) and lower than building integrated PV system. EPBT ranged 0.5-6.3 years, with APV slightly longer than GMPV but shorter than BAPV.	(1) Secondary data only (review, no primary LCA). (2) Results vary strongly with PV technology (Si, CdTe, CIS, perovskite). (3) Limited crop-level inventories.
Jouannais et al. [85]	2025	France	Generic fixed APV (parametric: wheat, soybean, alfalfa; multiple mounting structures; panel orientations)	Parametrized consequential LCA + scenario discovery to identify when APV is environmentally beneficial vs. conventional PV + crops	Two consequential FUs: 1 kWh electricity (when electricity is main product) or 1 kg crop (when crops are main product)	Consequential cradle-to-gate/use with ILUC	This LCA study of APV systems modelled 400,000 theoretical configurations and found that climate impacts vary wildly depending on design parameters, with some configurations achieving 33% lower emissions than conventional systems while others perform 33% worse, primarily determined by maintaining >90% electrical efficiency and limiting aluminium in mounting structures.	(1) EOL excluded. (2) Marginal crops assumed identical to conventional local crops; broader market effects (e.g., soy imports) not modelled. (3) Results highly sensitive to assumptions about marginal electricity and crop yield penalties. (4) Scenario discovery boxes cover parameter ranges, but extreme/unlikely configs possible outside boxes.

Critical patterns emerge from this synthesis. First, FU selection profoundly influences comparability, studies using monetary units often show favorable results due to revenue stacking, while energy-based assessments enable direct comparison with conventional electricity. Second, regarding system boundaries, most studies (~85%) employ either cradle-to-gate or cradle-to-end-of-use approaches, while only ~15% include EOL phases. Notably, the few cradle-to-grave studies in literature have centered on mono-facial PV modules, offering only limited relevance for bifacial technologies. The present work employs a methodological scope consistent with the dominant body of LCA research on APVs, thereby allowing results to be positioned within a directly comparable framework. Third, geographic and climatic context strongly influence performance, yet most studies remain limited to single locations, underscoring the value of the multi-location assessment conducted in this study.

3.2.5 Research gaps and study contributions

Despite expanding LCA research on APVs, critical knowledge gaps persist. First, comparative assessments of multiple configurations within unified frameworks remain absent, limiting understanding of optimal design selection. Notably, no prior study has comprehensively compared vertical, single-axis, and dual-axis configurations equipped with bifacial PV modules. Second, detailed material inventories, particularly for vertical and tracking systems, are frequently withheld due to confidentiality agreements, hampering reproducibility and technology advancement. Third, environmental impact assessments disproportionately emphasize climate change while neglecting equally important categories including ecosystem quality and resource depletion. Fourth, the integration of consequential and attributional LCA approaches remains underdeveloped, with most studies adopting single methodologies that fail to capture the complex interactions between energy conversion and agricultural systems. Comparative conclusions in agrivoltaics are inherently location dependent because feasible design space and deployment potential are shaped by spatially explicit constraints rather than solar resource alone [9], reinforcing the thesis choice to benchmark configurations under location-specific conditions and to treat geographic context as a first-order determinant when interpreting environmental rankings and generalizing conclusions. This study addresses these gaps through comprehensive LCA benchmarking of four bifacial APV systems including fixed vertical, interspace and overhead single-axis, and overhead dual-axis configurations, against conventional ground-mounted bifacial PV systems and country-specific electricity grid mixes. The assessment spans diverse European climatic conditions from Sweden, Kärrbo Prästgård (59.55°N) to Italy, Agrigento (37.21°N), capturing latitudinal variation in solar resource availability and agricultural productivity patterns. The analysis employs a hybrid LCA methodology combining

attributional assessment for PV components across ten environmental impact categories with consequential analysis for agricultural land-use change contributions to climate change. System boundaries explicitly encompass cradle-to-end-of-use phases, acknowledging the exclusion of EOL due to data limitations while maintaining consistency across all configurations. Critically, this research provides the first publicly available detailed material inventory for vertical APV systems. Monte Carlo Analysis ensures statistical robustness of conclusions. Through this comprehensive approach, the study identifies environmentally optimal APV configurations for sustainable food-energy co-production across European climatic gradients, providing actionable guidance for policymakers, developers, and agricultural stakeholders.

3.3 Methods

3.3.1 The Study area and system description

To capture climatic variation across Europe, the study includes four geographically sites namely Kärrbo Prästgård in Sweden (59.5549°N, 16.7585°E), Jeggeleben in Germany (52.7305°N, 11.0285°E), and Piacenza (45.0524°N, 9.6923°E) and Agrigento (37.20920°N, 13.81800°E) in Italy, as illustrated in Figure 3.2.

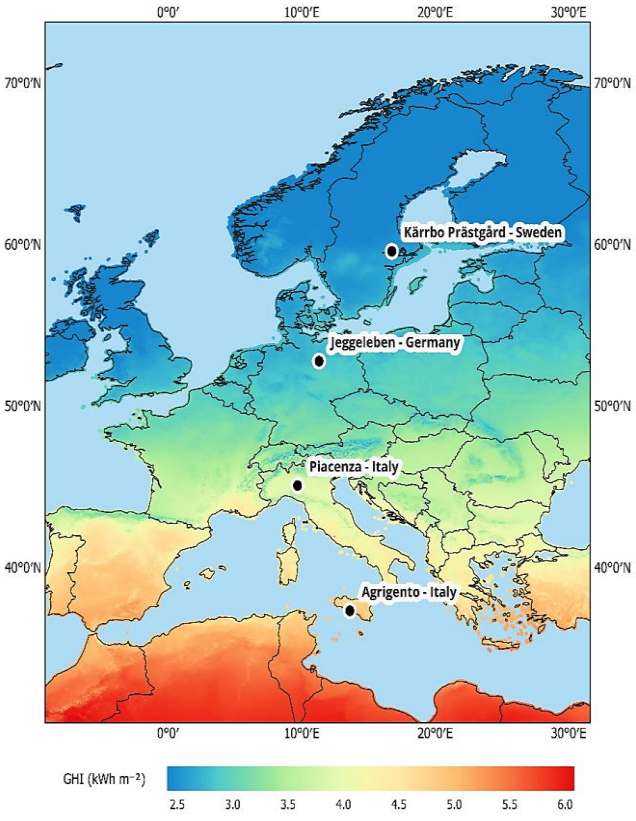

Figure 3.2 Geographic locations analyzed in this study with average daily Global Horizontal Irradiance (GHI) values.

To ensure accurate and location-specific energy yield simulations, typical meteorological years (TMYs) were constructed for each study site based on hourly reanalysis data from the ERA5 database [86], covering the period 2000-2024. Each TMY consisted of 8760 hourly values and was designed to represent long-term average weather conditions while minimizing computational demand. The TMY construction followed the methodology established by the U.S. National Renewable Energy Laboratory (NREL) for TMY2 and TMY3 datasets [87] and conforms to ISO 15927-4:2005 standards [88]. For each calendar month, all candidate months in the dataset were evaluated using the Finkelstein-Schafer (FS) statistic, which quantifies the deviation between a candidate month's cumulative distribution function (CDF) and the long-term CDF. Daily values of Global horizontal irradiance (GHI), air temperature (T_a), and relative humidity (RH) were used as evaluation variables. A weighted FS score was computed for each candidate month, with weights of 60% for GHI, 30% for T_a, and 10% for RH, reflecting their relative importance in PV performance modeling. The candidate month with the lowest weighted FS score was selected as most representative for each calendar month. These 12 months were then chronologically concatenated to create a synthetic year preserving intra-month weather patterns and irradiance variability. The resulting TMY datasets were used as standardized inputs for energy simulations, as shown in Figure 3.3.

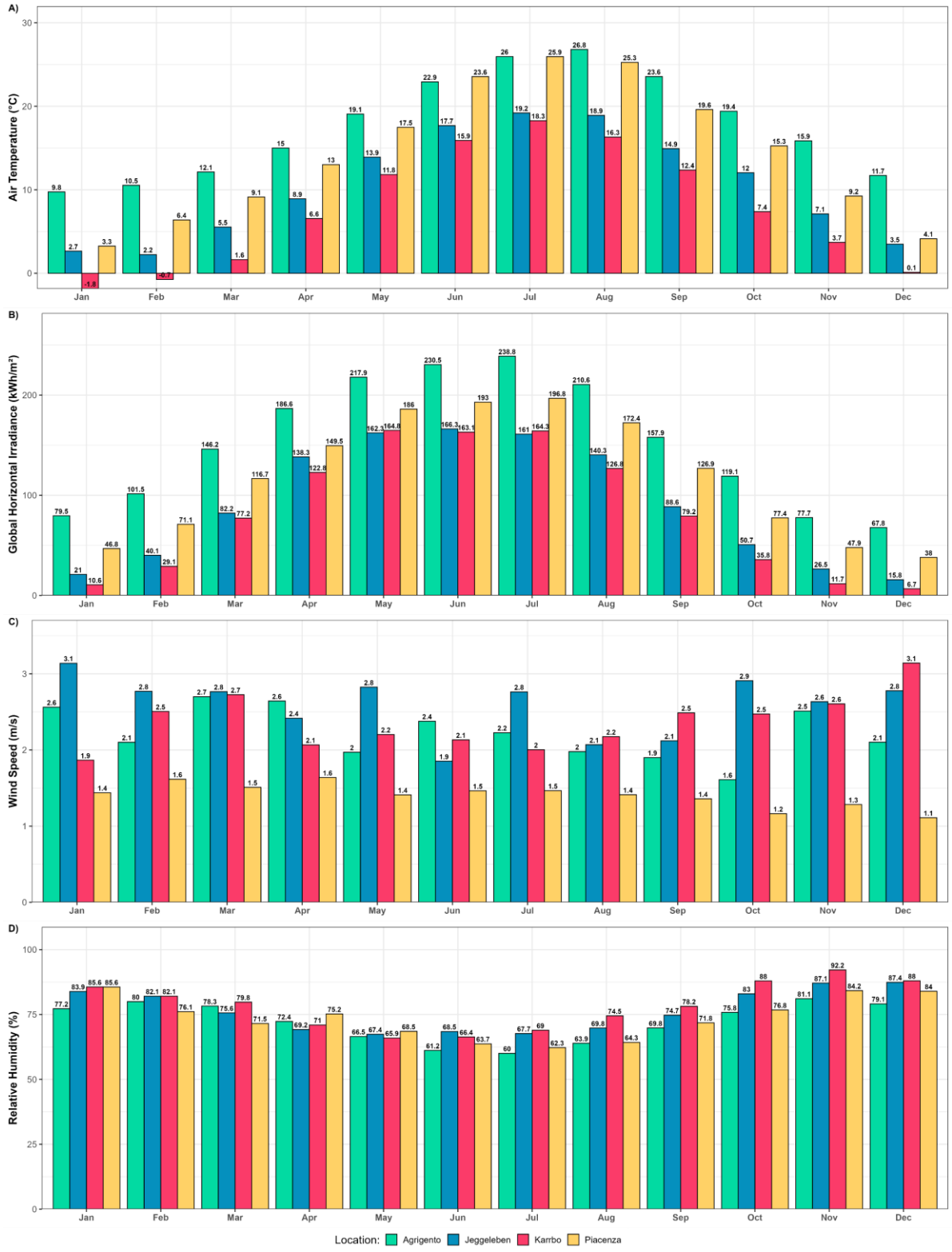

Figure 3.3 Summary of key annual meteorological data from the TMY datasets for each study location.

This study examines four APV configurations, which include a fixed vertical system, an interspace single-axis setup, and two overhead tracking systems comprising single-axis and dual-axis

mechanisms. These configurations reflect current industry standards and have been widely documented in previous research [2]. The different systems are depicted in Figure 3.4.

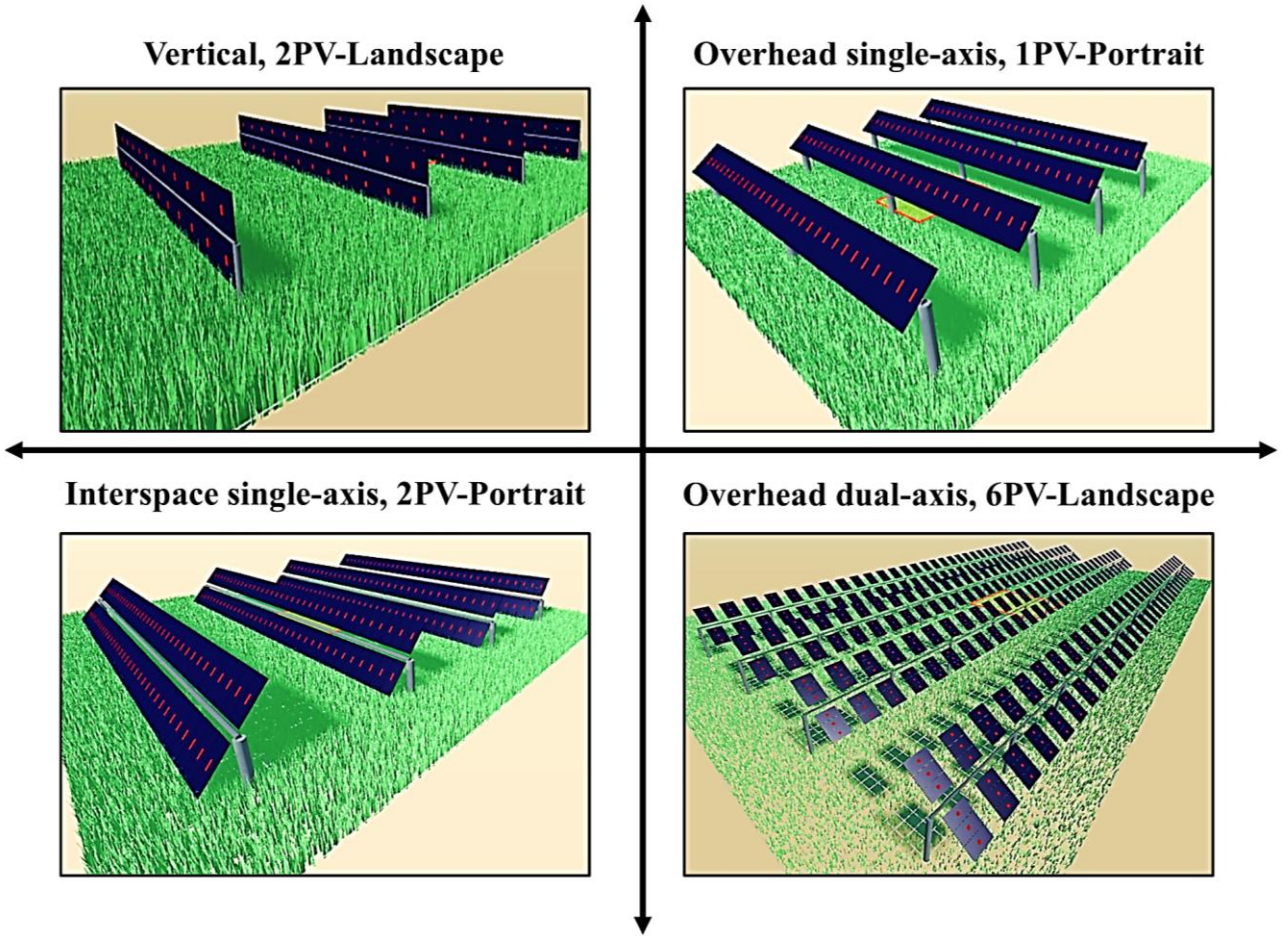

Figure 3.4 Different APV layouts investigated in the present study.

To establish fair performance comparisons, this study standardized the same PV module technology across all configurations. A 450 W_p bifacial module with 21.13% efficiency and a 75% bifaciality factor was selected. It weighs 29 kg, degrades by 0.5% annually, and has a surface area of 2.13 m² (2.13m×1m). A key decision was the selection of a representative, high-efficiency bifacial module, as this technology is central to modern APV systems [89]. Since Ecoinvent database lacks an inventory of bifacial PV module, this model was chosen based on the detailed life cycle inventory (LCI) provided by Jia et al. [90]. The albedo was assumed to be 0.2, representing the fraction of global irradiation reflected from the ground onto the front and rear sides of bifacial modules [91]. This value is commonly used as a baseline assumption in PV performance modeling for installations over vegetated or mixed ground surfaces [92]. While actual albedo may fluctuate depending on factors such as crop type, soil moisture, ground cover, and seasonal variations, the chosen value of 0.2 serves

as a conservative and widely accepted average for generalized APV system simulations [51, 82]. The inverters used are three-phase, grid tied units operating at 50 Hz with an efficiency of 97.9% [94]. Soiling and wiring losses were assumed to account for 2% of the total system losses [59]. The fixed vertical system had module rows aligned north-south, with vertically mounted modules (tilted 90°) facing east on one side and west on the other. The tracking systems also had north-south aligned rows and rotated from east to west to follow the sun's path, overhead single-axis trackers with a ±55° rotation range and interspace single-axis trackers with a ±45° range along the north-south axis. Dual-axis trackers rotated along both the north-south and east-west axes to fully track the sun. In contrast, the baseline system, conventional ground-mounted photovoltaic (CGMPV), had east-west aligned rows with modules facing north-south at a fixed tilt angle specific at each location. Each APV system type was analyzed under three different row pitches following the methodology outlined by Bellone et al. [48], beginning from a baseline minimum spacing. A reduced pitch was allowed if it did not obstruct agricultural machinery or cause significant PV self-shading. To facilitate comparison across APV configurations, the three row pitch distances evaluated for each system, starting from the minimum feasible value, are referred to throughout the study as low, medium, and high pitch, respectively. The electricity output for a 1 MW_p capacity of each APV system and CGMPV at each location was simulated using PVSOL® software [56], with detailed results provided in [95]. Optimal tilt angles for the CGMPV system were also determined using the same software, resulting in values of 35° for Agrigento, 40° for both Piacenza and Jeggeleben, and 45° for Kärrbo Prästgård. Table 3.2 summarizes the layout and key design features of each system.

Table 3.2 The settings of CGMPV and different APV systems used in this study.

APV type	Array layout	Height* (m)	Pitch (m)	Land use (ha/MW_p)
CGMPV (baseline)	2PV-Portrait	0.7	5	1.32
Fixed vertical	2PV-Landscape	0.7	8, 12, 16	1.95, 2.88, 3.82
Overhead single-axis	1PV-Portrait	2.8	6, 10, 14	1.44, 2.38, 3.34
Interspace single-axis	2PV-Portrait	2.3	10, 14, 18	1.21, 1.7, 2.16
Overhead dual-axis	6PV- Landscape	5	14, 18, 22	1.98, 2.48, 3.05

* In vertical system, the clearance from the ground to the bottom edge of the first PV panel is 70 cm. In tracking systems, this distance refers to the clearance from the hub to the ground.

3.3.2 Goal of the study

This study aims to evaluate the environmental impacts of different APV configurations across varied layouts and geographical settings spanning northern to southern Europe including Kärrbo Prästgård

in Sweden, Jeggeleben in Germany, Piacenza and Agrigento in Italy as shown in Figure 3.2. The objective is to improve understanding of their environmental performance during manufacturing and operation, supporting informed decision-making by farmers, industry stakeholders, and policymakers regarding optimal system selection for different regions.

3.3.3 Scope of the study

An attributional LCA is applied for the PV components of all APV systems, while the impact on agricultural production is assessed in terms of land losses by APV structures and shading-induced crop yield with a consequential LCA approach. FU is 1 kWh of electricity conversion by various APVs. This choice aligns with the international energy agency (IEA) recommendation, which suggests it as a viable FU for solar PV-based systems [96].

The system boundary for PV systems follows an attributional cradle-to-end-of-use approach, encompassing raw material extraction, bifacial PV modules, mounting structures, inverters, tracking motors (where applicable), and electrical BOS components such as cables for each APV configuration. In contrast, the crop-related assessment adopts a consequential LCA framework and considers only the indirect land use impacts resulting from APV system deployment, which is discussed in detail later. The overall analysis spans 30 years, consistent with the expected lifetime of PV modules and structural components. Figure 3.5 depicts the full system boundaries.

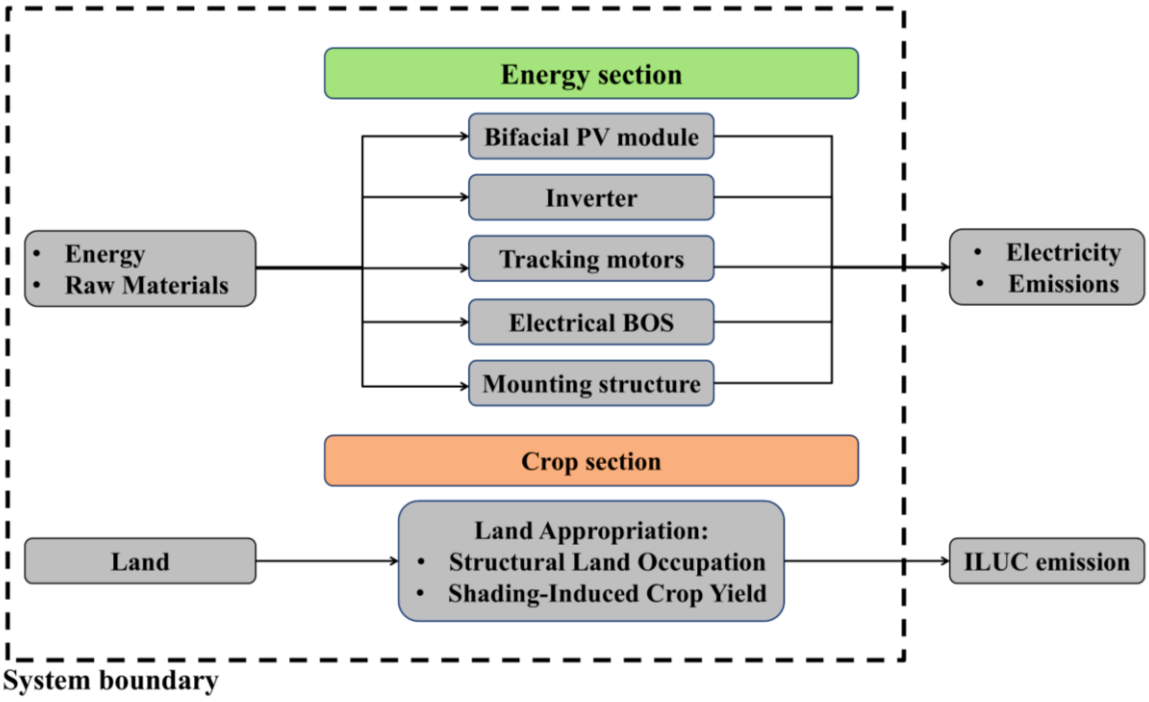

Figure 3.5 System boundary of this research.

In this study, EOL phase for different systems, which involves dismantling the plant, waste processing, disposal, and recycling of all relevant plant components, were excluded due to the lack of sufficient and reliable information. This decision was made because the study focused solely on the construction and use phase. Although the EOL of PV modules can influence the LCA result, the modules used in all scenarios were identical, leading to the assumption that the EOL aspects would not significantly impact the comparison. This approach aligns with established methodologies in many LCA studies for APVs found in literature [50, 61, 63, 67, 68, 69].

3.3.3.1 Consequential impacts on crop production

Consequential crop impact is assessed using the indirect land use change (ILUC) method reported by Searchinger et al. [97], which accounts for GHG emissions when APVs occupy arable land, potentially shifting crop production to other regions and increasing CO_2 emissions due to agricultural displacement [19]. ILUC emissions were estimated using the factor of 1595 kg CO_{2eq}/ha [98], consistent with EU methodological guidelines. ILUC factors are derived from global economic and land use models (e.g., GLOBIOM, GTAP (88, 89) that simulate market-mediated land displacement and associated carbon stock changes. In this study, ILUC emissions were calculated as the product of excluded agricultural area and reduction/increase in crop productivity, the ILUC factor per hectare, and the project lifetime (30 years). While this static factor does not capture regional variability, it ensures methodological consistency. The arable land loss due to APV structures is calculated using a security buffer around APV mounting rows (support structures/trackers), representing the area excluded from cultivation for safe agricultural mechanization [71]. A 0.75 m buffer on both sides of each mounting row leads to the exclusion of 1.5 square meters of land per meter length of mounting row, accounting for the pillar diameter. The only exception applies to the interspace single-axis configuration, which uses a wider buffer of 1.5 m per side, resulting in 3 square meters of excluded land per meter of row. This exclusion is scaled according to the number of rows required to install 1 MW_p of capacity, yielding the total structurally non-cultivable land area. This area is then multiplied by the ILUC factor and the 30-year project lifetime to estimate the GHG emissions associated with permanent land occupation. In addition to land exclusion caused by the APV structures, dynamic impacts on crop yield are also considered. Crop yield reductions can occur due to changes in the microclimate induced by APV structures, particularly reduced photosynthetically active radiation (PAR). Unlike the previous factor, which quantified structural land occupation, this component captures dynamic yield penalties related to shading effects. To estimate crop yield reduction, a multiple linear regression (MLR) model developed by Tekie et al. [101] was adopted. This model was constructed from a meta-analysis of empirical yield data collected under APVs across various

shading conditions. It includes five predictors: the shading level (X_1), and four climatic indicators (X_2: mean, X_3: minimum, X_4: maximum, X_5: standard deviation) derived from the standardized precipitation evapotranspiration index (SPEI), which together allow quantification of both light limitation and drought stress. The shading predictor, X_1, was estimated using the irradiation model described by Amaducci et al. [73], with hourly weather data from the ERA5 database (2000-2024), identical to that used for generating TMYs in the energy yield analysis, thereby ensuring methodological coherence. The model determined the annual reduction in GHI beneath the APV array compared to a full light (FL) reference scenario. To accurately account for the spatial heterogeneity in irradiation and potential edge effects beneath the PV arrays, shading was first calculated at a high spatial resolution of 0.5 m. This initial calculation encompassed the entire area between PV strings, capturing detailed light distribution patterns. From this high-resolution map, a single mean shading percentage, the required input for the subsequent yield estimation model, was derived by spatially averaging the values exclusively within the defined cultivated plot. The security buffer areas were deliberately omitted from this final averaging step to ensure the shading value accurately represented the conditions experienced by the crops and to avoid overestimation. Climatic predictors (X_2-X_5) were derived from SPEI-1, a 1-month timescale index capturing short-term soil moisture variations. Monthly SPEI-1 values were calculated from the same weather dataset by modeling potential evapotranspiration via the Thornthwaite method and computing the climatic water balance. The resulting time series was fitted to a log-logistic distribution using the SPEI R package [91, 92] to standardize the drought indices. These predictors were parameterized on a basis specific to each crop. For each growing season, the four statistical moments were calculated using only the SPEI-1 data corresponding to that crop's defined growth cycle (X_2-X_5). This methodology accounted for the distinct phenological cycles of different crop types, including single-season annuals, winter crops with growth periods spanning two calendar years, and perennials for which a full 12-month period was considered. The MLR model was then used to estimate relative yield reduction as a function of shading and drought stress. The final set of calibrated MLR equations is reported in Table 3.3 for seven non-irrigated crop categories.

Table 3.3 Regression equations derived from the MLR models for non-irrigated crop categories **[101]**.

Crop type	Equations
C3 Cereals	$Y= 71.34 - 0.76X_1 + 5.84X_2 + 12.47X_3 - 8.01X_4 + 67.09X_5$
Berries	$Y= 111.58 + 0.021X_1 - 16.78X_2 - 7.84X_3 - 50.16X_4 + 70.31X_5$
Maize	$Y= 86.84 - 0.47X_1 + 58.21X_2 - 9.55X_3 - 46.76X_4 + 49.29X_5$
Grain Legumes	$Y= 126.25 - 0.87X_1 - 37.61X_2 + 48.93X_3 - 5.39X_4 + 38.47X_5$
Fruits	$Y= 107.06 - 0.42X_1 + 6.52X_2 - 5.42X_3 - 2.22X_4 - 5.94X_5$
Root crop	$Y= 20.59 - 0.81X_1 - 26.50X_2 - 17.96X_3 - 22.61X_4 + 84.89X_5$
Forage	$Y= 78.68 - 0.93X_1 + 86.36X_2 - 31.22X_3 - 64.20X_4 + 123.21X_5$

*Y indicates the predicted crop yield (% of reference yield).

These equations allow direct integration of shading-climate interactions into APVs planning, enabling context-specific yield reduction assessments. Additional details on model structure, accuracy, and validation are provided by Tekie et al. [101]. Once relative yield reductions are estimated, the associated emissions are calculated by multiplying the percentage yield loss by the net cultivable area (excluding the security buffer areas), the ILUC factor, and the project lifetime. As the ILUC factor is defined on a per-hectare basis and not crop-specific, yield losses are interpreted as land-equivalent losses. For instance, a 20% reduction in crop yield is considered equivalent to a 20% reduction in productive land area. This assumption allows for the integration of shading-induced productivity losses into a land-based emission framework in a methodologically consistent and reproducible manner, in line with the principles of consequential LCA. Conversely, in cases where crop yield under the APVs improves due to the adoption of shade-tolerant crops or favorable microclimatic conditions, a credit is assigned using the same methodological approach. The resulting gain in yield is interpreted as an equivalent increase in productive land area and leads to negative ILUC emissions, reflecting the avoided land use that would otherwise be required to achieve the same level of agricultural output. Finally, the GHG emissions resulting from the consequential approach were combined with the GHG emissions associated with attributional approach. To ensure consistency with the study's functional unit (kWh), the total emissions were normalized by the cumulative electricity generation of each 1 MW_p APV configuration at each location over the system's lifetime. The resulting values were then assigned to the climate change impact category within the LCA framework.

3.3.4 Life cycle inventory (LCI)

Ecoinvent v3.8 datasets [104] were used to model all system components, excluding PV modules, for the APV configurations and the country-specific electricity grid mix (electricity, medium voltage [75]). Detailed national electricity mix compositions are provided in Figure 3.6.

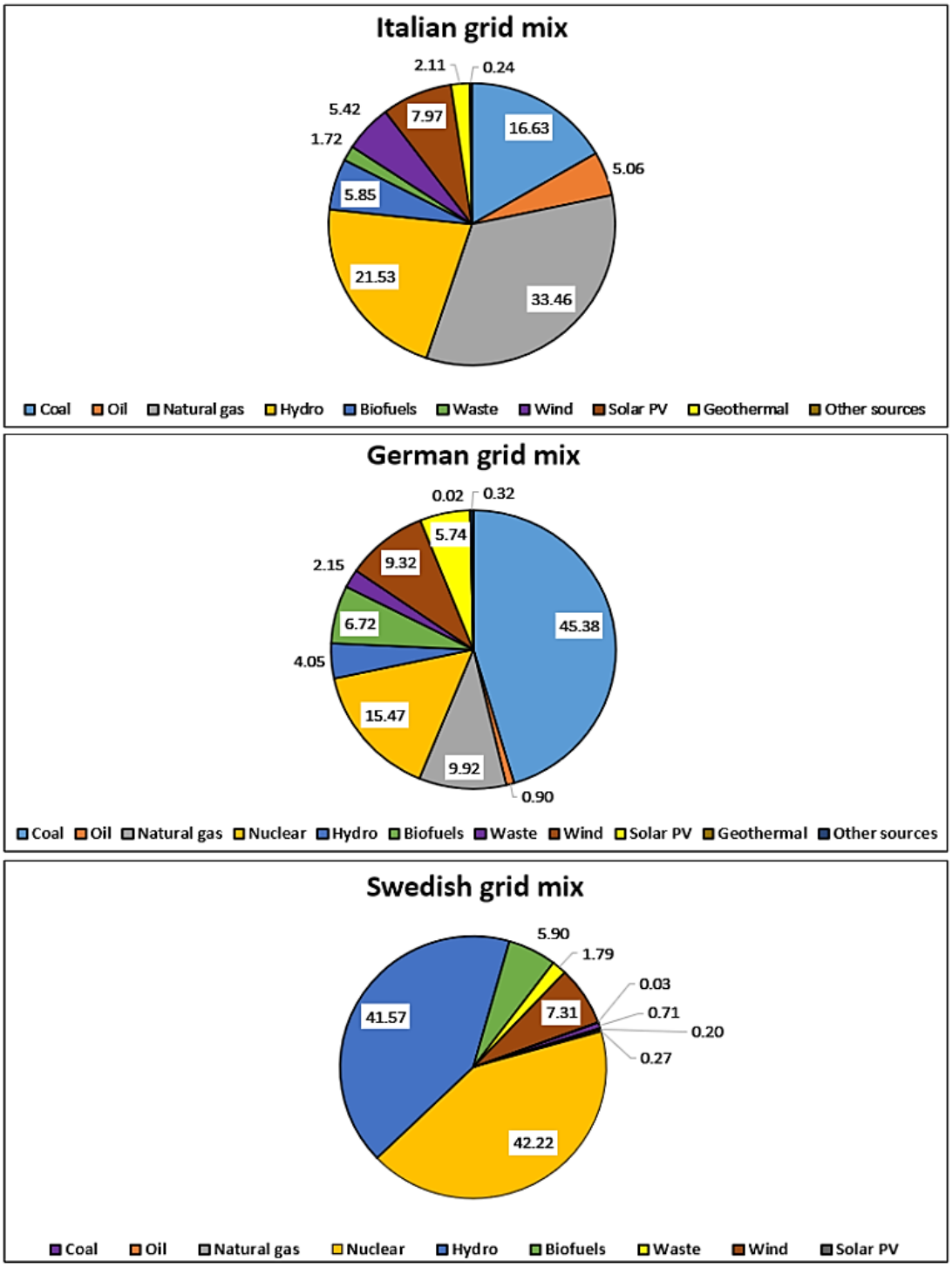

Figure 3.6 The country-specific electricity grid mix contribution (Data was obtained from **[104]**).

The analyses were conducted using the allocation, cut-off by classification system model, which is consistent with standard practice for attributional LCA [105]. Since the studied systems are not modeled as multifunctional (the functional unit is defined as 1 kWh of electricity), no additional allocation procedures were required. As this Ecoinvent database does not include a dedicated dataset for bifacial PV modules, a new process was created within the SimaPro® software to model the

selected 450 W_p module. The inventory for this process was adapted from the study by Jia et al. [90]. Specifically, the material and energy inputs were derived from their inventory for the "166-BF (72)" module, which corresponds to a 450 W_p bifacial module. The data reported by Jia et al. [90] is normalized per 1 kW_p of capacity; therefore, all values were scaled by a factor of 0.45 to accurately represent the inputs for a single 450 W_p module. The resulting inventory is detailed in Table 3.4.

Table 3.4 Life Cycle Inventory for a single 450 Wp Bifacial PV Module. Data adapted from **[90]**.

Materials	Life Cycle Stage	Flow Type	Units	Values	Remarks
Silicon wafer	Cell Manufacturing	Input	kg	0.833	Silicon, single crystal, Czochralski process, photovoltaics (RoW) | market for |
Metallization paste, back side	Cell Manufacturing	Input	kg	0.0107	Metallization paste, back side (RoW) | market for |
Metallization paste, back side, Aluminum	Cell Manufacturing	Input	kg	0.0107	Metallization paste, back side, aluminum (RoW) | market for |
Metallization paste, front side	Cell Manufacturing	Input	kg	0.0107	Metallization paste, front side (RoW) | market for |
HF	Cell Manufacturing	Input	kg	0.6484	Hydrogen fluoride (RoW) | market for|
HNO_3	Cell Manufacturing	Input	kg	0.6484	Nitric acid, without water, in 50 % solution state (RoW) | market for |
HCI	Cell Manufacturing	Input	kg	0.6484	Hydrochloric acid, without water, in 30 % solution state (RoW) | market for |
H_2SO_4	Cell Manufacturing	Input	kg	0.6484	Sulfuric acid (RoW) | market for |
KOH	Cell Manufacturing	Input	kg	0.6484	Potassium hydroxide (GLO) | market for |
H_2O_2	Cell Manufacturing	Input	kg	0.6484	Hydrogen peroxide, without water, in 50 % solution state (RoW) | market for |
O_2	Cell Manufacturing	Input	kg	0.6484	Oxygen, liquid (RoW) | market for |
NH_3	Cell Manufacturing	Input	kg	0.6484	Ammonia, liquid (RoW) | market for |
$POCI_3$	Cell Manufacturing	Input	kg	0.6484	Phosphorus oxychloride (GLO) | market for |
N_2	Cell Manufacturing	Input	kg	0.6484	Nitrogen, liquid (RoW) | market for |
POE	Module Assembly	Input	kg	2.376	Polyolyaltha Olfin, replaced by Polyethylene, low density, granulate (GLO) | market for |
Ribbons	Module Assembly	Input	kg	0.212	Copper (GLO) | market for |
Solar glass	Module Assembly	Input	kg	21.281	Solar glass, low - iron (GLO) | market for |
Aluminum frame	Module Assembly	Input	kg	2.3	Aluminum alloy, AlMg3 (GLO) | market for |
Tap water	Cell & Module Manufacturing	Input	kg	188.28	Tap water (RoW) | market for |
Electricity	Cell & Module Manufacturing	Input	kWh	24.503	Electricity, low voltage | market group for |

For the CGMPV system, the Ecoinvent dataset was modified to align with the selected bifacial PV module technology and to standardize the configuration to a 1 MW_p capacity over a 30-year project lifetime. These adjustments ensure a consistent basis for fair comparison with the APV configurations in terms of system design and energy yield. The default PV modules in the Ecoinvent dataset were

replaced with the custom-modeled 450 W_p bifacial modules used in the APV systems. The inverter inventory was revised to include two 500 kW_p inverters and one replacement at year 15, reflecting a more realistic operational lifetime [20] and resulting in four units over the system lifespan. The BOS inventory was proportionally scaled from the Ecoinvent dataset of a 570 kW_p electrical and mounting installation, using a scaling factor of 1.754 to represent a 1 MW_p system. PV modules and mounting structures were assumed to have a lifespan of 30 years, in line with the project lifetime [79, 95]. Table 3.5 presents the aggregated component inventories for electricity generation in both CGMPV and APV systems, standardized to a 1 MW_p capacity over the 30-year lifetime.

Table 3.5 Aggregated life cycle inventory of material inputs for 1 MWp capacity of CGMPV and four APV typologies, over a 30-year lifetime.

Components	Materials	Units	CGMPV (2P)	Fixed vertical (2L)	Overhead single-axis (1P)	Interspace single-axis (2P)	Overhead dual-axis (6L)	Dataset and References
PV module	Bifacial photovoltaic panel, single-Si, 450 W_p	Pieces	2223	2223	2223	2223	2223	[90]
Inverter	Inverter 500 kW_p	Pieces	2+2	2+2	2+2	2+2	2+2	Ecoinvent, Inverter 500 kW_p (GLO) | market for | [104]
Tracking motor	Steel, copper, plastic	kg	—	—	621	391	650	Ecoinvent, Electric motor, vehicle (GLO) | market for | [93, 96, 97]
Wiring	Copper, plastic	kg	Included in Ecoinvent dataset	1300	2710	2445	2950	Ecoinvent, Cable (GLO) | market for [50, 61, 98] Ecoinvent, Electric installation, for CGMPV (GLO) | market for | [104]
Structural BOS			Included in Ecoinvent dataset					Ecoinvent, Photovoltaic mounting system, for CGMPV (GLO) | market for | [104]
	Steel	kg	—	60000	114108	53785	236158	Ecoinvent, Reinforcing steel (GLO) | market for | [96, 97, 99]
	Aluminium	kg	—	140	227	171	7.15	Ecoinvent, Aluminium, wrought alloy (GLO) | market for | [96, 97, 99]
	Zinc	kg	—	2100	4021	2690	3900	Ecoinvent, Zinc (GLO) | market for | [96, 97, 99]

It is important to highlight that the material inventories used, particularly those related to tracking motors and structural BOS components for the different APV configurations, were obtained through direct personal communication with industry sources. These inventories may vary across manufacturers due to proprietary designs, patented innovations, and differences in structural design and material composition. In particular, some systems may employ lighter or heavier support structures (trackers) or utilize materials with higher or lower environmental impacts. Such variations

can significantly influence LCA results and should be carefully considered when generalizing findings across different APV technologies. The structural design of each APV followed a specific commercial reference including Agrivoltaico Tracker 3D-T2.1 for the dual-axis system (REM TEC® [110]), CONVERT TRJ15 for the overhead single-axis system (Valmont Solar® [107]), CONVERT TRJ72 for the interspace single-axis configuration [65], and SkyGre P2-DUO for the vertical system (SentNet® [108]). Table 3.6 details the technical specifications of the fixed vertical and tracking APVs, as provided by industry partners for the life cycle inventories. These specifications formed the basis for the estimation of material and energy flows. All inventories were scaled to a uniform system size of 1 MW_p to ensure comparability.

Table 3.6 Key technical specifications of the vertical and tracking APV systems.

	Fixed vertical (2L)	**Overhead single-axis (1P)**	**Interspace single-axis (2P)**	**Overhead dual-axis (6L)**
Number of PV modules per support structure/tracker	24	15	72	18
Total PV capacity per support structure/tracker (kW_p)	10.8	6.75	32.4	8.1
Total number of support structures/trackers required/1 MW_p	93	148	31	124
Length of each support structure/tracker (m)	26	18	41	10.5

Finally, the inventory of all material used was modeled using SimaPro® software [111], a leading software for LCA calculations [112].

3.3.5 Life cycle impact assessment (LCIA)

The environmental footprint (EF) method recommended by the international life cycle data (ILCD) System [113] was adopted for assessing environmental impacts in this study. This method translates life cycle inventory data into quantitative contributions to specific environmental concerns. An EF impact category denotes a particular type of resource use or environmental impact associated with the life cycle inventory data, and each impact category is represented by a quantifiable indicator. Although the EF method defines 16 impact categories, the present study selected 10 of them. This selection was guided by their methodological robustness, consistency with previous scientific literature on APVs [19], and alignment with recommendations provided by the European Commission guidelines [113]. Table 3.7 summarizes the selected EF categories, and their corresponding indicators used in this study.

Table 3.7 EF impact categories and their corresponding indicators used in this study.

Impact category	Indicator	Unit
Climate change	Global Warming Potential (GWP100)	g $CO_{2\ eq}$
Ozone depletion	Ozone Depletion Potential (ODP)	*µg CFC-11 $_{eq}$
Respiratory inorganics (Particulate matter)	Impact on human health	Disease incidence
Photochemical Ozone formation	Tropospheric ozone concentration increase	**mg NMVOC $_{eq}$
Acidification	Accumulated Exceedance (AE)	mmol $H+_{eq}$
Eutrophication, terrestrial	Accumulated Exceedance (AE)	mmol N $_{eq}$
Eutrophication, freshwater	Fraction of nutrients reaching freshwater end compartment (P)	mg P $_{eq}$
Eutrophication, marine	Fraction of nutrients reaching marine end compartment (N)	mg N $_{eq}$
Resource use, minerals and metals	Abiotic resource depletion (ADP ultimate reserves)	mg Sb $_{eq}$
Resource use, fossils	Abiotic resource depletion - fossil fuels (ADP-fossil), Uranium is included	MJ

*CFC-11= Trichlorofluoromethane, **NMVOC= Non-Methane Volatile Organic Compounds

3.3.6 Uncertainty analysis in LCIA

The uncertainty analysis aimed to quantify the influence of background data variability on the results across all impact categories for APV systems. It considered two distinct components. The first was the background processes, which were modeled as stochastic variables using Ecoinvent v3.8 “market for” datasets with global (GLO) coverage, as detailed in Table 3.5. These background flows were treated as stochastic, characterized by lognormal uncertainty distributions inherent to the database. Specifically, the uncertainty for these background processes, particularly for emissions and resource inputs, was estimated using the Pedigree matrix approach. This methodology, integrated within SimaPro and explained in its official documentation, assesses the data quality of each background data point based on six criteria including reliability, completeness, temporal correlation, geographical correlation, technological correlation, and a basic uncertainty factor [114]. The overall squared geometric standard deviation σ^2 for each data point’s uncertainty, which defines the spread of its lognormal distribution, is calculated as follows:

$$\sigma^2 = \sum_{n=1}^{6} \sigma_n^2 \qquad \text{Eq. 3.1}$$

The second component was the foreground data, referring to the quantities of materials and components used in each APV configuration. These were treated as deterministic values and were primarily derived from direct communication with industry sources. While no probability distributions were assigned to these values, they were included in the Monte Carlo analysis alongside

the background data to preserve model consistency. To perform the uncertainty analysis, a Monte Carlo analysis was executed using SimaPro's built-in functionality. This simulation, carried out for 10000 iterations, randomly sampled values from the defined probability distributions, including those determined by the Pedigree matrix for background data. The resulting uncertainty was expressed as 95% confidence intervals, indicating the statistical range within which the true mean value is expected to lie with 95% probability. For a more detailed explanation of the Pedigree matrix and uncertainty calculation methods within SimaPro, readers are referred to the software's official introduction manual [111].

3.4 Results

3.4.1 GHG emissions caused by structural land occupation

Understanding how APV infrastructure affects agricultural land availability is essential for evaluating system sustainability. The structural footprint of each configuration was quantified to estimate non-cultivable land area and its corresponding GHG emissions using the ILUC method, as summarized in Table 3.8. These values represent a consequential component of the LCA, highlighting how design choices influence environmental trade-offs between clean energy conversion and land preservation.

Table 3.8 Consequential GHG emissions of structural land occupation of 1 MWp APV systems.

APV system type	Fixed vertical (2L)	Overhead single-axis (1P)	Interspace single-axis (2P)	Overhead dual-axis (6L)
Total non-cultivable area per 1 MW_p (m^2)	3627	3996	3813	1953
ILUC-related GHG emissions for non-cultivable area per 1 MW_p ($kgCO_{2eq}$)	578.5	637.4	608.2	311.5
ILUC-related GHG emissions over 30-year project lifetime ($tonCO_{2eq}$)	17.35	19.12	18.47	9.35
Pitch between PV string	8m/12m/16m	6m/10m/14m	10m/14m/18m	14m/18m/22m
Total land area required per 1 MW_p (ha)	1.95/2.88/3.82	1.44/2.38/3.34	1.2/1.7/2.16	1.98/2.48/3.05
Net cultivable land area available per 1 MW_p (ha)	1.59/2.52/3.46	1.04/1.98/2.94	0.83/1.32/1.78	1.78/2.28/2.85

The results reveal significant design-dependent variability. The overhead dual-axis system was the most land-efficient, occupying only 1953 m^2/MW_p [48] and generating the lowest lifetime emissions (9.35 t CO_{2eq}). In contrast, the overhead single-axis configuration had the largest non-cultivable footprint at 3996 m^2/MW_p [48] and, consequently, the highest emissions (19.12 t CO_{2eq}). This was primarily due to its lower module density, which necessitated the highest number of trackers per MW_p [48]. The fixed vertical (3627 m^2/MW_p) and interspace single-axis (3813 m^2/MW_p) systems demonstrated intermediate performance [48], with the latter showing a modest 4.8% reduction in non-cultivable area compared to the overhead single-axis design, despite having a much longer structural

length. These findings on the contribution of APV structural land occupation to the ILUC-related GHG emissions represent one component that should be integrated with other factors, including the GHG impacts from crop yield variations and the emissions from PV component materials in each APV configuration. Only after this comprehensive integration and normalization per FU can a conclusive LCA benchmark the overall environmental performance of the various APV systems.

3.4.2 GHG emissions caused by crop yield variations

Evaluating how different APV system designs influence crop yields is essential to understanding their broader environmental impacts. Figure 3.7 illustrates the GHG emissions associated with crop yield variations under APV configurations for each location at medium pitch spacing across the selected crops in this study. A reduction in yield leads to increased GHG emissions due to the need for compensatory production elsewhere, while an increase in yield results in GHG savings by offsetting production in other regions [50, 64]. Results for lower and upper pitches are provided in [95].

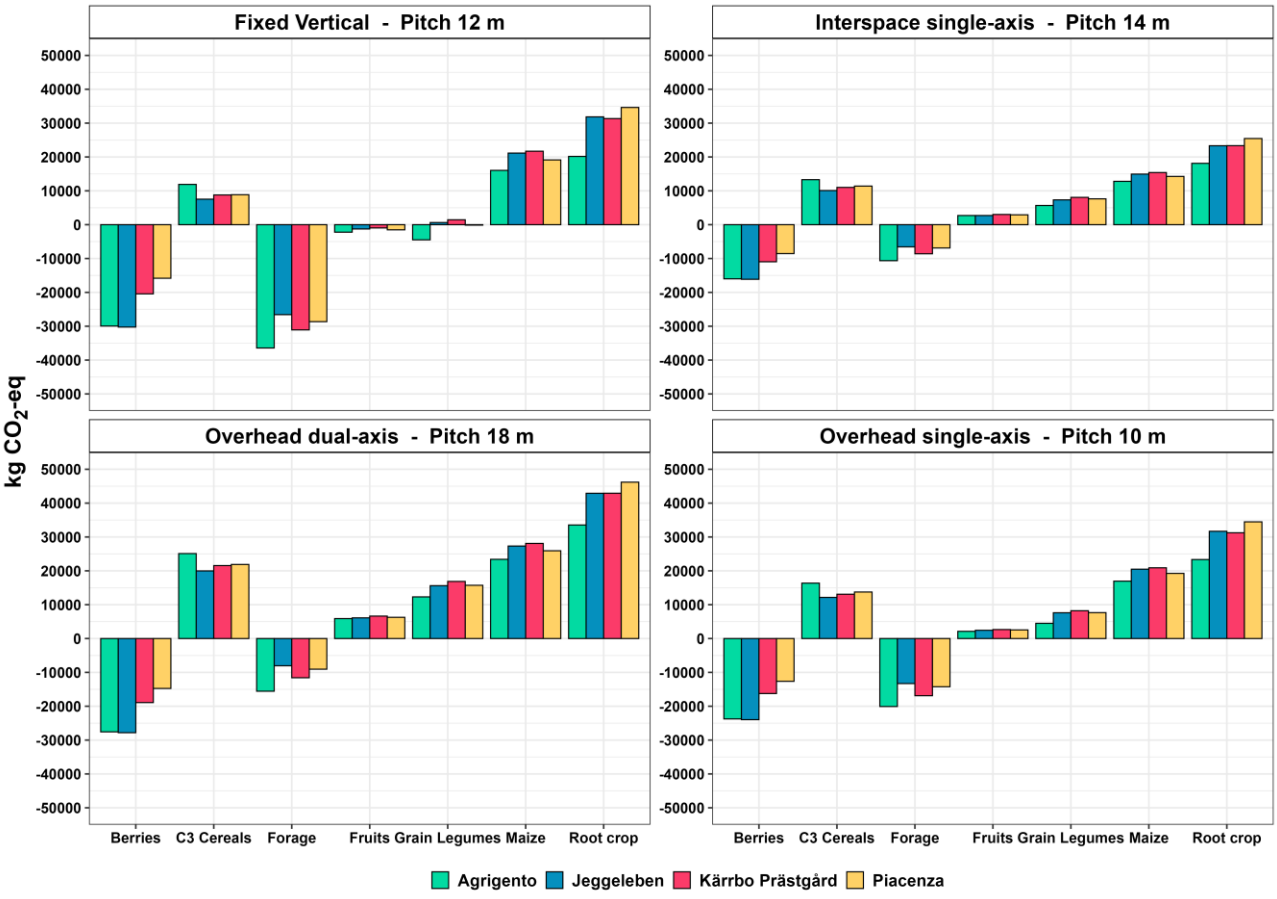

Figure 3.7 GHG emissions and credits associated with crop yield variation under medium pitch APV configurations across crop groups and locations.

Among tracking APV systems, a consistent trend emerges across crops and locations, with root crops demonstrating the highest ILUC-related GHG emissions due to their pronounced sensitivity to shading-induced yield reduction. Conversely, berries consistently deliver substantial GHG emission savings (credits), attributable primarily to their inherent shade tolerance. Cereals, maize, grain legumes, fruits, and root crops all experience their highest yield-induced GHG emissions in the overhead dual-axis APV system, consistent with broader assessments that associate APV design choices with climate impacts [21]. Despite the interspace design having higher shading levels at all locations, resulting from its lower height and the use of two PV modules instead of one in portrait orientation, it consistently shows lower ILUC-related GHG emissions and credits compared with the overhead single-axis system. For example, in Piacenza, the shading level for the interspace single-axis system was calculated at 26%, whereas the overhead single-axis system showed 21.52%. The significantly smaller net cultivable land area remaining available per MW_p installed capacity (approximately 50%) for the interspace system, compared to the overhead counterpart, ultimately led to lower ILUC-related GHG emissions and credits [50, 64]. The vertical APV system exhibits a similar general pattern, with root crops again recording the highest ILUC-related GHG emissions, reflecting their heightened shade sensitivity under medium pitch spacing across all APV configurations. However, for fruits and grain legumes, overall positive GHG emission contributions are observed, driven by yield enhancements at shading levels of up to 14%. Specifically, fruit yields improved at all locations, whereas grain legumes exhibited yield increases in most locations except Kärrbo Prästgård and Jeggeleben. In contrast to the tracking systems where berries delivered the highest GHG emission savings, forage crops within the vertical APV system consistently demonstrated the greatest emission reductions across all locations. Specifically for forage within the vertical APV system, which recorded the highest ILUC-related GHG credits among all APV configurations, Agrigento showed the greatest yield increase (+30.2% relative to open-field condition), followed by Kärrbo Prästgård (+25.8%), Piacenza (+23.8%), and Jeggeleben (+22.1%). Detailed data on shading levels and yield variations across locations and APV configurations at various pitches are provided in [95]. These findings will be integrated with GHG emissions from APV structural land occupation as well as materials used in PV components. The normalization process, detailed in Section 3.5.4.1, will be applied following this integration to ensure comprehensive assessment and enable conclusive interpretation of environmental impacts.

3.4.3 GHG emission contribution of PV components

Figure 3.8 depicts the GHG emissions associated with the electrical and structural material inputs across APV configurations. The emissions provide a detailed breakdown for key PV components such as PV modules, inverters, tracking motors, wiring and structural BOS.

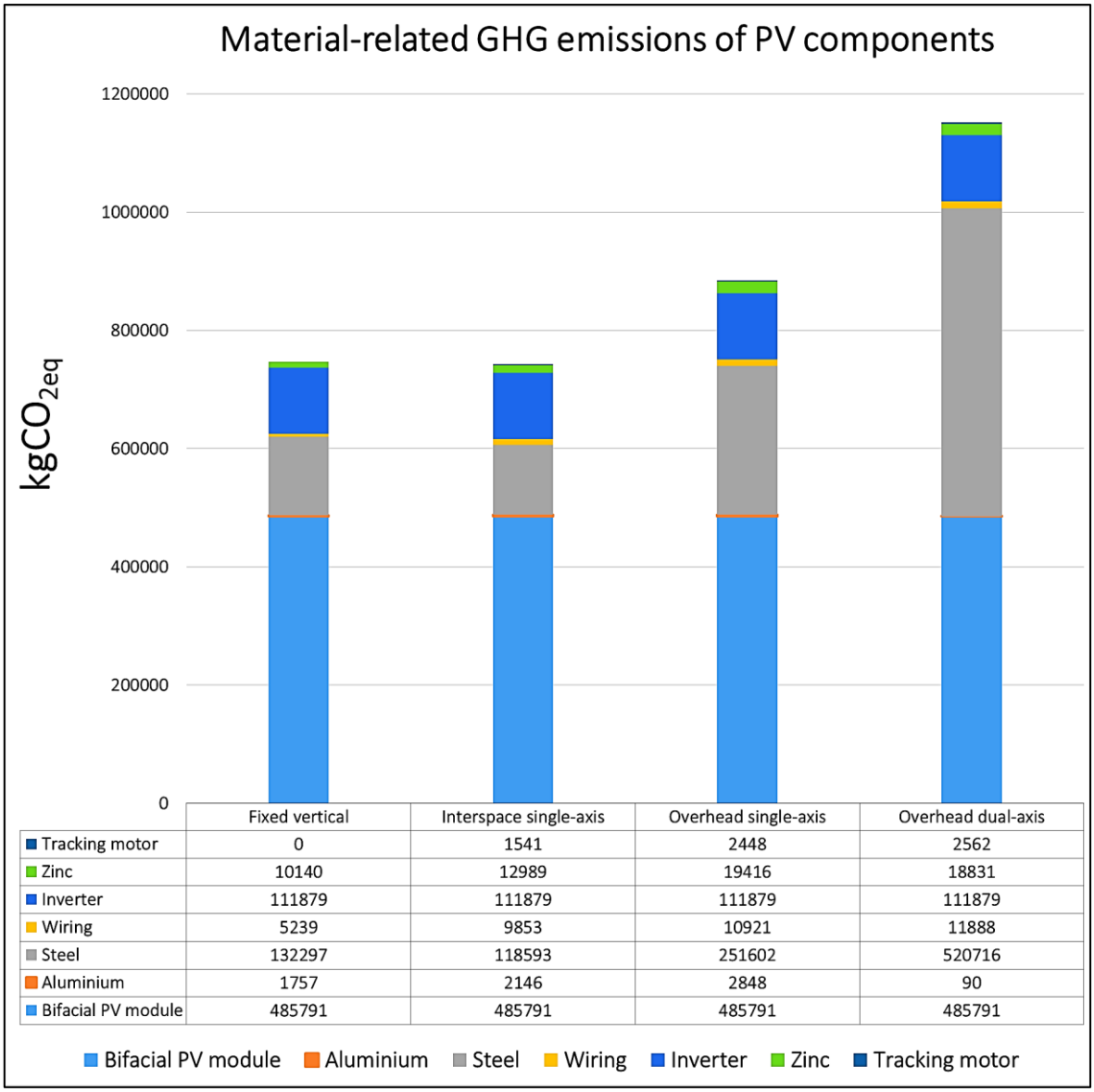

	Fixed vertical	Interspace single-axis	Overhead single-axis	Overhead dual-axis
Tracking motor	0	1541	2448	2562
Zinc	10140	12989	19416	18831
Inverter	111879	111879	111879	111879
Wiring	5239	9853	10921	11888
Steel	132297	118593	251602	520716
Aluminium	1757	2146	2848	90
Bifacial PV module	485791	485791	485791	485791

Figure 3.8 GHG contributions of PV component materials for various APV systems, calculated per 1 MWp.

The results demonstrate a clear correlation between system complexity and material-related emissions. The overhead dual-axis system had the highest emissions at 1151.8 t CO_{2eq}, a full 55% higher than the least impactful design. This was driven by its substantial steel requirement of 236.2 tons, needed to support a 5 m installation height. The interspace single-axis configuration was the best performer (742.8 t CO_{2eq}), benefiting from a reduced height (2.3 m) that required only 53.8 tons

of steel. The fixed vertical system (747.1 t CO_{2eq} from 60 tons of steel) and the overhead single-axis system (884.9 t CO_{2eq}) had intermediate emissions. The overhead single-axis design produced about 19% more emissions than the interspace system, consistent with its moderate structural requirements at a height of 2.8 m. Emissions from bifacial PV modules (485.8 t CO_{2eq}) and inverters (111.9 t CO_{2eq}) were constant across all configurations, while tracking motors added a smaller contribution of 1.5-2.6 t CO_{2eq} depending on the system. This pattern corroborates the trends reported in prior studies [50, 64].

3.4.4 Overall environmental impact assessment

In this section, all impact categories listed in Table 3.7 are assessed across all APV configurations compared to the baseline system (CGMPV) and country-level electricity grid mix at all locations at medium pitch spacing, with all systems normalized per functional unit for fair comparison. It should be noted that increasing row pitch reduces GHG emissions per kWh. This effect is due to minimizing near-shading losses between PV strings, which in turn improves the overall electricity conversion efficiency [48]. Consequently, with a fixed material inventory for a given capacity, a higher energy output effectively dilutes the life cycle impacts when normalized by the FU (kWh). The complete numerical results for all impact categories across all systems, locations and pitches are provided in [95].

3.4.4.1 Climate change

Assessing climate impacts across system types and regions provides insight into the decarbonization potential of APVs. Figure 3.9 presents the normalized GHG emissions across different APV configurations, crop groups, and locations, alongside comparisons with the country-specific electricity grid mix and CGMPV system.

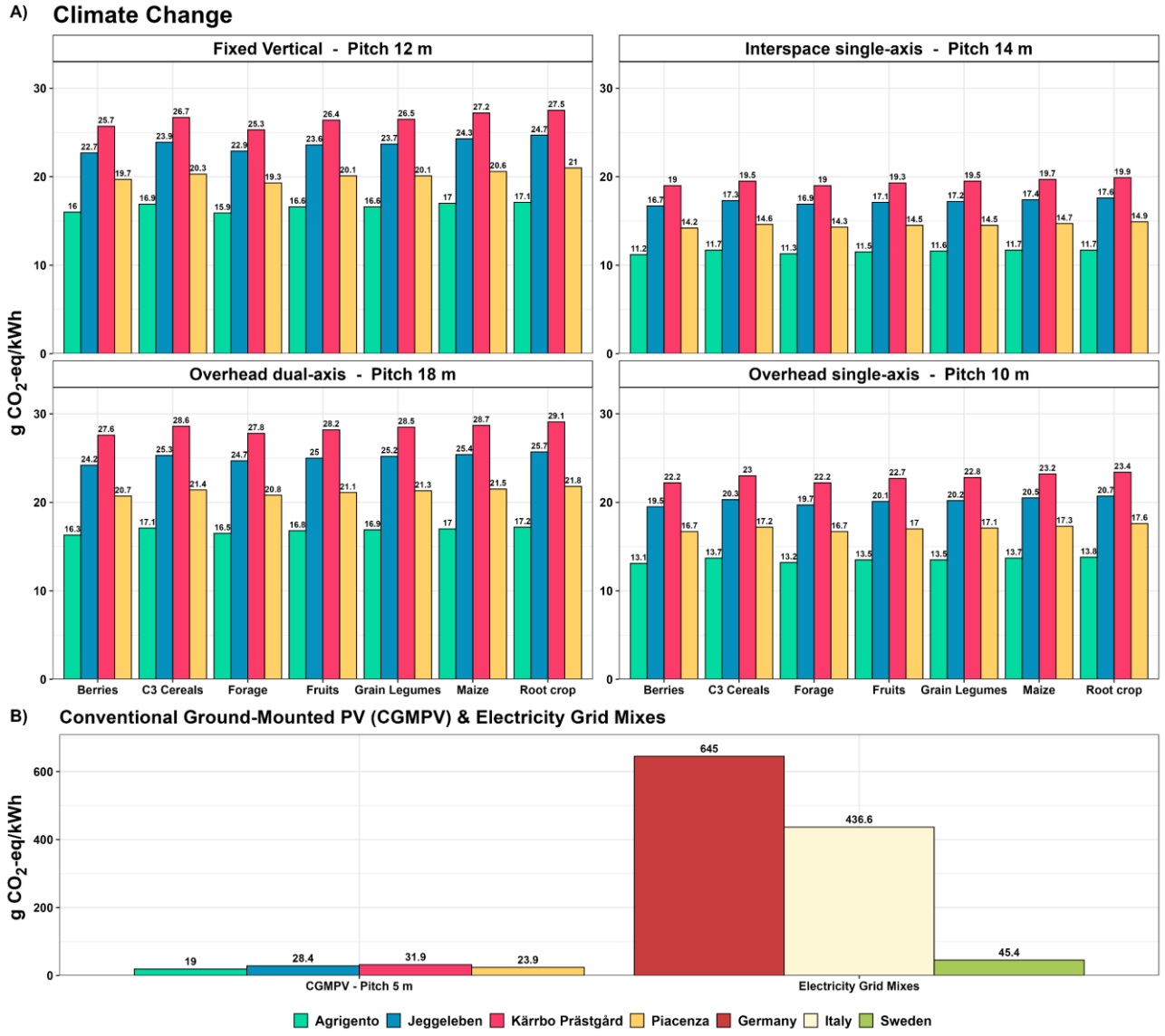

Figure 3.9 Comparative GHG emissions of APVs at the medium pitch per each configuration, CGMPV, and electricity grid mixes, normalized per kWh across multiple locations and crop groups.

The interspace single-axis system consistently demonstrates the lowest GHG emissions across all locations and crop types (11.2-19.8 g CO_{2eq}/kWh). The overhead dual-axis system consistently exhibits the highest GHG emissions per unit of electricity across all locations and crop types (16.3-29.1 g CO_{2eq}/kWh). The fixed vertical system depicts the second highest emissions (15.8-27.5 g CO_{2eq}/kWh), exceeding those of the interspace single-axis design [21]. The overhead single-axis system shows intermediate emissions (13.1-23.4 g CO_{2eq}/kWh), reflecting moderate structural requirements and additional tracking components compared to the fixed vertical system.

A pronounced geographic trend emerges across all system types, with Agrigento consistently yielding the lowest GHG emissions per kWh, followed by Piacenza, Jeggeleben, and Kärrbo Prästgård. Under

the interspace single-axis configuration, Agrigento achieves the lowest observed emission value for berries (11.2 g CO_{2eq}/kWh), while the same system for the same crop type in Kärrbo Prästgård emits nearly 19 g CO_{2eq}/kWh due to significantly lower solar intensity.

APV structural land occupation has a relatively minor influence on overall climate change results. The variations range from a minimum of 0.13 g CO_{2eq}/kWh in Agrigento for dual-axis APV systems to a maximum of 0.62 g CO_{2eq}/kWh in Kärrbo Prästgård for fixed vertical APV systems. The differences among crop types also have relatively minor influence on overall climate change results. However, the variations demonstrate both positive and negative impacts on GHG emissions. For example, in Kärrbo Prästgård's fixed vertical APV system, root crops result in additional GHG emissions of 1.08 g CO_{2eq}/kWh, while forage crops provide GHG emissions savings of 1.07 g CO_{2eq}/kWh. The highest normalized GHG emissions occur with dual-axis configuration on root crops in Kärrbo Prästgård (29.1 g CO_{2eq}/kWh), while the lowest emissions are achieved with interspace single-axis configuration on berries in Agrigento (11.2 g CO_{2eq}/kWh).

National grid mixes show the largest footprints among the electricity sources considered, with 645 g CO_{2eq}/kWh for Germany, 436.6 g CO_{2eq}/kWh for Italy, and 45.4 g CO_{2eq}/kWh for Sweden. Across all locations, APV configurations outperform both grid electricity and CGMPV systems, consistent with previous research [50, 60, 61, 65, 68, 69].

3.4.4.2 Photochemical ozone formation, and ozone depletion

Figure 3.10 shows the normalized photochemical ozone formation potential (POFP) and ozone depletion potential (ODP) of various APV configurations compared to the CGMPV system and the national electricity grid mix.

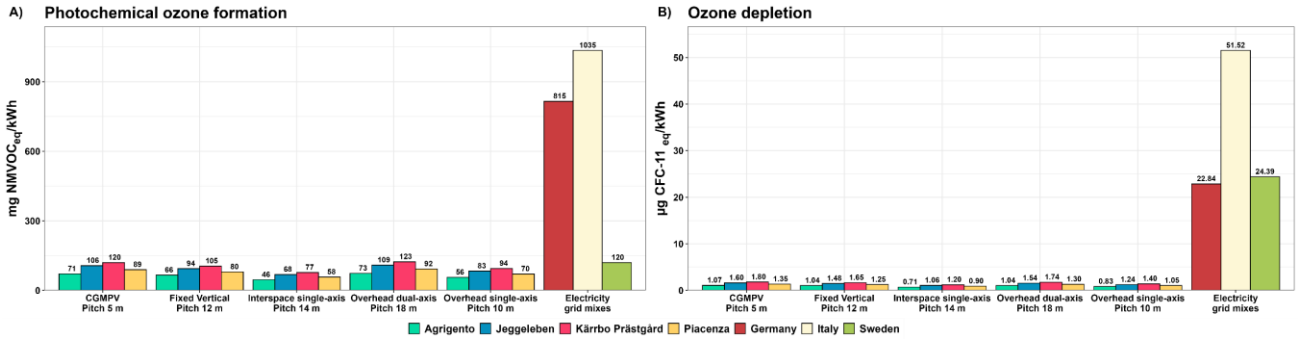

Figure 3.10 Normalized photochemical ozone formation potential (A) and ozone depletion potential (B) of APV systems across different configurations and locations compared to CGMPV system and national electricity grid mix.

For POFP (Figure 3.10A), APV systems range from 46 to 123 mg NMVOC$_{eq}$/kWh. The interspace single-axis system in Agrigento (highest irradiance) demonstrates the lowest POFP (46 mg

$NMVOC_{eq}$/kWh). Conversely, the overhead dual-axis APV system in Kärrbo Prästgård (lowest irradiance) exhibits the highest POFP (123 mg $NMVOC_{eq}$/kWh) due to its higher material intensity, complexity, and lower solar availability, leading to elevated normalized emissions. Most APV configurations generally outperform CGMPV systems, which average 106 mg $NMVOC_{eq}$/kWh and a peak of 120 mg $NMVOC_{eq}$/kWh in Kärrbo Prästgård. However, the worst-performing APV system in Kärrbo Prästgård slightly exceeds the peak CGMPV impact (overhead dual-axis at 123 mg $NMVOC_{eq}$/kWh). APV systems exhibit 8 to 23 times lower POFP than the Italian grid mix (1035 mg $NMVOC_{eq}$/kWh) and 7-18 times lower than the German grid mix (815 mg $NMVOC_{eq}$/kWh). While they are 1.1 to 2.6 times lower than the relatively clean Swedish grid (120 mg $NMVOC_{eq}$/kWh), the overhead dual-axis APV system in Kärrbo Prästgård (123 mg $NMVOC_{eq}$/kWh) shows a slightly higher impact than the Swedish grid. Regarding ODP (Figure 3.10B), APV systems range from 714 to 1740 µg $CFC\text{-}11_{eq}$/kWh. Consistent with POFP, the interspace single-axis system in Agrigento shows the lowest ODP (714 µg $CFC\text{-}11_{eq}$/kWh), while the overhead dual-axis APV system in Kärrbo Prästgård exhibits the highest (1740 µg $CFC\text{-}11_{eq}$/kWh), primarily driven by material intensity and energy yields. All APV configurations and CGMPV systems consistently demonstrate significantly lower ODPs compared to country-level electricity grids. For instance, APV systems are 29 to 71 times lower than the Italian grid mix (51.52 µg $CFC\text{-}11_{eq}$/kWh), and 12 to 31 times lower than both the German (22.84 µg $CFC\text{-}11_{eq}$/kWh) and Swedish (24.39 µg $CFC\text{-}11_{eq}$/kWh) grid mixes. Notably, unlike POFP, the German grid shows a marginally lower ODP than the Swedish grid. Compared to CGMPV systems (ranging from 1070 to 1800 µg $CFC\text{-}11_{eq}$/kWh), even the worst-performing APV system (overhead dual-axis in Kärrbo Prästgård at 1740 µg $CFC\text{-}11_{eq}$/kWh) shows a slightly lower ODP than the peak CGMPV.

3.4.4.3 Respiratory Inorganics

Figure 3.11 represents the normalized respiratory inorganics (particulate matter) potential.

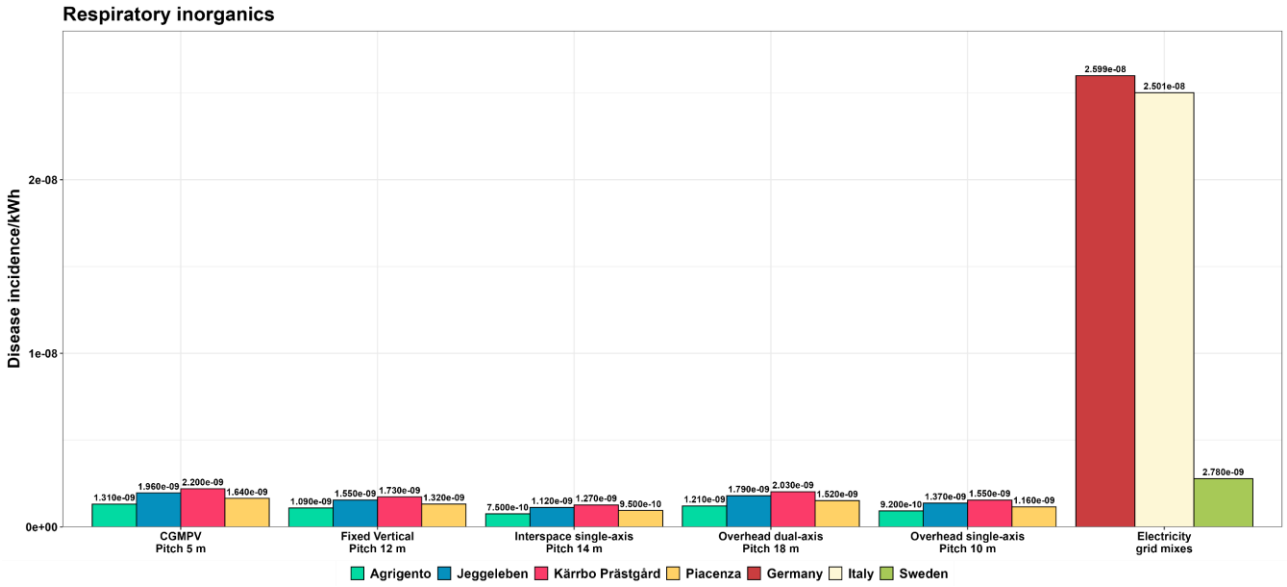

Figure 3.11 Normalized respiratory inorganics potential of APV systems across different configurations and locations compared to CGMPV system and national electricity grid mix.

Within the APV configurations, impacts vary from 7.5E-10 to 2.03E-09 Disease incidence/kWh. The interspace single-axis system in Agrigento records the lowest impact (7.54E-10 Disease incidence/kWh). Conversely, the overhead dual-axis APV system in Kärrbo Prästgård shows the highest impact (2.03E-09 Disease incidence/kWh), primarily due to its greater material intensity and complexity, coupled with lower local solar availability, which inflates normalized emissions. APV systems demonstrate a significantly lower impact, ranging from 12 to 33 times less than the Italian electricity grid (approx. 2.5E-09 Disease incidence/kWh), 13-34 times less than the German grid (approx. 2.6E-08 Disease incidence/kWh), and 1.4-3.7 times less than the Swedish grid (approx. 2.78E-09 Disease incidence/kWh). The German grid shows a marginally higher impact than the Italian grid, while the Swedish grid, consistent with its generally cleaner profile, presents a significantly lower impact than both German and Italian grids in this specific category. Comparing APV to the CGMPV system, most APV systems exhibit superior performance. CGMPV impacts range from 1.31E-09 Disease incidence/kWh (Agrigento) to a peak of 2.2E-09 Disease incidence/kWh in Kärrbo Prästgård, with an average of 1.77E-09 Disease incidence/kWh. Notably, even the worst-performing APV system (overhead dual-axis in Kärrbo Prästgård at 2.03E-09 Disease incidence/kWh) shows a lower impact than the peak CGMPV system. A similar trend has been documented by [50, 60, 61, 65].

3.4.4.4 Acidification

Figure 3.12 signifies the normalized acidification potential.

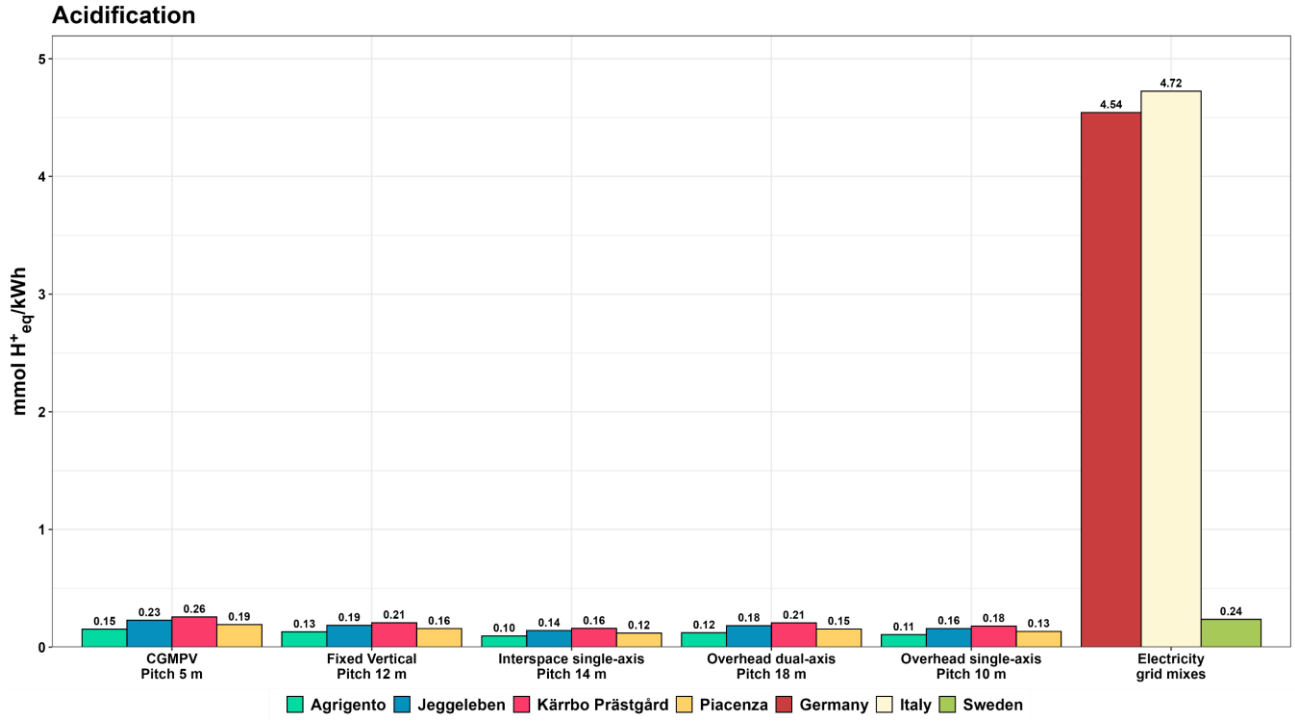

Figure 3.12 Normalized acidification potential of APV systems across different configurations and locations compared to CGMPV system and national electricity grid mix.

Examining the APV configurations, acidification impacts range from a low of 0.1 mmol $H+_{eq}$/kWh for the interspace single-axis system in Agrigento to a high of 0.21 mmol $H+_{eq}$/kWh for the fixed vertical APV system in Kärrbo Prästgård. APV systems demonstrate impacts that are 22 to 48 times lower than the Italian grid (approx. 4.72 mmol $H+_{eq}$/kWh) and 22 to 47 times lower than the German grid (approx. 4.54 mmol $H+_{eq}$/kWh). Even against the comparatively cleaner Swedish grid (approx. 0.24 mmol $H+_{eq}$/kWh), APV systems achieve a significant reduction, showing impacts 1.1 to 2.4 times less. Notably, the Swedish grid exhibits a substantially lower acidification burden than both its Italian and German counterparts, reflecting distinct profiles of acidifying substance emissions from their respective energy generation and industrial activities. When contrasted with the CGMPV system, APV systems generally present a more favorable environmental profile. CGMPV impacts span from 0.15 mmol $H+_{eq}$/kWh (Agrigento) to a peak of 0.26 mmol $H+_{eq}$/kWh in Kärrbo Prästgård, with an average of 0.18 mmol $H+_{eq}$/kWh. Crucially, even the highest-impact APV system records a lower impact than the peak CGMPV system and national grid mix, which are in line with [50, 60, 61, 65].

3.4.4.5 Eutrophication: freshwater, terrestrial, and marine

Figure 3.13 presents the normalized eutrophication potential for freshwater eutrophication (A), terrestrial eutrophication (B), and marine eutrophication (C).

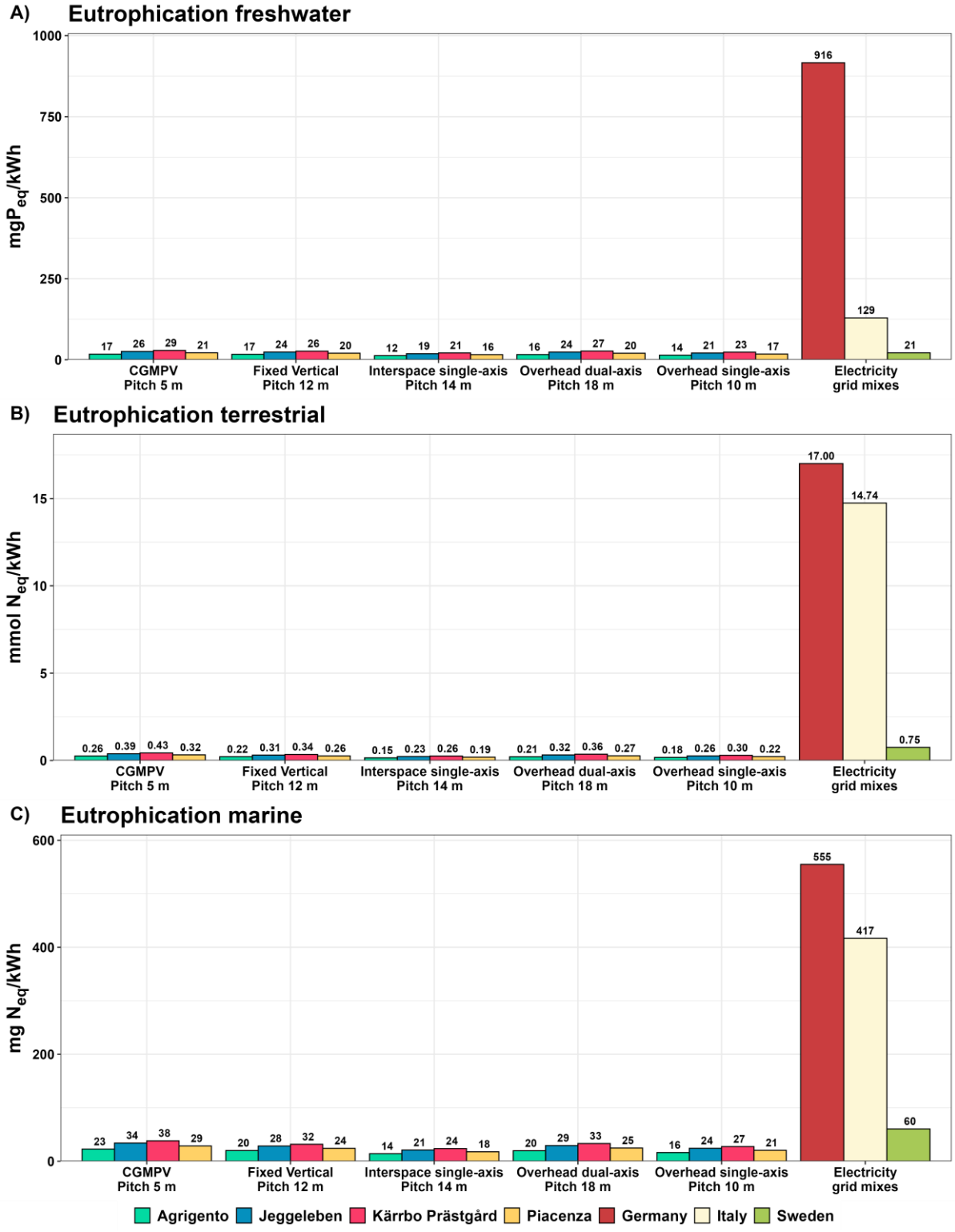

Figure 3.13 Normalized eutrophication potentials for freshwater (A), terrestrial (B), and marine (C) across various APV configurations compared to the CGMPV system and the national electricity grid mix.

For Freshwater Eutrophication (Figure 3.13A), the German grid shows the highest impact at ~916 mg P_{eq}/kWh, far exceeding the Italian (~129 mg P_{eq}/kWh) and Swedish (~21 mg P_{eq}/kWh) grids. APV systems are much lower, 12-26 mg P_{eq}/kWh, which is 34.5-73.6 times less than the German grid and 4.9-10.4 times less than the Italian grid. APV is generally comparable to or only slightly higher (≤1.3 times) than the Swedish grid. The interspace single-axis in Agrigento records the lowest impact (12 mg P_{eq}/kWh), while the overhead dual-axis in Kärrbo Prästgård is highest (26 mg P_{eq}/kWh). Compared with CGMPV (17-29 mg P_{eq}/kWh), most APV systems perform better, with the best achieving a 27% reduction and even the highest APV below the CGMPV peak. In terms of Terrestrial Eutrophication (Figure 3.13B), Germany again leads with ~17 mmol N_{eq}/kWh, followed by Italy (~15 mmol N_{eq}/kWh) and Sweden (~0.75 mmol N_{eq}/kWh). APV systems (0.15-0.36 mmol N_{eq}/kWh) are 47-111 times lower than Germany and 42-98 times lower than Italy, though up to 2.3 times higher than Sweden. The interspace single-axis in Agrigento has the lowest value (0.15 mmol N_{eq}/kWh) and the overhead dual-axis in Kärrbo Prästgård the highest (0.36 mmol N_{eq}/kWh). Most APVs outperform CGMPV (0.26-0.43 mmol N_{eq}/kWh), with the most efficient APV showing a 40% reduction and the highest APV still below the CGMPV peak. For Marine Eutrophication (Figure 3.13C), the German grid reaches ~555 mg N_{eq}/kWh, followed by Italy (~417 mg N_{eq}/kWh) and Sweden (~60 mg N_{eq}/kWh). APV systems (14-33 mg N_{eq}/kWh) are 16-39 times lower than Germany and 12-29 times lower than Italy, and up to 4.2 times lower than Sweden. The interspace single-axis in Agrigento records the lowest impact (14 mg N_{eq}/kWh), while the overhead dual-axis in Kärrbo Prästgård records the highest (33 mg N_{eq}/kWh). Compared with CGMPV (23-38 mg N_{eq}/kWh), APV generally performs better, with the most efficient APV reducing impacts by 27 % and the highest APV still below the CGMPV peak. All eutrophication results align with prior studies [50, 60, 61, 65].

3.4.4.6 Resource use

Figure 3.14 presents the normalized resource use for fossil (energy carriers), and for minerals and metals.

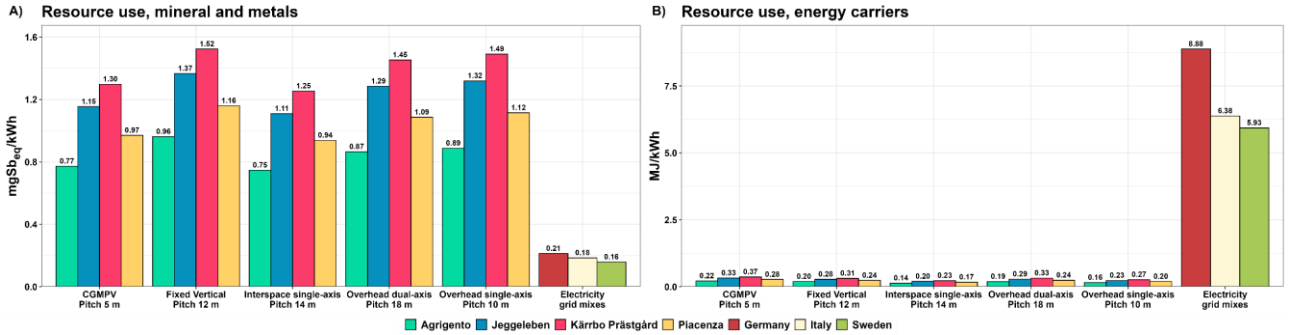

Figure 3.14 Normalized resource use potentials- minerals and metals (A) and fossils (B)-for various APV systems and locations, compared to the CGMPV system and national electricity grid mix.

A pronounced disparity in "Resource use, fossils" (Figure 3.14B) is evident between country-level electricity grids and solar PV technologies. Grids exhibit significantly higher impacts due to reliance on fossil fuels, directly depleting non-renewable energy carriers. The German grid records the highest impact at approximately 8.88 MJ/kWh, followed by the Italian and Swedish grids at around 6.38 and 5.93 MJ/kWh. In contrast, APV systems range from 0.14 to 0.33 MJ/kWh, equal to 18-64 times less than the respective grids. CGMPV spans 0.22-0.37 MJ/kWh, and the most efficient APV configuration achieves a 37% reduction versus the lowest CGMPV, while even the highest-impact APV remains below the peak CGMPV. This trend is consistent with [50, 60, 61, 65, 68].

Regarding "resource use, mineral and metals" category (Figure 3.14A), a distinct trend emerges relative to other categories. National grids show lower impacts, with Sweden at approximately 0.16 mg Sb_{eq}/kWh, Italy at around 0.18 mg Sb_{eq}/kWh, and Germany at approximately 0.21 mg Sb_{eq}/kWh. APV systems range from 0.75 to 1.52 mg Sb_{eq}/kWh, which is 3.5-7.2 times higher than Germany's grid, 4.1-8.3 times higher than Italy's, and 4.7-9.6 times higher than Sweden's. Within APV, the fixed vertical system in Kärrbo Prästgård is highest at 1.52 mg Sb_{eq}/kWh, largely due to ~12% higher steel intensity and lower solar availability inflating normalized results, while the interspace single-axis in Agrigento is lowest at 0.75 mg Sb_{eq}/kWh. CGMPV ranges from 0.77 to 1.30 mg Sb_{eq}/kWh; the most efficient APV is only marginally above the lowest CGMPV, whereas the highest-impact APV can exceed the peak CGMPV. These findings align with [50, 60, 61, 65].

3.4.5 Uncertainty analysis

To assess the robustness of the results, a Monte Carlo analysis was performed using SimaPro. The analysis focused solely on the PV component materials, as their contribution exceeded 95% of the total GHG emissions across all configurations, whereas the consequential elements accounted for less

than 5% (see Sections 3.4.1-3.4.3). Due to this imbalance, the uncertainty analysis was restricted to the attributional portion of the LCA.

Among the ten impact categories evaluated, Climate Change and Resource Use (Minerals and Metals) were selected for uncertainty analysis, as these categories showed the highest sensitivity in distinguishing between different APV configurations and the CGMPV system (see Section 3.4.4). Country-level electricity grid mixes were excluded from this analysis as their absolute impact values were orders of magnitude higher than those of APV and CGMPV systems. Furthermore, SimaPro defines grid inventories per unit of energy produced, making it incompatible with fixed-capacity comparisons like the 1 MW_p system size used here.

To improve visual interpretability, the probability distributions were smoothed using a moving average with a window size of three. Figure 3.15 presents the resulting distributions for the selected categories across all APV configurations and the CGMPV system, normalized to 1 MW_p installed capacity.

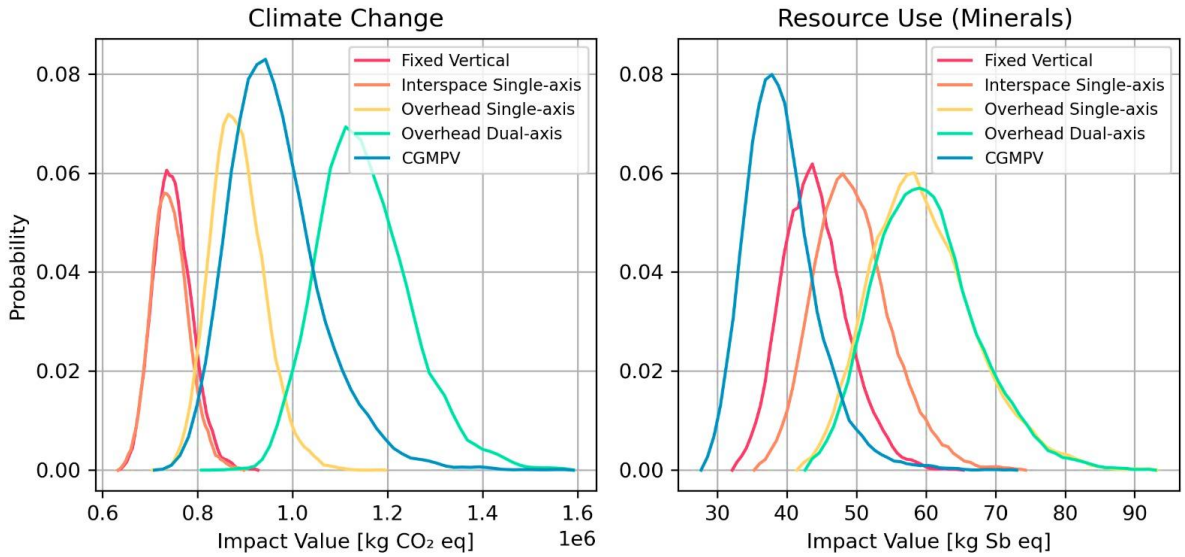

Figure 3.15 Smoothed probability distributions of life cycle impact values for APV configurations and CGMPV system (Monte Carlo uncertainty analysis for Climate Change and Resource Use impact categories, normalized to 1 MWp system capacity, PV components only).

In the climate change category (left), the fixed vertical and interspace single-axis systems exhibit very similar distributions, both displaying narrow peaks concentrated at lower CO_{2eq} values. This suggests a consistently low climate impact across simulations for these two APV configurations. Their probability distributions are skewed, with most values falling between approximately 600 and 850 t CO_{2eq}, indicating that they are likely to result in lower emissions compared to the other systems analyzed. Interestingly, the overhead single-axis system performs better than might be expected for

an elevated structure. Its distribution is generally lower than that of the CGMPV, with most values concentrated below 850 t CO_{2eq}. Although its climate impact is slightly higher than the fixed vertical and interspace single-axis configurations, it remains relatively modest. This indicates that the elevated mounting structure does not necessarily translate to significantly higher emissions, especially when compared to CGMPV systems. Notably, despite being structurally more demanding than its interspace counterpart, the overhead single-axis system exhibits lower average climate impacts than CGMPV, potentially due to more efficient use of materials such as steel and foundation elements.

The CGMPV system shows a broader distribution centered around 900 t CO_{2eq}, suggesting greater variability and a tendency toward higher emissions. It typically results in more substantial climate impacts than the fixed vertical, interspace single-axis, and overhead single-axis systems. Nonetheless, its distribution does overlap with those of other configurations, reflecting that in specific contexts or design implementations, CGMPV can still achieve relatively low emissions. In contrast, the overhead dual-axis system exhibits the highest climate change impacts overall, with a distribution that is both wide and right-skewed, extending up to approximately 1,600 t CO_{2eq}. This indicates a combination of high average emissions, likely driven by the increased structural and mechanical complexity required for dual-axis tracking and elevated module mounting. However, it is important to note that, despite the generally higher impacts associated with overhead dual-axis systems, the sensitivity analysis occasionally reveals lower emissions compared to CGMPV or overhead single-axis configurations. Such outcomes are consistent with scenarios in which competing systems underestimate their material requirements or where dual-axis designs achieve reduced material needs. The right panel shows the results for mineral resource use, where CGMPV demonstrates the lowest impact across all systems. Its sharply peaked distribution, centered around 38 kg Sb_{eq}, reflects low and consistent material demands. The fixed vertical system also performs well, with its distribution confined mainly to the 32-60 kg Sb_{eq} range. This suggests modest material requirements, likely due to its ground-mounted, structurally simple design. The interspace single-axis configuration displays a somewhat broader distribution that overlaps with the fixed vertical system but also extends toward higher impact values. While it can match the resource efficiency of simpler systems in some cases, it also shows a higher probability of increased mineral use, possibly due to additional tracking mechanisms or structural reinforcement. The overhead single-axis and overhead dual-axis systems show nearly identical and significantly wider distributions, peaking around 60 kg Sb_{eq} and extending beyond 90 kg Sb_{eq}. These results reflect the substantial material requirements for elevated, mechanically tracked systems. The similarity between these two configurations suggests that the elevated structure itself, rather than the number of tracking axes, is the dominant contributor to

mineral resource intensity. While overhead systems are clearly more resource-intensive [19], they offer key functional advantages such as increased clearance for machinery access, and crop operations [48]. These design benefits may be crucial in certain APV applications despite the environmental trade-offs. The remaining categories exhibited minimal variability, with impact values clustering tightly as shown in Figure 3.16.

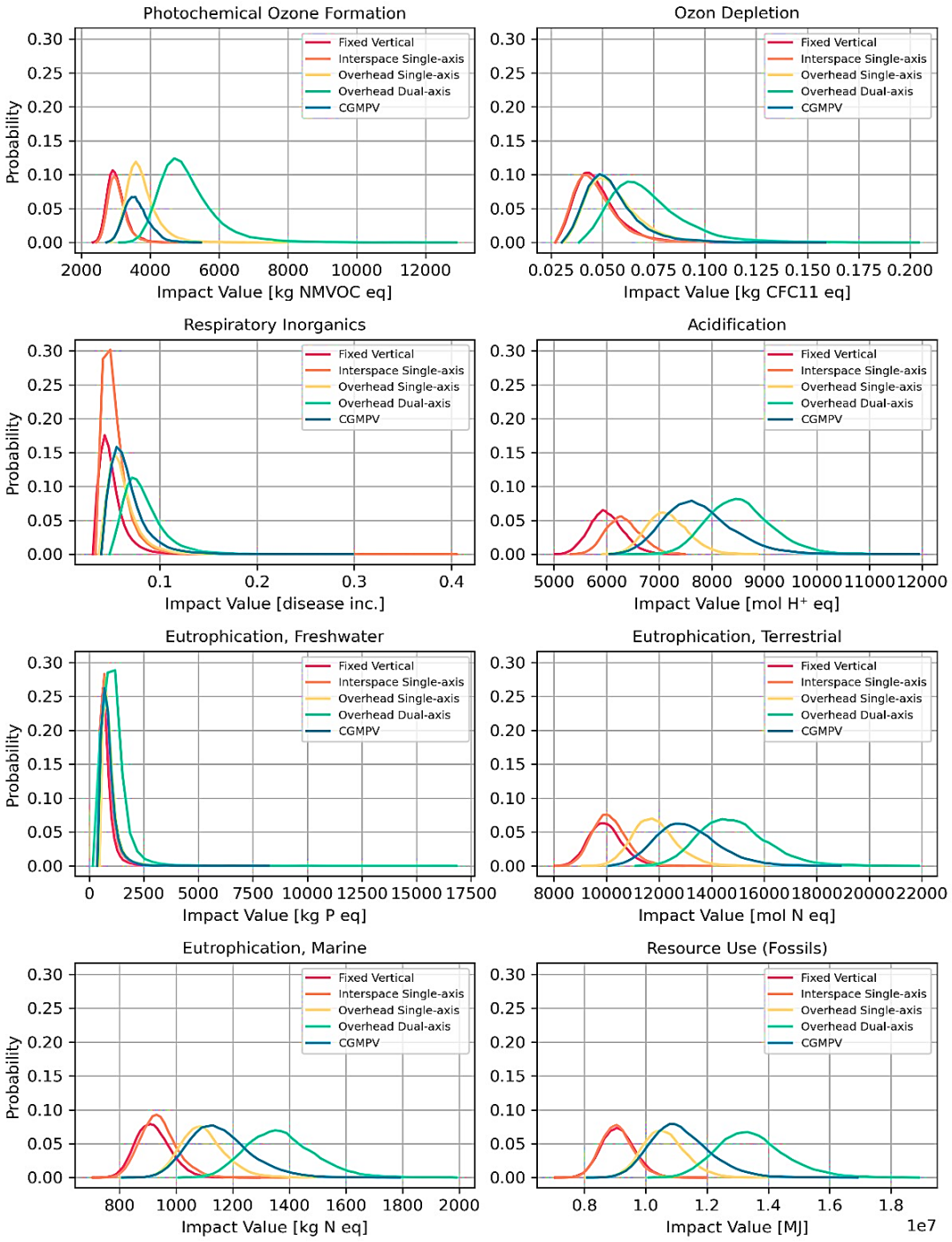

Figure 3.16 Probability distributions of additional environmental impact categories, including photochemical ozone formation, ozone depletion, respiratory inorganics, acidification, eutrophication (freshwater, terrestrial, marine), and fossil resource use, for all APV configurations and the CGMPV system.

Overall, the fixed vertical and interspace single-axis APV systems consistently exhibit lower impacts across most categories, particularly for respiratory inorganics, acidification, and eutrophication (freshwater and terrestrial). The CGMPV system generally performs well in resource use (fossils) and ozone depletion, showing compact distributions skewed toward lower values. The overhead dual-axis system tends to show the highest impacts in nearly all categories, especially for acidification, marine eutrophication, and fossil resource use, likely due to its greater structural and mechanical complexity similar to what was noted for Climate Change and Resource Use (Minerals). These results support the main findings by demonstrating that simplified or interspaced APV systems (i.e., fixed vertical and interspace single-axis) offer advantages not only in climate and mineral impacts but also across a broader range of environmental indicators. The CGMPV system remains efficient in certain categories but shows limitations in others. While overhead configurations may be advantageous for facilitating agricultural machinery access, improving crop management, or ensuring adequate ground clearance, they come at the cost of substantially higher environmental impacts, particularly in terms of emissions and resource use, highlighting the importance of carefully balancing agronomic functionality with environmental performance.

3.5 Discussion

3.5.1 APV structural land occupation

The nearly twofold variation in land occupation across designs therefore translates directly into a similar variation in environmental impact. The poor performance of the overhead single-axis system is not just a matter of occupying more space; its extensive land exclusion is the direct cause of it generating the highest GHG emissions (19.12 t CO_{2eq}). Conversely, the superior land-use efficiency of the overhead dual-axis system, achieved through its optimized design of moderate module density and short structural lengths [110], allows it to produce the lowest emissions (9.35 t CO_{2eq}). Interestingly, while the interspace single-axis system has a much longer structural length [107], its exceptionally high module density reduces the number of trackers needed (Table 3.6), leading to slightly better land-use efficiency. These findings highlight that structural design is a key factor in balancing energy conversion with agricultural land preservation while also determining ILUC-related GHG emissions and their resulting climate impacts.

3.5.2 Crop yield variations

The higher GHG emissions observed for most crops under the overhead dual-axis system are attributable to its greater shading intensity relative to single-axis configurations, consistent with previous studies linking APVs design choices to higher climate impacts [21]. A noteworthy observation emerges when comparing the two single-axis configurations. Although the interspace single-axis system has higher shading levels, it consistently shows lower total GHG emissions from yield loss than the overhead single-axis system. This occurs because the interspace system has a substantially smaller net cultivable land area available per megawatt, approximately 50% less (Table 3.8), which reduces the total crop loss and the resulting ILUC-related GHG emissions [31, 50, 64].

3.5.3 PV components

GHG emissions from PV components underscore the importance of structural optimization for the environmental performance of APVs. Steel was the dominant contributor, accounting for 118.6 t CO_{2eq} in the interspace system and up to 520.7 t CO_{2eq} in the dual-axis system. This finding confirms that structural BOS components are key environmental hotspots, as consistently reported in previous studies [50, 64]. The substantial variation, up to 55% between the most and least material-intensive configurations, can be attributed almost entirely to the amount of steel required for mounting structures, which is largely determined by design parameters such as installation height. These results clearly demonstrate that structural design choices have a decisive influence on the overall climate impact of APV installations.

3.5.4 Climate change

Across APV configurations, the climate change hierarchy is governed by structural height and associated steel demand, together with the added complexity of dual-axis actuation, which raises GHG impacts relative to single-axis alternatives, consistent with previous studies [19]. Systems with lower installation heights, such as the interspace single-axis design, require less steel and therefore achieve the lowest embodied emissions across sites. By contrast, the overhead dual-axis configuration has the highest impacts because taller supports and more complex mechanisms substantially increase material needs. Normalizing by electricity generation reduces but does not eliminate differences. Higher-yield trackers spread embodied burdens over more kWh, which is why the overhead single-axis system outperforms the fixed vertical configuration despite additional components. The geographic gradient from Agrigento to Kärrbo Prästgård reflects the primacy of solar resource, as higher irradiation in southern Europe lowers carbon intensity per kWh. Land occupation and crop-specific yield effects become minor once normalized, with crop responses to shading remaining

secondary to structural material intensity and energy yield. Grid footprints mirror generation mixes (Figure 3.6). Sweden's grid is predominantly low-carbon, with nuclear 42.2% and hydropower 41.6%. As shown in Figure 3.6, Italy is led by natural gas at 33.5%, with hydropower 21.5% and coal 16.6%. Germany is the most fossil-intensive, dominated by coal at 45.4%, with nuclear 15.5% and natural gas 9.9%. These structural differences in electricity generation technologies, particularly Germany's heavy reliance on coal, directly explain the pronounced variation in GHG emissions across the countries. Benchmarked against CGMPV and national grids, all APV systems show lower GHG intensities, in line with [50, 60, 61, 65, 68, 69]. The advantage is greatest where coal dominates, as in Germany, yet remains evident even against Sweden's low-carbon mix. Overall, the results underscore the decarbonization potential of APV and confirm that minimizing steel while maintaining high energy yield is critical to achieving the lowest climate impacts.

3.5.5 Photochemical ozone formation, and ozone depletion

The analysis of APV systems highlights their performance for both POFP and ODP, showing strong dependence on system design, material intensity, and solar irradiance. The interspace single-axis system performs best due to its optimized balance of material inputs and energy yield, achieving a 57% reduction in ozone precursor emissions compared with the average CGMPV. This also illustrates that not all APV configurations consistently outperform CGMPV, particularly in low-irradiance settings where the advantage narrows. Significant environmental gains arise when APV displaces grid electricity. Both impact categories underscore the importance of renewable deployment for reducing tropospheric ozone precursors and protecting the stratospheric ozone layer, particularly when substituting fossil fuel-intensive electricity. Interestingly, in contrast to POFP, the German grid exhibits a slightly lower ODP than the Swedish grid. This finding is counter-intuitive, given that Germany's electricity generation is largely coal-based (45.38%), whereas Sweden relies predominantly on low-carbon sources (Figure 3.6). However, this outcome reflects the specific life-cycle inventory data in the Ecoinvent v3.8 database, which attribute higher ODP to the upstream supply chains of nuclear and hydropower technologies in Sweden. Overall, APVs generally perform comparably to or better than CGMPV for ozone depletion, even under less favorable conditions, consistent with previous findings [50, 60, 61].

3.5.6 Respiratory inorganics

Respiratory-inorganics impacts are driven by combustion emissions and their precursors, so cross-country differences closely follow generation portfolios. Germany's coal-intensive grid mix (Figure

3.6) produces the highest disease-incidence burden, Italy shows intermediate impacts due to its natural-gas dominance with residual coal, and Sweden is much lower because nuclear and hydropower supply most of its generation. Against these baselines, all APV configurations are far lower. Within APV, performance reflects structural material intensity and solar resource. The interspace single-axis configuration achieves the lowest impacts in high-irradiance locations, where optimized structures and higher yields dilute manufacturing-phase particulate emissions per kWh. The overhead dual-axis configuration shows the highest impacts in low-irradiance northern sites, where greater mechanical complexity and lower generation raise normalized burdens. APV systems generally outperform CGMPV at the same sites, showing that yield gains from tracking and lean BOS inventories offset the simpler ground-mounted baseline, consistent with previous studies [50, 60, 61, 65]. Overall, replacing combustion-based electricity with APV provides substantial public-health benefits, with the greatest marginal gains in coal-heavy grids. Prioritizing configurations that minimize structural material while maximizing generation further reduces respiratory-inorganics impacts and strengthens APVs' role in mitigating adverse respiratory health outcomes.

3.5.7 Acidification

Acidification impacts are mainly driven by sulfur and nitrogen oxides from combustion. Germany's coal-heavy mix substantially elevates sulfur dioxide (SO_2) and nitrogen oxides (NO_x) emissions, creating the largest gap between its grid mix and APV systems. Italy's natural-gas-dominated mix lowers SO_2 but retains significant NO_x and a coal share, yielding intermediate impacts. Sweden's reliance on nuclear and hydropower suppresses combustion-related precursors and narrows the margin to APV, though APV still retains a clear advantage. Within APVs, impacts depend on structural material intensity and solar resource. Lean, high-yield designs, such as the interspace single-axis system in Agrigento, dilute manufacturing emissions per kWh, whereas heavier structures in low-irradiance sites, such as the fixed vertical system in Kärrbo Prästgård, raise normalized burdens. Overall, the most efficient APV achieves a 48% reduction in acidification impacts compared with the average CGMPV, confirming APV's consistent environmental advantage across conditions and supporting previous findings [50, 60, 61, 65].

3.5.8 Eutrophication: freshwater, terrestrial, and marine

Germany's coal-heavy mix releases the most phosphorus- and nitrogen-bearing precursors, explaining the large gap to PV. Italy's natural-gas-led mix yields intermediate burdens, while Sweden's nuclear and hydropower dominance suppresses combustion precursors and results in much lower values, especially for terrestrial and marine outcomes. These differences explain APVs' 34.5-

73.6 times advantage over Germany, 4.9-10.4 times over Italy in freshwater eutrophication, and similarly wide margins in the other subcategories. Within PV, differences are driven by structural mass and solar resource. Material-efficient, high-yield designs such as the interspace single-axis in Agrigento dilute manufacturing emissions, while heavier structures in low-irradiance sites, such as the overhead dual-axis or fixed vertical in Kärrbo Prästgård, raise normalized burdens but remain below CGMPV and far below grid levels. Overall, displacing combustion-based electricity with APV greatly reduces eutrophication across freshwater, terrestrial, and marine environments. The largest gains occur in coal-heavy grids, and within APVs the most effective strategy is combining lean support structures with high-irradiation sites to minimize impacts.

3.5.9 Resource use

For fossil resource use, the grid ranking reflects fuel portfolios. Germany's coal-heavy mix, Italy's substantial natural-gas share with residual coal, and Sweden's comparatively lower-fossil mix explain the order and the wide margins to PV. Solar PV avoids fuel combustion during operation; residual burdens stem from material supply chains and are diluted at high-irradiance sites, which is why APV options fall 18-64 times below the grids and frequently below CGMPV.

For mineral and metal resource use, the pattern reverses because the category tracks primary extraction of metals and minerals. Grid electricity relies largely on existing centralized assets with modest incremental material flows per kWh, whereas PV is fabrication-intensive. APVs increase structural demand relative to CGMPV, and designs with taller supports or greater steel content, coupled with low irradiance, raise normalized burdens. Thus the fixed vertical system in Kärrbo Prästgård sits at the upper end, while the interspace single-axis in Agrigento benefits from a material-efficient structure and strong yield. These trends in both subcategories of "Resource Use" are consistent with previous findings [50, 60, 61, 65, 68].

These contrasts point to actionable levers. For fossil resource use, any displacement of combustion-based electricity generation by APV confers immediate gains, with the largest benefits in fossil-intensive grids. For mineral and metal use, optimizing structural mass and layout, prioritizing high-irradiance siting, and advancing circularity and recycled content can materially reduce impacts. Overall, APV retains a clear advantage for non-renewable fossil resource depletion while requiring careful structural and supply-chain choices to manage mineral and metal use.

3.5.10 Study limitations and future directions

This comprehensive LCA study reveals clear environmental performance hierarchies while operating within methodological boundaries that inform future research priorities. The cradle-to-end-of-use

system boundary necessarily excludes EOL phase impacts due to insufficient reliable data for component recycling and disposal pathways. This limitation, though applied consistently across all configurations to maintain comparability, prevents full assessment of circular economy potential for systems containing substantial steel infrastructure ranging from 53.8 to 236.2 tons per megawatt peak.

Material inventories obtained directly from commercial manufacturers represent real-world deployed systems rather than theoretical designs, yet this specificity may limit generalizability across the broader technology landscape. While Monte Carlo analysis confirmed that performance rankings remain statistically robust despite input variability, absolute impact values may differ across manufacturers due to proprietary designs and structural variations. This uncertainty becomes particularly relevant given that steel consumption emerged as the dominant differentiating factor among configurations, suggesting that future research investigating alternative materials could substantially reduce both climate impacts and mineral resource depletion.

The assessment of agricultural impacts relies on meta-analytical regression models calibrated from existing APV studies rather than site-specific field measurements, introducing uncertainty in crop yield predictions across diverse pedoclimatic conditions. Similarly, ILUC emissions employ a static factor consistent with EU guidelines, which simplifies complex regional agricultural dynamics. However, these contributions proved relatively minor, accounting for less than 5% of total GHG emissions, suggesting that refinements to these factors would not substantially alter the comparative results.

The analysis utilizes Ecoinvent v3.8 integrated within SimaPro v9, which, while scientifically robust and widely cited, may not reflect the most recent refinements to background data, particularly for national electricity grid mixes found in newer database versions. Additionally, the temporal dimension of both electricity generation and climate conditions presents opportunities for enhanced analysis. Historical climate data spanning 2000 to 2024 captures substantial interannual variability including extreme events, yet assumes stationarity that may not adequately represent future conditions for infrastructure with thirty-year operational lifespans. Furthermore, the analysis based on annual average electricity production overlooks the potential value of tracking and vertical systems energy conversion during morning and afternoon peaks when they may displace carbon-intensive fossil fuel generation.

Future investigations should prioritize comprehensive cradle-to-grave assessments as recycling technologies mature and EOL data becomes available. Long-term field trials across diverse agricultural systems would strengthen crop yield models while accounting for emerging shade-

tolerant cultivars and management adaptations specific to APV environments. Integration of climate change projections would assess system resilience under non-stationary conditions, while social life cycle assessment (S-LCA) would capture broader sustainability dimensions including rural employment, energy justice, and community acceptance factors that influence successful deployment. These research directions would collectively strengthen the evidence base for optimizing APV systems within sustainable food-energy transitions.

3.6 Conclusion

This study conducted a comprehensive LCA to quantify the environmental performance of four APV configurations across different European climates, providing critical insights for sustainable energy and agricultural planning. The results clearly demonstrate that the choice of APV design is a paramount factor influencing its overall environmental footprint. The principal finding is the superior performance of the interspace single-axis APV system, which consistently yielded the lowest environmental impacts across nearly all ten investigated categories. For instance, its GWP ranged from approximately 11 to 20 g CO_{2eq}/kWh. In stark contrast, the overhead dual-axis system was the least environmentally favorable, with a GWP of 16 to 29 g CO_{2eq}/kWh.

In stark contrast, the overhead dual-axis system, despite its advanced tracking capabilities, it was still the least environmentally favorable configuration due to its significant material intensity, particularly due to the large quantity of steel required for its elevated structure. The fixed vertical and overhead single-axis systems showed intermediate performance, highlighting a clear trade-off between structural complexity, material demand, and energy conversion efficiency. The impacts from the consequential approach, accounting for crop yield variations and structural land occupation, contributed less than 5% to the total GHG emissions, making them secondary to the component-related impacts.

When benchmarked against conventional energy systems, all APV configurations offered dramatic improvements over electricity grid mixes in nine out of ten impact categories, underscoring their potential to drive deep decarbonization and mitigate issues like acidification, eutrophication, and air pollution. Furthermore, most APV designs outperformed CGMPV in environmental impacts, especially in climate change. This indicates that land dual-use does not inherently increase environmental burdens per unit of energy. Interspace single-axis, fixed vertical, and overhead single-axis APVs performed better overall, while the overhead dual-axis system, despite some benefits, underperformed CGMPV in certain high-impact cases, such as photochemical ozone formation in low-irradiance areas, due to its higher material intensity. The one exception was mineral and metal

resource use, where all PV systems were more impactful than grid electricity, highlighting the material intensity of PV infrastructure. Crucially, the Monte Carlo analysis confirmed the robustness of these findings. It showed that the performance rankings are statistically significant, with clear distinctions between the system configurations despite variability in background data. This gives strong confidence that the observed differences are inherent to the system designs rather than being artifacts of data uncertainty. While overhead systems provide greater clearance for agricultural machinery, this functionality comes at a considerable environmental cost. Our findings advocate for the preferential deployment of material-efficient like the interspace single-axis system where agricultural practices permit.

Chapter 4

Cross-validation of agrivoltaic simulation tools against field measurements under full-tracking and anti-tracking operation

4.1 Abstract

Advanced agrivoltaic (APV) plants increasingly combine bifacial modules with dual-axis tracking and crop-oriented operational modes, yet their energy performance is seldom validated under real operation, particularly for anti-tracking (AT). This study cross-validates PV simulation tools against field measurements from an overhead APV installation in Piacenza, Italy (507 kW_p), equipped with bifacial modules and horizontal dual-axis tracking, operating under both full-tracking (FT) and AT modes. Three commercial platforms (PVSOL, SAM, SISIFO) and an in-house developed tool (UCSC platform) were evaluated using three months of hourly energy conversion data (August–October 2025). Specific yield was computed as defined in IEC 61724-1, and model accuracy was quantified using standard statistical metrics. Under FT operation, the UCSC platform showed the closest agreement with measurements across monthly-to-hourly scales, maintaining deviations within 3.5%, whereas the commercial tools exhibited a systematic positive bias that increased toward autumn, reaching 20.9–27.5% overestimation in October. This divergence is consistent with limited support for the site's horizontal dual-axis tracking geometry and the inability to resolve module-to-module near-shading within multi-row tracker layouts. For AT operation, where no evaluated commercial tool provides a native modeling pathway, the UCSC platform captured the temporal dynamics of measured energy conversion (R^2>0.92), although errors increased under clear-sky conditions due to the sensitivity of AT to direct-beam deflection. Field measurements further quantified the climate dependence of the AT energy penalty, with daily yield reductions of 59.8% under clear-sky conditions but only 17.8% under overcast conditions. The findings indicate that energy yield assessments for advanced APV configurations and crop-prioritizing tracking strategies require specialized, site-validated modeling workflows to avoid optimistic yield projections.

Keywords: Agrivoltaic, Photovoltaic, Anti-tracking, Bifacial modules, Validation, Simulation.

4.2 Introduction

The escalating global demand for renewable energy and the urgent need to ensure food security amidst a changing climate have positioned agrivoltaic (APV) systems as a profoundly innovative and vital solution. By synergistically integrating solar electricity conversion with agricultural cultivation on the same land, APV systems directly address the pressing land-use conflict that often arises between these two critical sectors [115]. Beyond merely optimizing land utilization, APV systems offer multifaceted benefits, including mitigating agricultural yield losses, alleviating crop water stress, and providing crucial protection against extreme weather events such as heatwaves, frost, and drought [4, 13, 15, 109, 110]. Furthermore, these integrated setups can create a favorable microclimate beneath the solar panels, which has been shown to enhance the energy efficiency of the photovoltaic (PV) modules themselves [111, 112].

A pivotal advancement in optimizing the performance of APV installations lies in the implementation of dynamic solar tracking technologies [117], specifically dual-axis solar photovoltaic tracking (DASPT) systems. While fixed-tilt systems offer simplicity, dynamic systems, particularly those employing DASPT, are increasingly recognized for their superior capability to maximize solar energy capture by continuously adjusting PV module orientation throughout the day and across seasons [14, 110, 113]. In fact, DASPT systems can achieve up to a 30-45% enhanced power output compared to fixed PV systems [117]. Concurrently, the integration of bifacial PV modules further enhances the efficiency of these dual-use systems by harvesting sunlight from both their front and rear surfaces, effectively capitalizing on direct and reflected ground irradiance [3, 114, 115, 116, 117]. However, while these systems are inherently designed to maximize energy conversion, the core design challenge remains the trade-off between energy yield and crop requirements [3]. This unavoidable conflict necessitates flexible operational strategies, enabling the systems to shift from Full Tracking (FT), where panels are oriented perpendicular to the sun to maximize electricity [3, 108, 113], to Anti-Tracking (AT). In the AT mode, panels are positioned parallel to the sun’s direct beam to manage shading and prioritize crop light requirements, leading to increased light transmission to crops at the expense of energy conversion reduction [3, 14, 114].

It is imperative to acknowledge that "Anti-Tracking" represents a unique operational paradigm specific to the APV context, which explains the scarcity of literature on this specific topic. In standard PV applications, orienting panels away from the sun is counter-productive and economically baseless due to the deliberate loss of energy conversion. Consequently, scientific investigation into AT

performance has historically been minimal, as this mode possesses no utility in conventional solar farms. It is only within the APV environment, where the agricultural component demands sophisticated light management, that this strategy becomes relevant. More sophisticated approaches, termed Customized Tracking (CT) or Agronomic Tracking, involve intelligently time-multiplexing these modes to align with the varying light requirements of plants throughout their growth cycle [4, 15, 108]. These refined strategies necessitate using absolute light targets expressed in W/m^2 or $Wh/m^2/day$ rather than relying on estimated relative shading percentages [3]. This nuanced control over microclimatic factors contributes to substantial agronomic benefits, such as reducing sunburn damage in fruits, with studies showing a reduction from 13% damage in control apples to only 2% in apples under APV in one hot year [120]. Furthermore, dynamic APV systems have achieved remarkable water savings; studies on grapevine cultivation demonstrated a consistent reduction of crop reference evapotranspiration by approximately 65% over four consecutive seasons, resulting in irrigation water savings ranging from 37% to 62% [4]. In dryland ecosystems, the shading provided by PV arrays yields an Aridity Mitigation Potential, increasing Aboveground Net Primary Production by approximately 20% in dry years compared to open grasslands [121]. Novel tracking strategies, such as Critical-Time Anti-Tracking, optimize light distribution by applying Anti-Tracking only during critical crop physiological phases, enabling the achievement of nearly full commodity crop and energy production, maintaining 86.71% annual energy generation relative to solar tracking [23]. In a recent simulation-based study on single-axis APV systems, Tekie et al. [124] compared FT and AT modes alongside two novel crop-physiological tracking strategies such as Daily Light Integral Tracking (DLIT), which transitions from AT to FT once the crop's daily light requirement is satisfied, and Knee Point Tracking (KPT), which dynamically adjusts panel orientation based on the crop's light response curve. Their results for barley cultivation demonstrated that KPT achieved the optimal balance, with less than 2% reduction in crop yield compared to AT while maintaining over 85% of the energy output relative to FT.

Despite significant advancements in the conceptualization of these strategies, a key basic science and engineering challenge impedes broader commercial implementation including the lack of robust, real-time empirical validation of energy conversion performance for advanced APV systems under actual environmental conditions [23]. Although various simulation tools for the bifacial dual-axis APV performance under FT condition have been used so far [61, 119], systematic cross-validation against real-world measurements for AT operation has not yet been established [23]. This limitation is reinforced by the fact that most commercial platforms not only lack the native functionality to

simulate AT logic but also provide limited functionality for modeling advanced APV systems (overhead bifacial dual-axis) under FT condition with key installation parameters such as row pitch and installation height. These constraints hinder comprehensive and reliable comparative analyses. Addressing these limitations necessitates the use of specialized integrated simulation tools, which account comprehensively for geometric layout, dynamic shading, and bifacial performance [26].

This study directly addresses these identified gaps by conducting a systematic comparative analysis of FT and AT APV systems, cross-validated with both commercial tools and an in-house developed tool (UCSC platform). The research provides real-time field data from a cutting-edge overhead dual-axis APV installation equipped with bifacial PV modules in Piacenza, Italy, offering empirical insights into the energy conversion performance based on measured meteorological and energy output data collected between 1 August and 31 October 2025. Unlike previous studies restricted to single-axis or fixed-tilt systems [53, 108], this work quantifies the trade-offs in energy conversion resulting from operating in FT versus AT modes. Furthermore, a cross-simulation analysis was conducted using established commercial software tools, including PVSOL, SISIFO, and System Advisor Model (SAM), and the UCSC developed platform. By validating experimental findings through error analysis, this study aims to provide foundational knowledge for the sustainable deployment of APV systems, specifically supporting the advancement of renewable energy conversion capabilities under dual-land use.

4.3 Materials and methods

4.3.1 Study area and system configuration

The overhead dual-axis APV system examined in this study is situated at the Piacenza campus of Università Cattolica del Sacro Cuore, Italy (45.0378° N, 9.7303° E). Figure 4.1 provides a detailed view of an individual tracker, which is identical across the plant, and the overall layout of the field.

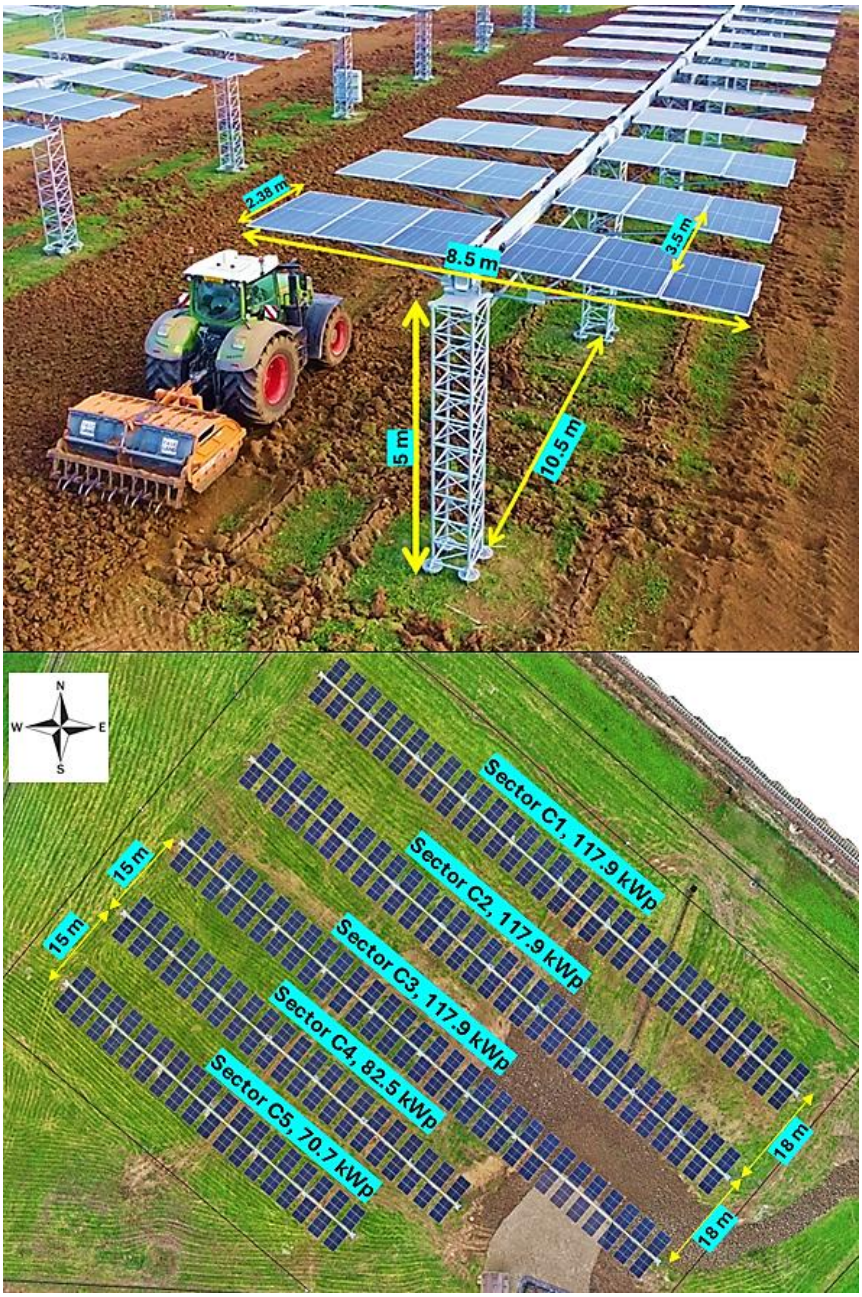

Figure 4.1 Design and layout of the on-site overhead horizontal dual-axis APV system located in Piacenza, at the Università Cattolica del Sacro Cuore campus.

The installation consists of 43 horizontal dual-axis trackers mounted on elevated structures with a ground clearance of 5 m (as shown in Figure 4.1), which enables the passage and operation of agricultural machinery. Each tracker is 10.5 m long and supports 3 rows of 6 PV modules in landscape orientation, yielding 18 modules per tracker and a total width of 8.5 m. Each PV module has a length of 2.38 m, with a module-to-module row spacing of 3.5 m. In total, the system comprises 774 bifacial PV modules rated at 655 W_p each, corresponding to an installed capacity of 506.97 kW_p and occupying an area of 0.72 ha. The APV plant was organized into 5 PV strings divided into two groups,

one with a pitch of 18 m corresponding to a Ground Coverage Ratio (GCR) of 30% and the other with a pitch of 15 m corresponding to a GCR of 35%. Due to site-specific land constraints, the PV arrays were oriented at an azimuth angle of 131° from north, deviating from the optimal south-facing direction (180°). Detailed technical specifications of the trackers, PV modules, and on-grid inverters are provided in Table 4.1.

Table 4.1 Technical characteristics of the APV plant as an input data in the simulation.

Parameters	Specifications
Tracker system	
Model	REM TEC®, HORIZONTAL TRACKER 3D – T2.1 [110]
Tracker max/min rotation angle of primary axis (°)	±41
Tracker max/min rotation angle of secondary axis (°)	±41
PV module	
Model	HISUNAGE, HSGDG655-132M12 [126]
Nominal capacity (W_p)	655
Efficiency (%)	21.09
Bifaciality factor (%)	75
Nominal Operation Module Temperature (°C)	44 (±2)
Temperature coefficient for P_{max} (%/°C)	-0.35
Number of cells	132 (66×2)
Dimension (L×W×H)	2.38×1.30×0.35 m
Inverter	
Model	GROWATT, MAX 125KTL3-X LV [127]
Nominal AC power	125 kW
Max. Efficiency (%)	98.8
Euro. Efficiency (%)	98.5
AC output	Triple-phase
Grid frequency range (Hz)	50/60
Grid voltage range (V)	230/400

4.3.2 Operational tracking strategies

Data collection for FT operation was carried out for the entire daytime period between 1 August and 31 October 2025. The dataset includes the hourly energy output measured by the APV system's sensors. In contrast, AT operation was monitored only over two full day periods on 7 October (clear-sky condition) and 21 October (cloudy condition). For these experiments, AT mode was applied

exclusively to Sectors C4 and C5 (as shown in Figure 4.1), representing two out of the five sectors in the APV field. This restricted testing was necessary because the APV plant under investigation is grid-connected for economic purposes and also supplies part of the university's electrical demand. Operating the entire installation in AT mode would impose substantial energy losses, making extended AT operation neither financially nor operationally justified. Accordingly, AT testing was limited in duration and spatial extent while still ensuring sufficient data to evaluate performance differences between FT and AT operation. The experimental setup comparing the two tracking modes at the Università Cattolica del Sacro Cuore campus on a clear-sky day is shown in Figure 4.2.

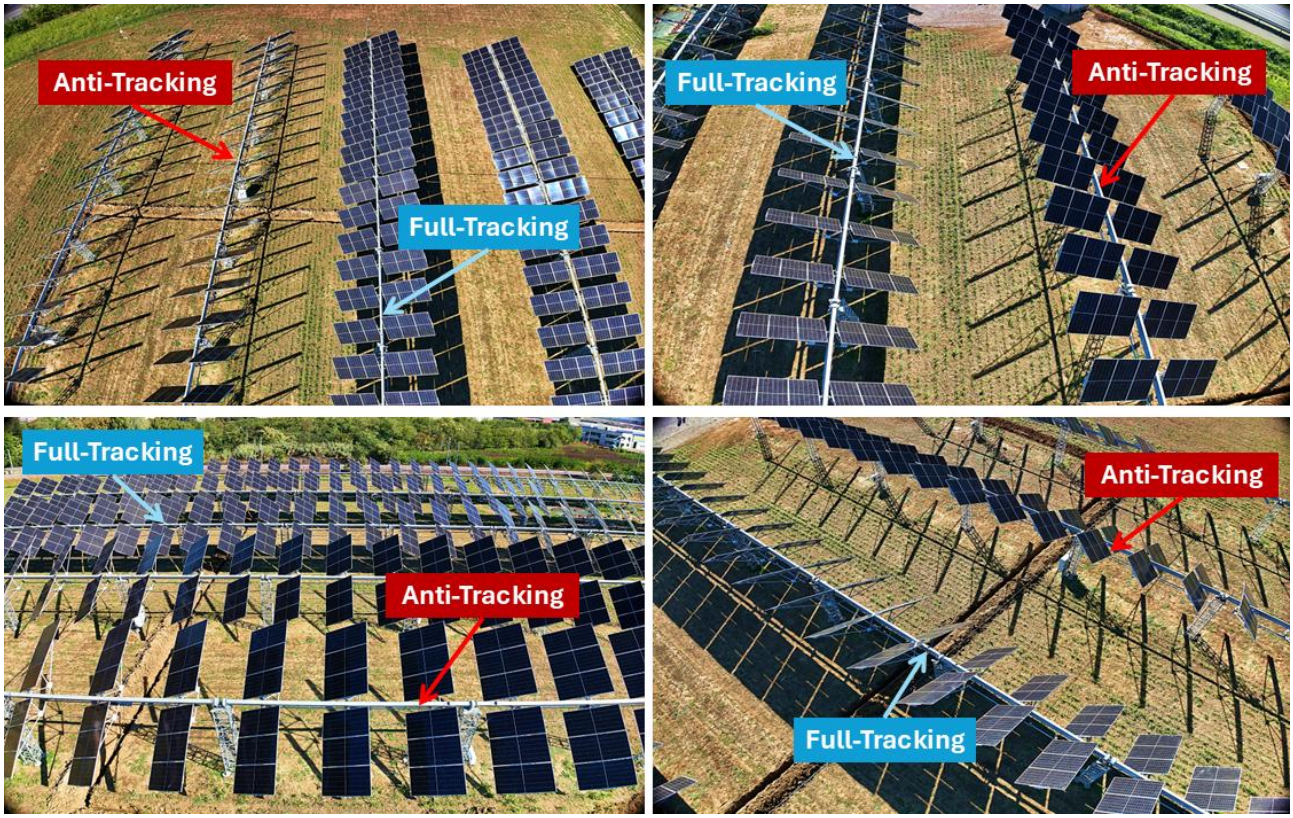

Figure 4.2 Aerial view of the APV plant at the Piacenza campus of Università Cattolica del Sacro Cuore, comparing FT and AT modes on a clear-sky day (7 October 2025, 12:00 CEST).

4.3.3 Software tools and simulation workflow

The selection of software for this study was performed through a comprehensive evaluation process designed to identify tools capable of simulating a complex system involving dual-axis tracking, bifacial PV modules, and the integration of measured meteorological data. This rigorous filtering was a critical first step to ensure the validity and reliability of the simulation results presented in this work.

The initial investigation included a broad range of software. To conduct this preliminary assessment efficiently and without a significant financial burden, a multi-tiered approach was adopted for access. Freely available, open-access versions of several platforms were used, which allowed for a rapid evaluation of their fundamental capabilities. For proprietary software, full-featured free trial periods were utilized, providing a crucial window to test specific, advanced functionalities essential to the present case study. This systematic method enabled the identification of limitations in many tools that, while excellent for standard simulations, could not meet the specific requirements of the advanced system under investigation. For example, it was observed that RETScreen is designed for simplified analyses and lacks the ability to natively model bifacial gain as a dynamic variable dependent on location and environmental conditions.

The comprehensive assessment included a total of seventeen platforms, comprising two distinct groups. Within the category of Standalone Desktop Software, it was determined that PVsyst, RETScreen, HOMER Pro, PV-F-Chart, Solarus PV, BlueSol, and Solar Pro were all limited in their ability to simulate both bifacial modules and dual-axis tracking simultaneously. Additionally, RETScreen, Solarus PV, and BlueSol were found to have a limitation in using measured meteorological data. For the Web-based Platforms, the same limitations regarding bifacial modules and dual-axis tracking applied to PVWATTS, PVGIS, Global Solar Atlas, Solargis, PROSPECT, HelioScope, and Sunny Design. Furthermore, PVGIS and Global Solar Atlas were limited in their use of measured meteorological data.

This thorough filtering process resulted in the selection of three distinct software platforms that possess the required capabilities for this study, namely PVSOL (v.R3, 2025), SAM (v.R1, 2025), and SISIFO (v3.3, 2025). These tools were used in a comparative analysis, along with the in-house tool (UCSC platform) developed by Università Cattolica del Sacro Cuore, to simulate the system's performance and to benchmark their results against actual hourly energy output measured by the operational site's sensors.

PVSOL is a dynamic simulation program with 3D visualization and shading analysis for the calculation of PV systems. Developed by Valentin Software, this commercial platform represents one of the most comprehensive tools available for PV system design and performance analysis [56]. The platform incorporates sophisticated modeling approaches including enhanced single-diode models for PV modules, thermal balance equations for temperature calculations, and various transposition models for solar irradiance analysis. PVSOL supports advanced system configurations including bifacial PV modules and tracking systems, making it particularly suitable for complex PV

installations. The software enables comprehensive loss analysis, while providing capabilities for defining critical installation parameters such as pitch, clearance height, and ground albedo values. In this study, PVSOL was accessed through its free trial period.

SAM is a performance and financial model developed and distributed by the National Renewable Energy Laboratory (NREL) [128]. This open-source desktop application represents a comprehensive techno-economic simulation platform specifically designed for renewable energy systems analysis. SAM incorporates bifacial irradiance model and employs the California Energy Commission single-diode model for PV module characterization and utilizes Isotropic or Perez transposition model for solar irradiance calculations [129]. SAM supports extensive system configurations including bifacial modules, tracking systems, and comprehensive loss mechanisms. The platform provides comprehensive capabilities for defining system geometry, including pitch spacing, module heights, and ground albedo parameters, making it particularly valuable for advanced APV system analysis. SAM is freely available as a desktop application.

SISIFO is an online, free-software simulator of PV systems developed by the Institute of Solar Energy at Universidad Politécnica de Madrid in the frame of the European project PVCROPS, allowing the simulation of PV system performance evaluation [130]. The software employs empirical PV module efficiency models combined with Nominal Operating Cell Temperature (NOCT) temperature modeling approaches. SISIFO provides comprehensive support for bifacial PV systems and tracking configurations, with particular strengths in modeling complex geometric arrangements. The platform uniquely offers explicit definition capabilities for module-to-module row spacing, a critical parameter often overlooked in other simulation tools but essential for accurate APV system modeling. SISIFO supports loss analysis, while enabling users to define essential installation parameters such as pitch, clearance height, and site-specific albedo values for enhanced accuracy in performance predictions. This approach of cross-referencing results across multiple capable platforms strengthens the integrity of the methodology and the findings. A comparative summary of the key capabilities of the selected tools is provided in Table 4.2. The structure and criteria of this comparison draw upon prior reviews and validation studies of PV simulation tools, which have systematically evaluated their general modeling frameworks, loss factors, and applicability across different case studies [124, 125, 126].

Table 4.2 Comparative capabilities of the PV simulation tools used in this study [124, 125, 126].

	PVSOL	**SAM**	**SISIFO**
Model of PV module	Enhanced single diode	Single diode (CEC model)	PV module efficiency model (empirical)
Temperature model	Thermal balance equation	NOCT	NOCT
Transposition model (Perez)	●	●	●
Bifacial PV support	●	●	●
Vertical dual-axis tracking support	●	●	●
Horizontal dual-axis tracking support	⊗	⊗	●
Primary axis rotation limit (user input)	●	⊗*	●
Secondary axis rotation limit (user input)	●	⊗*	●
AC/DC wiring loss	●	●	●
Mismatch loss	●	●	●
Soiling loss	●	●	●
Shading loss	●	●	●
Array pitch, height, albedo (user input)	●	●	●
Module-to-module row pitch	⊗	⊗	●
Hourly measured climatic data (user input)	●	●	●

(● = available; ⊗ = not available), *SAM provides only a single 'Tracker rotation limit' parameter accessible through single-axis mode though applied to dual-axis configuration in background simulations.

To ensure consistency and comparability across all simulations, the same PV module and inverter specifications (Table 4.1) and identical hourly meteorological datasets were used across the simulation tools. The dataset comprised GHI, ambient temperature, and wind speed, obtained from a real-time meteorological measuring station in Piacenza [134] at hourly intervals for the period from 1 August to 31 October 2025. Meteorological parameters were imported into the simulation tools at hourly resolution, while albedo values were incorporated at monthly resolution due to platform-specific constraints. A constant albedo value of 0.2 was applied throughout the simulation period, consistent with typical values reported in APV systems [125].

The simulations also reflected the real system configuration including APV orientation, pitch, clearance height from the ground, and PV module's layout as previously described in section 4.3.1. Soiling and mismatch losses were each assumed to contribute 2% to the total system losses, while AC/DC wiring losses were set at 3% in the performance simulations [135]. Additional losses were calculated automatically by the simulation tools.

Regarding UCSC developed platform, a Python-based simulation framework was employed to model hourly electricity conversion by APV systems equipped with bifacial PV modules. Meteorological inputs can be obtained from field measurements or external datasets, and the data are processed to derive the irradiance and atmospheric variables required for the simulations. Solar geometry is calculated using the astronomical algorithms available in PVLIB [136], which ensures consistency with widely used PV modeling practices. When direct and diffuse irradiance components are not available, GHI is decomposed into beam and diffuse components using the empirical models included in PVLIB. These models include ERBS, DIRINT, DISC and Boland. Tracking configurations are represented using PVLIB's formulation for single-axis trackers, while dual-axis tracking is implemented using a custom geometric optimization routine adapted from the REM TEC® methodology [110]. Backtracking and self-shading avoidance follow the method presented by [137]. Bifacial irradiance is calculated using the view-factor-based method implemented in PVLIB's pvfactors module [136]. This approach accounts for system geometry, inter-row shading, sky and ground reflections, and the angular distribution of irradiance on both sides of the module. Module operating temperature is estimated with NOCT model. The DC power output is computed using the De Soto five-parameter single-diode model [138], which is solved analytically with the Lambert-W formulation as implemented in PVLIB [139]. Front and rear irradiance contributions are combined using the module's bifaciality factor. Finally, system-level losses resulting from soiling, mismatch, wiring and inverter conversion are applied in order to obtain AC power. The complete computational workflow is presented in the following flowchart.

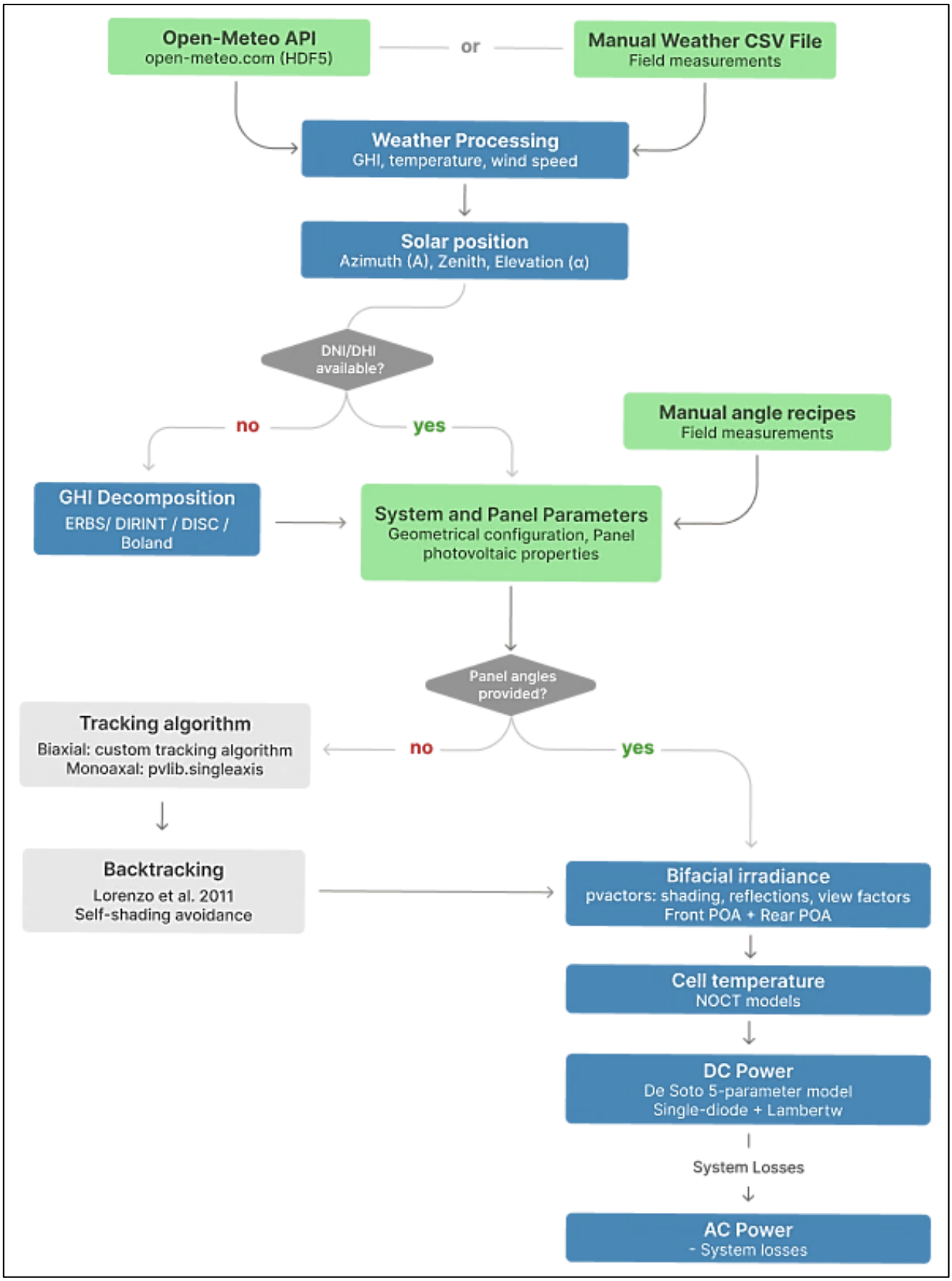

Figure 4.3 Flowchart of the UCSC developed framework used in the simulation process.

4.3.4 Performance indicator

The energy performance evaluation of the APV system was conducted using standardized performance indicators established by the International Electrotechnical Commission (IEC) 61724-1 standard [140]. The performance metric, specific yield (SY), was employed to quantify energy productivity under real operational conditions. SY quantifies the normalized energy conversion efficiency by expressing the ratio of net energy conversion by the APV plant to the nominal power capacity of the PV arrays, as shown in Eq. 4.1 [141]:

$$SY = \frac{E_{out}}{P_{nom}} \quad \text{Eq. 4.1}$$

Where SY denotes the specific yield (kWh/kW_p), E_{out} is the total energy output from APV system at each hour (kWh), and P_{nom} is the nominal power capacity (kW_p). SY enables performance benchmarking independent of system size and facilitates.

4.3.5 Statistical validation and error analysis

Model performance validation was conducted through comprehensive error analysis comparing simulated outputs from PVSOL, SAM, SISIFO, and UCSC developed platform against measured hourly energy output from the APV system's sensors. This cross-validation approach strengthens the robustness of the present work. The statistical framework employed five error metrics to assess prediction accuracy, systematic bias, and correlation strength, following established practices in PV performance modeling [135, 136].

All statistical computations in this study were performed using MATLAB (v.R2024b), a technical computing platform developed by MathWorks for numerical and statistical analysis [144], ensuring precision and reproducibility of the error analysis results. The complete error analysis framework is presented in Table 4.3.

Table 4.3 Error metrics for validation and performance assessment of PV simulation tools and UCSC developed platform in this study [124, 138].

Error metrics	Application	Formula
Mean Absolute Error (MAE)	Indicating the accuracy with which each software predicts energy outputs compared to actual measurements. A smaller value indicates better forecast accuracy.	$MAE=\frac{\sum_{i=1}^{n}\lvert\hat{y}_i-y_i\rvert}{n}$ Eq. 4.2
Root Mean Square Error (RMSE)	A standard way to measure the error of a model in predicting quantitative data, representing the square root of the average of squared differences between predicted and actual values, giving more weight to larger errors. A lower value indicates a better fit.	$RMSE=\sqrt{\frac{\sum_{i=1}^{n}(\hat{y}_i-y_i)^2}{n}}$ Eq. 4.3
Mean Absolute Percentage Error (MAPE)	Indicating the mean absolute error as a percentage of the actual values. A lower value indicates better predictive performance.	$MAPE=\frac{\sum_{i=1}^{n}\lvert\frac{\hat{y}_i-y_i}{y_i}\rvert}{n}\times 100$ Eq. 4.4
Coefficient of Determination (R^2)	Indicating the proportion of the variance in the actual data that is predictable from the model. A higher value signifies a better goodness of fit.	$R^2=1-\frac{\sum_{i=1}^{n}(y_i-\hat{y}_i)^2}{\sum_{i=1}^{n}(y_i-\bar{y}_i)^2}$ Eq. 4.5
Mean Bias Error (MBE)	Indicates the average bias in the model's predictions. A MBE close to zero is desirable.	$MBE=\frac{\sum_{i=1}^{n}(\hat{y}_i-y_i)}{n}$ Eq. 4.6

Note: $\hat{y}_i$ = Predicted values, y_i = Measured values, $\bar{y}_i$ = Mean of measured values, n = Number of observations.

4.4 Results and discussion

4.4.1 Monthly and weekly energy performance under full tracking operation

Figure 4.4 presents the monthly aggregated SY comparison between measured values and simulation outputs from all platforms over the three-month monitoring period.

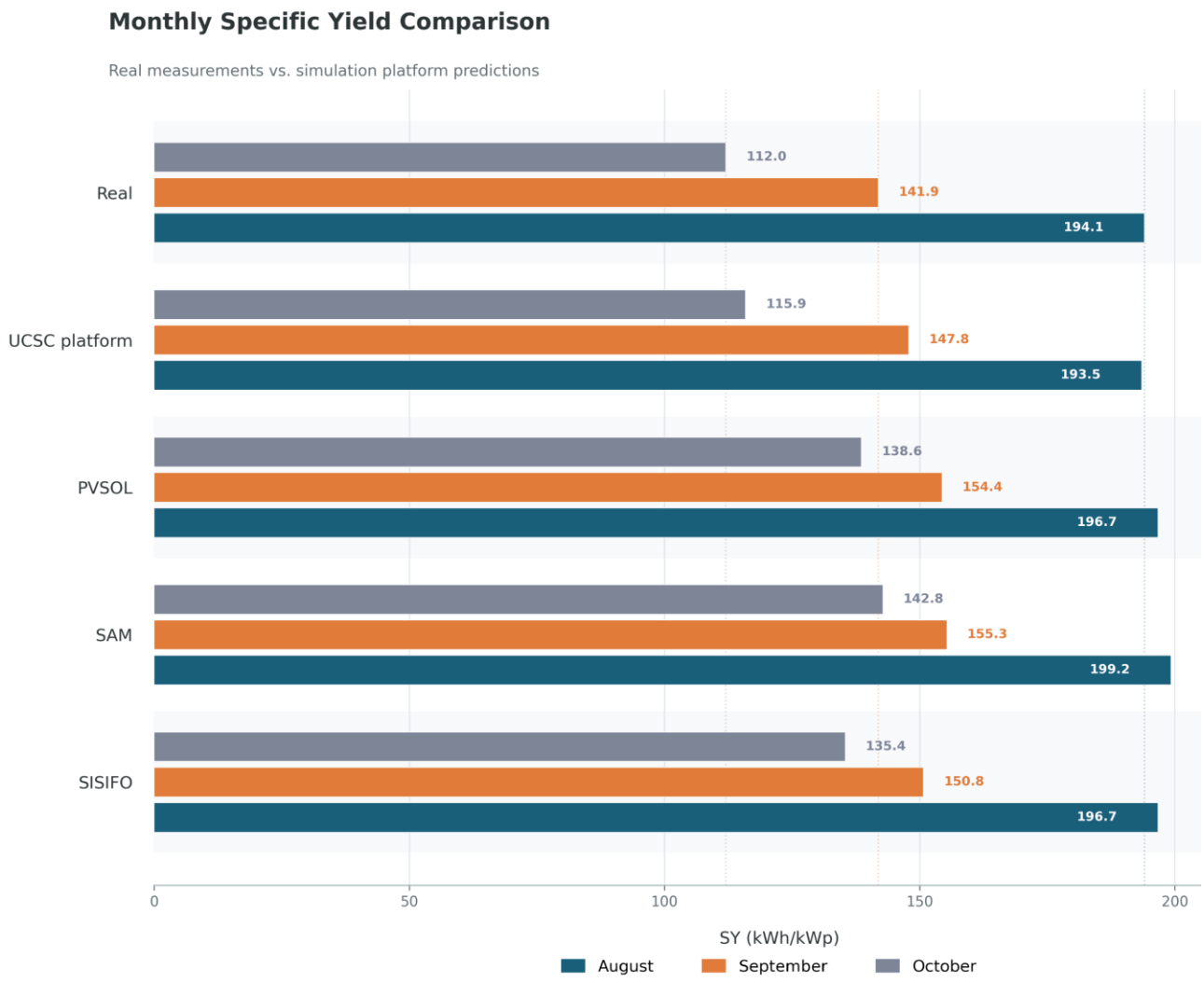

Figure 4.4 Comparison of measured and simulated SY at monthly temporal resolution for FT operation from August to October 2025.

The measured SY exhibited a pronounced seasonal decline from 194.1 kWh/kW$_p$ in August to 141.9 kWh/kW$_p$ in September and 112.0 kWh/kW$_p$ in October, representing an overall reduction of 42% attributable to decreasing solar elevation angles, shortened daylight duration, and increased cloud cover characteristic of autumn in northern Italy. The UCSC platform demonstrated superior agreement with measured values across all months, predicting 193.5, 147.8, and 115.9 kWh/kW$_p$ for August, September, and October respectively, with deviations consistently within 3.5%. Commercial tools exhibited systematic positive bias that intensified progressively. In October, PVSOL, SAM, and SISIFO overestimated measured values by 23.8%, 27.5%, and 20.9% respectively, compared to only 3.5% for the UCSC platform.

The weekly disaggregation shown in Figure 4.5 provides finer temporal resolution across the 13-week monitoring campaign.

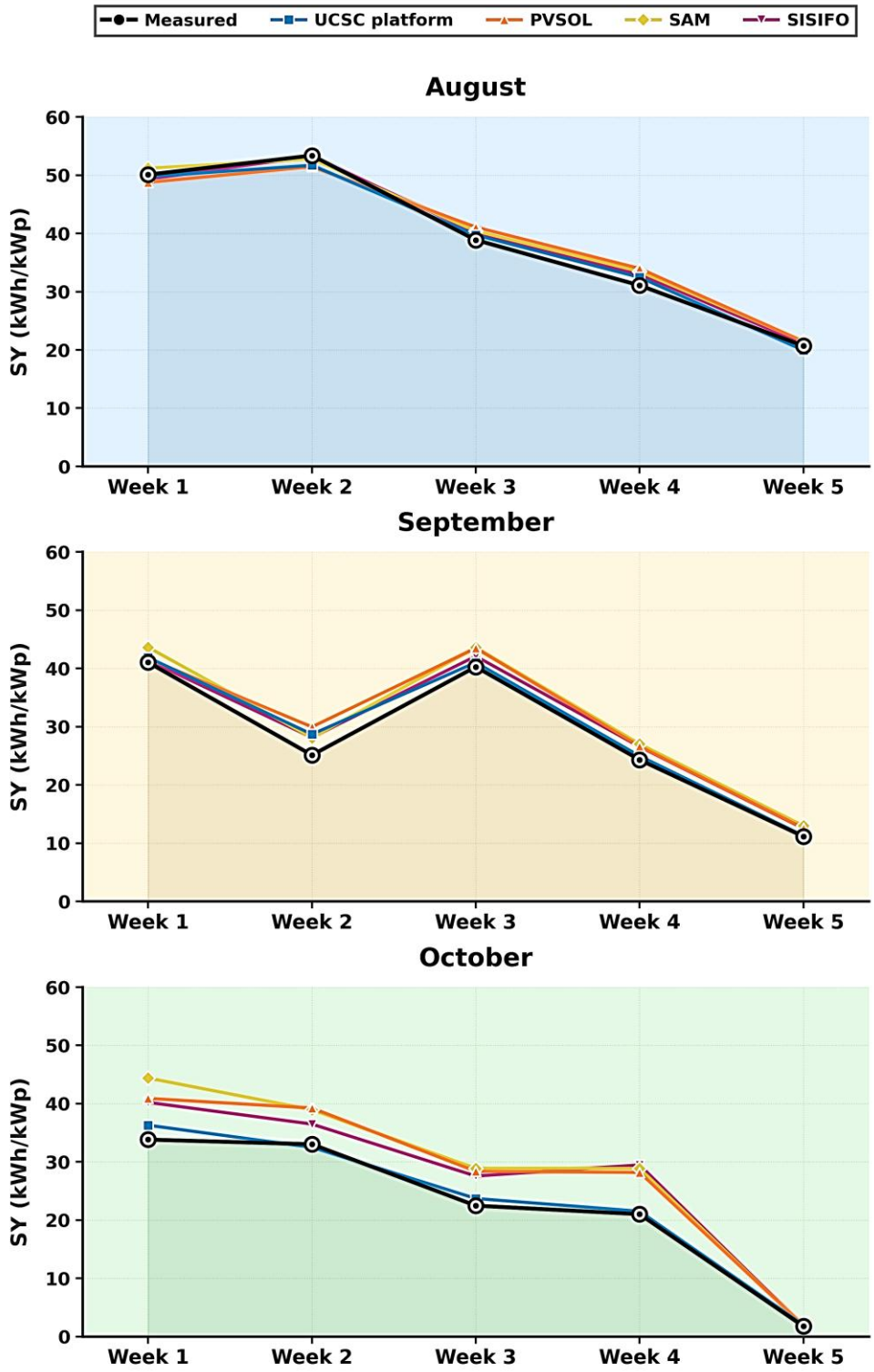

Figure 4.5 Comparison of measured and simulated SY at weekly temporal resolution for FT operation from August to October 2025.

During August, all tools achieved acceptable agreement with weekly SY values ranging from 35 to 55 kWh/kW_p. The UCSC platform maintained high tracking fidelity while commercial tools showed modest overestimation. Week 5 of September (comprises the residual days of each month), characterized by extended overcast conditions, represents an important validation case demonstrating increased relative errors across all platforms under diffuse-dominated conditions. The transition into October revealed amplified systematic bias in commercial predictions, with tools consistently projecting values 5-10 kWh/kW_p above measurements while the UCSC platform maintained close agreement. This divergence indicates that commercial platforms inadequately account for loss mechanisms becoming significant at reduced solar elevation angles.

4.4.2 Daily performance variability

Figure 4.6 depicts daily SY time series for August (top panel), September (middle panel), and October (bottom panel), enabling examination of day-to-day variability under diverse meteorological conditions.

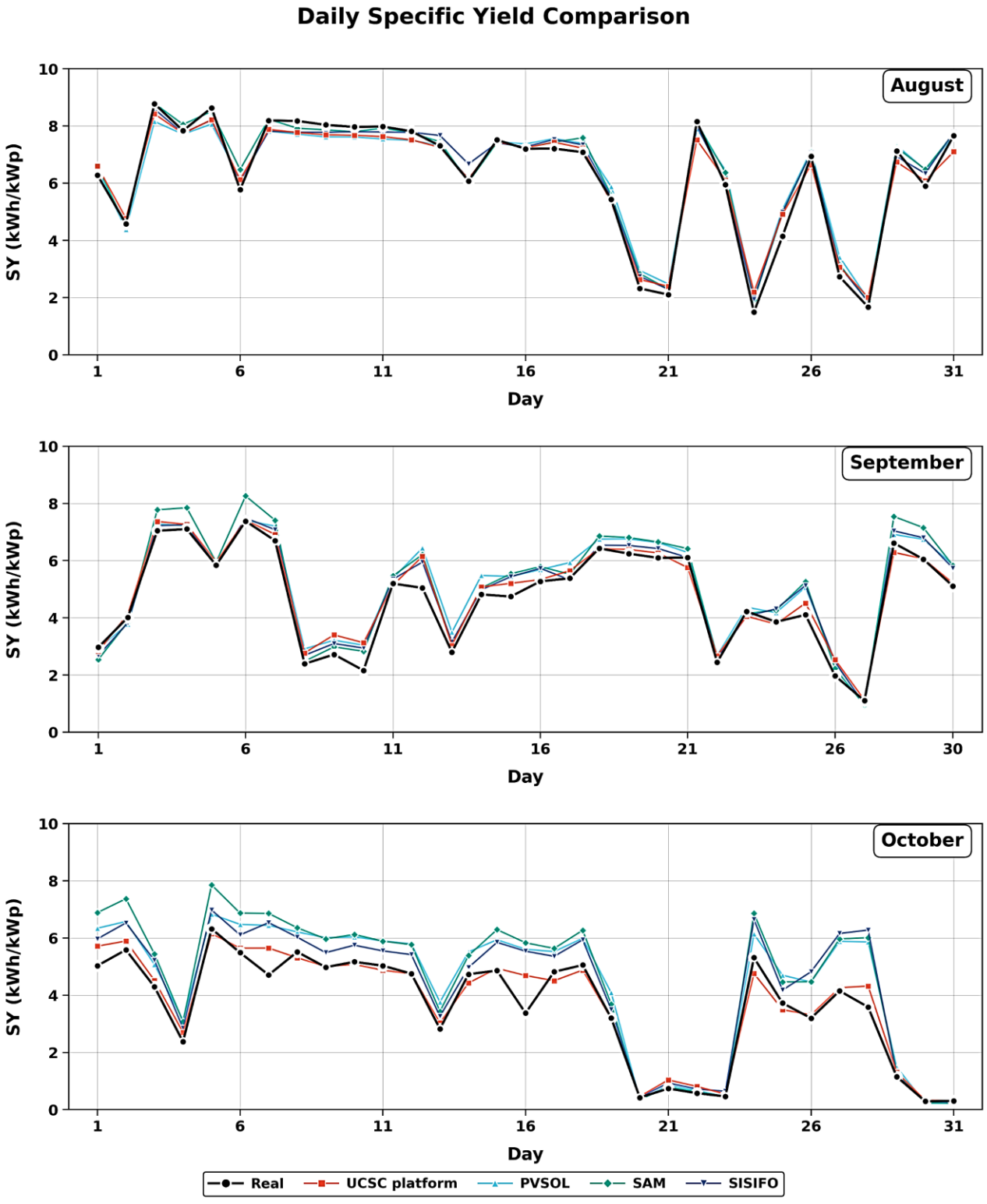

Figure 4.6 Daily SY time series comparing measured values with simulation outputs from UCSC platform, PVSOL, SAM, and SISIFO for August (top), September (middle), and October (bottom) 2025.

The August data demonstrate characteristic fluctuation between clear-sky days exceeding 7 kWh/kW_p/day and overcast periods producing approximately 1-2 kWh/kW_p/day, with all tools exhibiting commendable tracking of the measured profile. September reveals increased meteorological variability with peak values decreasing to 7–8 kWh/kW_p/day; systematic divergence among tools becomes apparent during partially cloudy conditions, suggesting variable errors in diffuse irradiance modeling under intermediate sky states. The October panel provides compelling evidence for differential simulation accuracy. Clear-sky days achieved measured SY of approximately 5-6 kWh/kW_p/day, yet commercial tools consistently predicted 6-7 kWh/kW_p/day under identical meteorological inputs. The UCSC platform maintained agreement within ±0.5 kWh/kW_p/day throughout October. The extended low-production period between Days 18-23 corresponds to persistent overcast and rainy conditions during which all tools exhibited increased absolute errors but comparable relative accuracy.

4.4.3 Hourly profile analysis under clear-sky conditions

Figure 4.7 presents hourly SY profiles for three representative clear-sky days spanning the monitoring period.

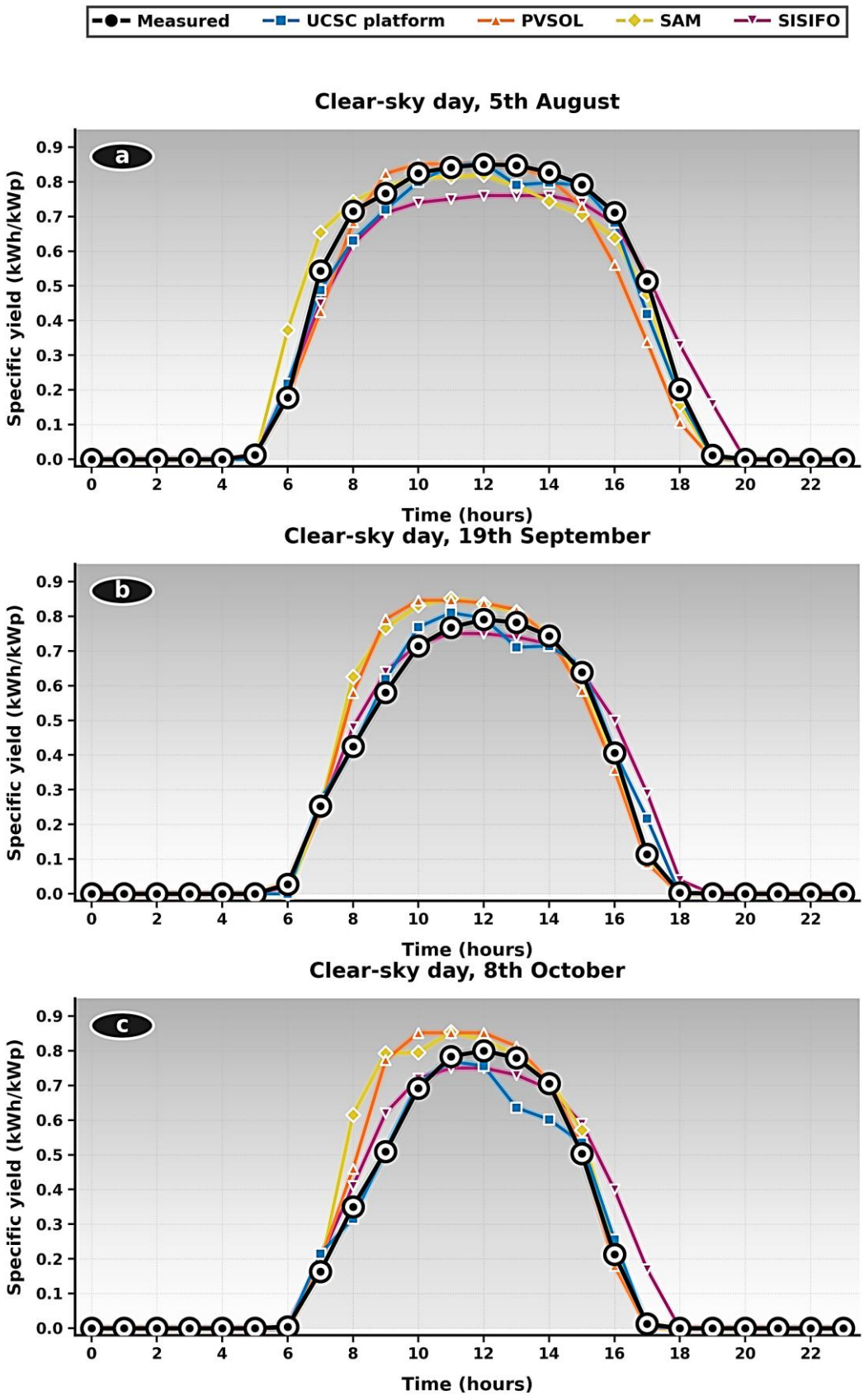

Figure 4.7 Hourly SY profiles under clear-sky conditions: a) 5th August (top), b) 19th September (middle), and c) 8th October (bottom) 2025.

The 5th August profile (top panel) shows measured peak hourly values of approximately 0.85 kWh/kW$_p$ between 11:00-13:00 with a production window extending approximately 13 hours (06:00-19:00). All tools demonstrate reasonable agreement during morning ramp-up, with PVSOL and SAM exhibiting slightly elevated predictions reaching 0.82-0.86 kWh/kW$_p$ at midday. The 19th September profile (middle panel) reflects seasonal transition with measured peak values of approximately 0.79 kWh/kW$_p$ and contracted production window of approximately 11 hours. Commercial tool overestimation becomes clearly discernible in the midday region where PVSOL and SAM predict 0.83-0.84 kWh/kW$_p$, while the UCSC platform accurately captures the measured production curve. The 8th October profile (bottom panel) reveals the most pronounced divergence. Measured peak values of approximately 0.8 kWh/kW$_p$ contrast with PVSOL and SAM predictions of 0.83-0.86 kWh/kW$_p$ during midday hours, while the UCSC platform maintains excellent agreement throughout the 9-hour production window (08:00-17:00). This superior performance derives from the platform's correct implementation of horizontal dual-axis tracking geometry and explicit near-shading modeling, capabilities absent in commercial tools as discussed in Section 4.4.5.

An important methodological consideration affects interpretation of these hourly comparisons. The meteorological station providing input data is located approximately 5 km from the APV site. This spatial separation introduces uncertainty when localized cloud activity creates discrepancies between recorded and actual irradiance conditions. Transient clouds shadowing the APV site but not the weather station cause measured production to fall below simulated values based on clear-sky irradiance data. This effect is stochastic and affects all tools equally, contributing to baseline scatter that cannot be eliminated without co-located irradiance measurements.

4.4.4 Statistical validation and error analysis

Table 4.4 presents comprehensive error metrics at hourly resolution for the three monthly periods, quantifying prediction accuracy through MAE, RMSE, MAPE, and MBE.

Table 4.4 Statistical error metrics comparing simulation platforms against measured hourly energy output for FT operation across three monthly periods.

	PVSOL	SAM	SISIFO	UCSC platform
	FT operation, 1 August-31 August, Hourly resolution			
MAE (kWh/kW$_p$)	0.035	0.037	0.039	0.025
RMSE (kWh/kW$_p$)	0.065	0.069	0.076	0.047
MAPE (%)	23.25	28.09	52.19	18.47
MBE (kWh/kW$_p$)	0.004	0.007	0.004	-0.001
	FT operation, 1 September-30 September, Hourly resolution			
MAE (kWh/kW$_p$)	0.037	0.038	0.033	0.026
RMSE (kWh/kW$_p$)	0.074	0.076	0.064	0.055
MAPE (%)	29.33	27.12	42.25	22.75
MBE (kWh/kW$_p$)	0.017	0.019	0.012	0.008
	FT operation, 1 October-31 October, Hourly resolution			
MAE (kWh/kW$_p$)	0.040	0.046	0.040	0.021
RMSE (kWh/kW$_p$)	0.090	0.105	0.086	0.049
MAPE (%)	38.42	44.38	79.54	21.04
MBE (kWh/kW$_p$)	0.036	0.041	0.031	0.005

During August, the UCSC platform demonstrated superior accuracy with MAE of 0.025 kWh/kW$_p$, RMSE of 0.047 kWh/kW$_p$, MAPE of 18.47%, and MBE of -0.001 kWh/kW$_p$ indicating essentially zero systematic bias. Among commercial tools, PVSOL achieved MAE of 0.035 kWh/kW$_p$ and RMSE of 0.065 kWh/kW$_p$, followed by SAM with MAE of 0.037 kWh/kW$_p$ and RMSE of 0.069 kWh/kW$_p$. SISIFO exhibited the highest MAPE (52.19%) and RMSE (0.076 kWh/kW$_p$), reflecting limitations that became more pronounced as the monitoring period progressed.

September results show maintained UCSC accuracy with MAE of 0.026 kWh/kW$_p$ and RMSE of 0.055 kWh/kW$_p$. Commercial tools exhibited increased positive bias with MBE values of 0.017, 0.019, and 0.012 kWh/kW$_p$ for PVSOL, SAM, and SISIFO respectively, indicating systematic overestimation of energy production.

October provided the most stringent accuracy test. The UCSC platform achieved its lowest MAE (0.021 kWh/kW$_p$), RMSE of 0.049 kWh/kW$_p$, MAPE of 21.04%, and MBE of only 0.005 kWh/kW$_p$. Commercial tools showed pronounced degradation with SAM exhibiting RMSE of 0.105 kWh/kW$_p$, MAPE of 44.38%, and MBE of 0.041 kWh/kW$_p$. SISIFO demonstrated the highest MAPE across the entire study (79.54%), while PVSOL showed intermediate performance with MBE of 0.036

kWh/kW_p. These elevated MBE values confirm the systematic positive bias and demonstrate that modeling deficiencies become increasingly significant during autumn operation. Figure 4.8 presents scatter plot comparisons between measured and simulated hourly energy production, with the coefficient of determination (R^2) quantifying the correlation strength for each platform-month combination.

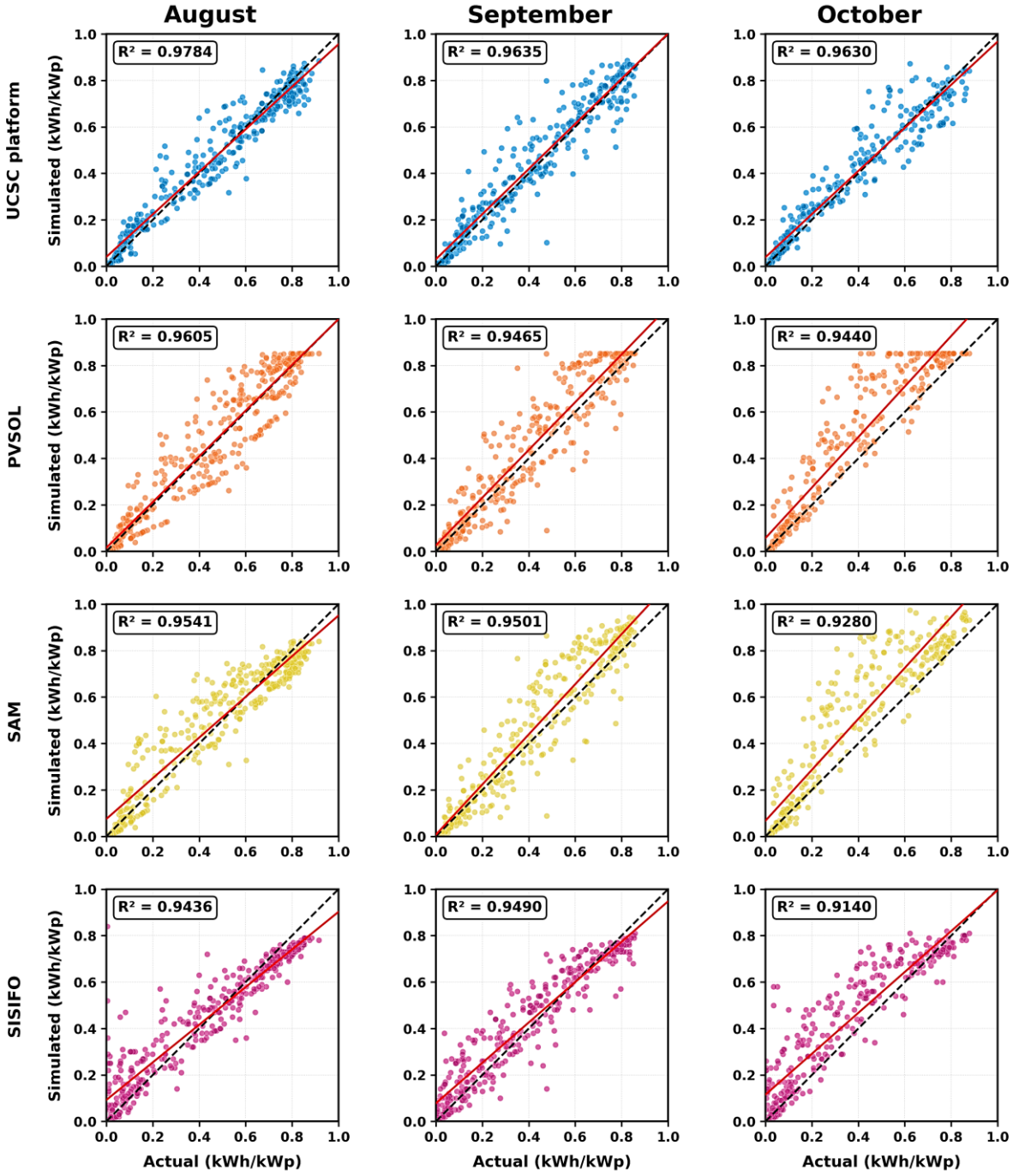

Figure 4.8 Scatter plots comparing actual (measured) versus simulated hourly specific yield (kWh/kW_p) for four simulation platforms across three monthly periods. Dashed lines indicate the 1:1 reference; solid red lines show linear regression fits.

During August, all platforms achieved R^2 exceeding 0.94, indicating strong correlation with measurements. The UCSC platform exhibited the tightest clustering around the 1:1 line with R^2 = 0.978, demonstrating superior predictive capability. Commercial platforms showed progressively lower correlations: PVSOL (R^2 = 0.961), SAM (R^2 = 0.954), and SISIFO (R^2 = 0.944).

September scatter plots reveal maintained correlation strength, with UCSC platform achieving R^2 = 0.964. Commercial platforms demonstrated comparable correlations: PVSOL (R^2 = 0.947), SAM (R^2 = 0.950), and SISIFO (R^2 = 0.949). The visual inspection of scatter distributions reveals systematic deviation above the 1:1 line for commercial tools, consistent with the positive MBE values reported in Table 4.4.

October scatter plots demonstrate the most pronounced inter-platform differences. The UCSC platform maintained robust correlation (R^2 = 0.963) with data points closely aligned to the 1:1 reference line. Commercial platforms exhibited increased scatter and reduced correlation coefficients: PVSOL (R^2 = 0.944), SAM (R^2 = 0.928), and SISIFO (R^2 = 0.914). The regression lines for commercial platforms consistently lie above the 1:1 reference, visually confirming the systematic overestimation quantified by MBE values in Table 4.4. This graphical evidence demonstrates that prediction accuracy degrades more substantially for commercial tools during autumn operation when low solar elevation angles amplify geometric modeling limitations.

4.4.5 Mechanistic interpretation of simulation discrepancies

The systematic investigation conducted in this study identified two fundamental limitations in commercial platforms that primarily account for their overestimation relative to the UCSC platform and measured values. These limitations concern tracking system geometry representation and near-shading loss modeling, both largely overlooked in existing PV simulation validation literature.

The APV installation employs horizontal dual-axis tracking wherein the primary rotation axis is horizontal, fundamentally different from vertical dual-axis systems where the primary axis enables azimuth rotation. A critical finding is that none of the commercial platforms could accurately simulate this configuration. PVSOL and SAM include only vertical dual-axis tracking options, lacking horizontal dual-axis capability entirely. While SISIFO nominally includes horizontal dual-axis tracking, operational difficulties during simulation setup precluded its reliable use. Consequently, all commercial platforms were configured with vertical dual-axis tracking, creating fundamental geometric mismatch with the actual installation.

This geometric mismatch has significant implications for energy yield estimation. Horizontal dual-axis trackers face mechanical constraints limiting tracking capability during low solar elevation conditions, particularly morning and evening hours when the primary axis rotation limits (±41° for the REMTEC system) may prevent optimal orientation. Vertical dual-axis systems can typically track through full azimuth range regardless of elevation angle. By simulating the system as vertical dual-axis, commercial platforms assume tracking capabilities exceeding those of the actual installation, resulting in systematically overestimated yields during morning and evening periods. This effect amplifies during autumn when lower solar elevation angles throughout the day cause tracking limitations to affect larger portions of the production window.

The second critical limitation concerns near-shading losses from module-to-module row interactions. Each tracker supports two module rows with 3.5 m row spacing; at low solar elevation, upper rows can shade lower rows, reducing irradiance to affected surfaces. Neither SAM nor PVSOL provides functionality to specify module-to-module row pitch, treating dual-axis trackers as single-plane entities without internal geometric complexity. While SISIFO includes this capability, the necessity of using vertical dual-axis tracking negated its utility. Vertical dual-axis algorithms typically assume negligible row-to-row shading because continuous tracking theoretically positions panels perpendicular to the sun; this assumption fails for multi-row arrangements where backtracking cannot eliminate internal shading.

The UCSC platform addresses both limitations through implementation of actual horizontal dual-axis tracking geometry with measured rotation angles and explicit near-shading modeling via PVLIB's pvfactors module [136], which calculates view factors with consideration of geometric layout parameters. The platform's superior accuracy, particularly during October when low solar elevation maximizes these effects, validates the importance of these modeling capabilities.

The identified limitations carry significant implications for APV project assessment. The systematic positive bias exhibited by commercial tools, reaching 21–28% overestimation in October, means energy yield projections for horizontal dual-axis APV systems generated by these platforms are likely unrealistically optimistic. This optimism bias can lead to erroneous techno-economic feasibility conclusions, potentially resulting in investment decisions based on inflated performance expectations that actual operation will not achieve. It should be noted that other modeling components including transposition algorithms, bifacial calculations, and irradiance decomposition methods are well-standardized across modern platforms with minimal inter-tool differences; the tracking geometry and

near-shading limitations therefore represent the dominant factors explaining differential accuracy for this APV configuration.

4.4.6 Anti-tracking operation: Validation of the UCSC platform

AT operational mode represents a paradigm unique to APV applications, wherein PV modules are deliberately oriented parallel to the solar beam to prioritize light transmission to underlying crops at the expense of energy conversion. Given that no commercial simulation platform currently incorporates AT logic, the UCSC platform constitutes the sole available tool for predicting energy output under this operational strategy. Validation was conducted using measured data from two representative days including 7 October (clear-sky conditions) and 21 October (overcast conditions), with AT mode applied exclusively to Sectors C4 and C5 (Figure 4.1). Figure 4.9 presents the validation results for UCSC platform simulation of AT operation at hourly resolution, comparing measured and simulated SY (kWh/kW_p) alongside error metrics and operational mode comparisons.

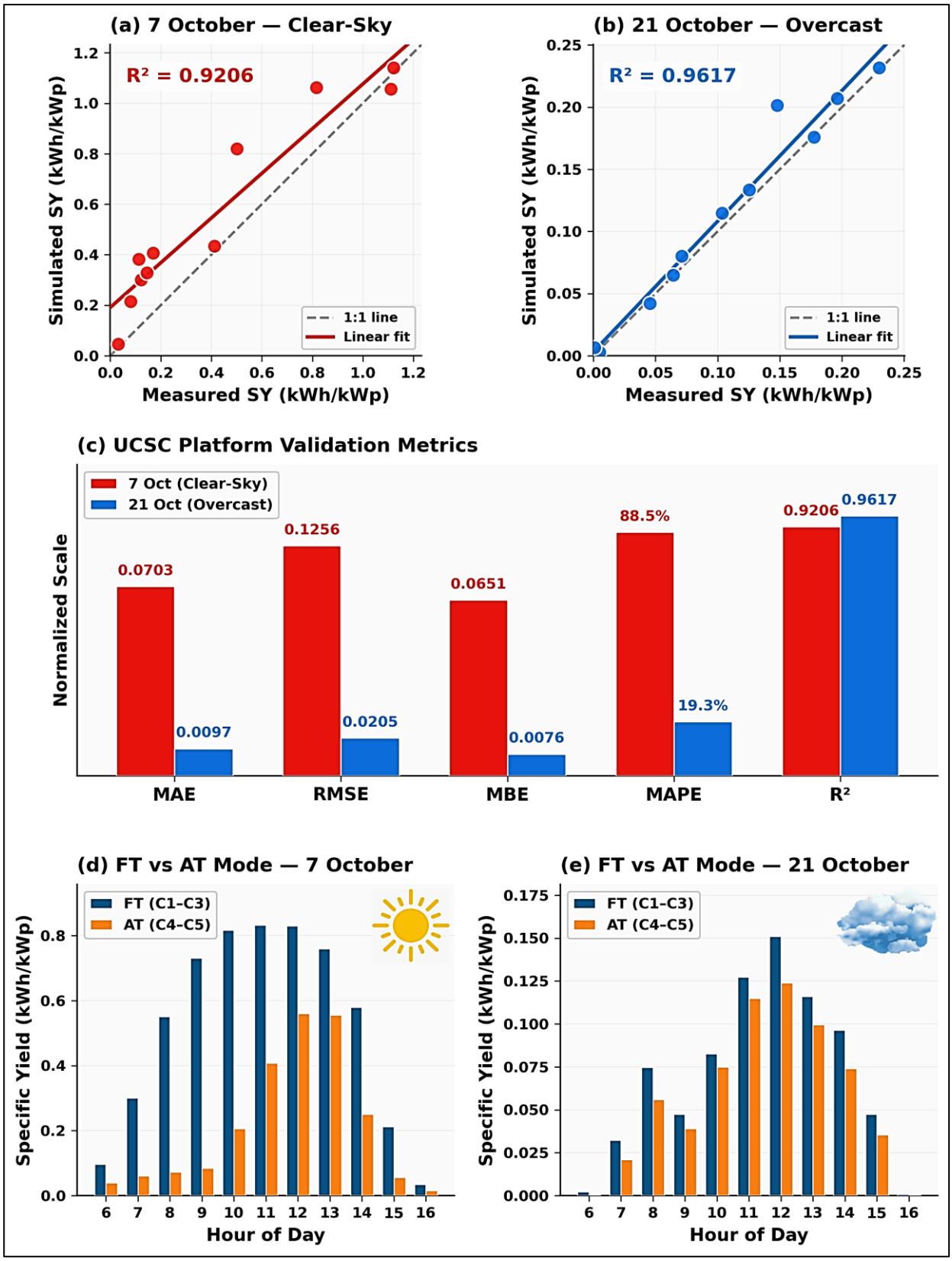

Figure 4.9 Validation of UCSC platform simulation for AT operation at hourly resolution comparing clear-sky and overcast conditions. Panels (a) and (b) present scatter plots of measured versus simulated specific yield with R^2 values and linear regression fits. Panel (c) displays error metrics. Panels (d) and (e) show hourly specific yield comparison between FT and AT operational modes.

The scatter plots (panels a and b) demonstrate strong correlation between measured and simulated hourly SY values under AT operation. For the clear-sky day, the platform achieved $R^2 = 0.9206$, indicating that the simulation explains over 92% of the variance in measured hourly production. The overcast day exhibited even stronger correlation with $R^2 = 0.9617$. Both days show data points closely aligned with the 1:1 reference line, with slight positive bias evident under clear-sky conditions where simulated values tend to exceed measured values during peak production hours.

The error metrics (panel c) reveal distinct performance characteristics between meteorological conditions. The clear-sky day exhibited substantially higher absolute errors with MAE of 0.0703 kWh/kW_p, RMSE of 0.1256 kWh/kW_p, and MBE of 0.0651 kWh/kW_p compared to the overcast day with MAE of 0.0097 kWh/kW_p, RMSE of 0.0205 kWh/kW_p, and MBE of 0.0076 kWh/kW_p. When expressed as MAPE, the clear-sky day yielded 88.5% compared to 19.3% for the overcast day. This difference in relative error does not indicate superior model performance under diffuse conditions but rather reflects the fundamental physics of AT operation. Under clear-sky conditions, AT mode actively deflects substantial direct normal irradiance away from the front surface while the rear surface orientation similarly reduces ground-reflected irradiance capture, creating large absolute differences between FT and AT production that amplify modeling uncertainties. Under overcast conditions, direct irradiance is minimal regardless of module orientation, resulting in similar low production values for both operational modes and consequently reduced absolute errors in AT simulation. The positive MBE values across both conditions confirm systematic overestimation by the UCSC platform.

The hourly comparison between FT and AT modes (panels d and e) quantifies the energy sacrifice associated with crop-priority operation. Under clear-sky conditions, the FT sectors (C1–C3) achieved a daily SY of 5.75 kWh/kW_p compared to 2.31 kWh/kW_p for AT sectors (C4–C5), representing a SY loss of 3.43 kWh/kW_p (59.8%) and corresponding energy loss of 526 kWh for the AT-configured capacity of 153.2 kW_p. The temporal profile reveals that AT losses are concentrated during midday hours when direct normal irradiance is highest and the AT orientation most effectively diverts solar radiation away from the module surfaces. Under overcast conditions, the performance differential diminishes substantially. The FT sectors achieved 0.78 kWh/kW_p compared to 0.64 kWh/kW_p for AT sectors, yielding a reduced SY loss of 0.138 kWh/kW_p (17.8%) and energy loss of only 21.2 kWh. This 3.4-fold reduction in relative energy sacrifice under cloudy conditions underscores that AT

operation imposes minimal penalty when diffuse irradiance dominates, as the isotropic nature of diffuse radiation renders module orientation less consequential for energy capture.

The validation results enable direct comparison of UCSC platform accuracy between operational modes. Under FT operation, the platform achieved R^2 values of 0.963–0.978 with MAPE ranging from 18.47% to 22.75% across the three-month monitoring period. Under AT operation, R^2 values of 0.9206 and 0.9617 were achieved for clear-sky and overcast conditions respectively, while MAPE reached 88.5% under clear-sky conditions and 19.3% under overcast conditions. The elevated MAPE under clear-sky AT conditions reflects the inherent difficulty of modeling irradiance capture when modules are oriented to minimize rather than maximize solar interception. The geometric complexity of AT orientation, where modules maintain parallelism with the solar beam throughout the day, presents modeling challenges distinct from those encountered in FT operation. The irradiance incident on module surfaces under AT conditions comprises predominantly diffuse and edge-intercepted components, which are inherently more difficult to model accurately than the direct normal irradiance dominant in FT operation. Additionally, bifacial gain calculations become particularly uncertain under AT mode, as the rear surface irradiance patterns differ substantially from those assumed in conventional bifacial models developed for energy-maximizing orientations.

The R^2 values exceeding 0.92 indicate that the temporal dynamics of AT production are reasonably captured, which may suffice for applications requiring relative rather than absolute performance predictions. The systematic positive bias identified in this validation represents a specific target for model refinement. The consistent overestimation across both clear-sky and cloudy conditions suggests that one or more model components systematically overpredict irradiance capture under AT geometry. Potential refinement pathways include recalibration of the diffuse irradiance transposition model for the steep module tilt angles characteristic of AT operation, adjustment of bifacial gain algorithms for configurations where modules face away from the sun, and incorporation of empirically-derived correction factors specific to AT operation.

4.4.7 Study limitations and future directions

This comparative validation study establishes benchmark accuracy metrics for APV simulation platforms while operating within methodological boundaries that warrant acknowledgment. The three-month monitoring period (August-October 2025) captures only late summer and autumn conditions, omitting winter months when low solar elevation angles persist throughout the day and spring periods. Furthermore, this single-site validation at Piacenza, Italy represents Mediterranean-Continental transitional climate conditions. Extended validation campaigns spanning complete

annual cycles across diverse climate zones would strengthen generalizability and reveal climate-dependent model performance characteristics that cannot be assessed from this limited temporal and geographic scope.

The meteorological input data originates from a station located approximately 5 km from the APV site, introducing spatial separation uncertainties. Localized cloud activity can create discrepancies between recorded irradiance and actual on-site conditions, particularly during transient cloud passages that affect the installation but not the weather station. While this stochastic effect impacts all simulation platforms equally and contributes to baseline scatter, co-located irradiance measurements would eliminate this source of uncertainty and improve validation precision.

The validation of AT operational mode introduces distinct methodological challenges reflecting the pioneering nature of this investigation. As the first empirical validation of any simulation tool for AT operation of advanced APV systems (overhead bifacial dual-axis), this work necessarily confronts elevated prediction uncertainties absent from conventional PV simulation validation. The 88.5% MAPE observed under clear-sky AT conditions reflects the geometric complexity of maintaining beam-parallel orientation, where incident irradiance comprises predominantly diffuse and edge-intercepted components requiring fundamentally different calculation approaches than those validated in energy-maximizing contexts. The absence of alternative validation frameworks precludes comparative assessment and independent verification of modeling approaches for this APV-specific operational mode.

The scope boundaries of this investigation reflect a deliberate focus on energy performance validation rather than comprehensive APV system assessment. This study does not address agricultural productivity impacts, omitting crop yield measurements, photosynthetically active radiation distribution analysis, or soil moisture dynamics. Consequently, while the energy sacrifice associated with AT operation is rigorously quantified, the corresponding agricultural benefits remain unquantified. Additional methodological simplifications warrant acknowledgment. The constant albedo value (0.2) applied throughout represents a necessary simplification of dynamic ground reflectance that varies with crop phenology and soil moisture, affecting bifacial gain calculations. Soiling effects were not separately quantified, and module degradation was not explicitly tracked through periodic measurements. These simplifications were necessary given the primary objective of platform validation but should be addressed in comprehensive APV system assessments that integrate energy simulation with crop modeling and agronomic monitoring.

4.5 Conclusion

This study presents the first comprehensive cross-validation of PV simulation platforms against field measurements from an advanced APV system (overhead bifacial dual-axis) operating under both FT and AT modes. The systematic comparison of three commercial tools (PVSOL, SAM, SISIFO) and the UCSC platform against three months of hourly energy conversion data (August to October 2025) from a 507 kW_p installation in Piacenza, Italy, yields several significant findings with direct implications for APV system design and assessment. Under FT operation, the UCSC platform demonstrated consistently superior accuracy with deviations within 3.5% of measured values and R^2 exceeding 0.96 across all monthly periods. In contrast, commercial platforms exhibited systematic positive bias that intensified progressively throughout the monitoring campaign, reaching overestimation levels of 21–28% during autumn when reduced solar elevation angles amplified modeling deficiencies. This investigation identified two fundamental limitations in commercial software responsible for these discrepancies, namely the inability to accurately represent horizontal dual-axis tracking geometry and the absence of functionality for modeling module-to-module near-shading losses. These capability gaps result in unrealistically optimistic energy yield projections that could lead to flawed investment decisions for such advanced APV configurations. For AT operation, this study provides the first empirical validation of any simulation tool for this APV-specific operational mode. The UCSC platform achieved R^2 values of 0.92 and 0.96 for clear-sky and overcast conditions respectively, establishing its utility for AT performance prediction despite accuracy limitations under high direct irradiance conditions. The field measurements quantify the energy sacrifice associated with crop-priority operation, revealing 59.8% yield reduction under clear-sky conditions compared to only 17.8% under overcast conditions. This pronounced weather-dependence indicates that AT strategies impose substantially lower energy penalties in climates characterized by frequent cloud cover, thereby informing site-specific operational planning for APV installations worldwide. These findings carry actionable implications for multiple stakeholders. Project developers should apply conservative correction factors when using commercial PV tools for this system typology or adopt specialized APV platforms such as the UCSC framework. Software developers should prioritize implementation of horizontal dual-axis tracking algorithms and near-shading calculations to address the identified capability gaps. Future research should extend validation across complete annual cycles, multiple climate zones, and integrated agricultural-energy performance metrics to support comprehensive optimization of advanced APV systems.

Chapter 5

Synthesis

5.1 Overview

This thesis investigated the techno-economic optimization, environmental performance, and simulation accuracy of agrivoltaics (APV) systems through three complementary studies. This chapter synthesizes the collective insights that emerge when these investigations are viewed as an integrated body of work.

5.2 Main results

A convergent finding across the economic and environmental assessments is that single-axis tracking configurations occupy a favorable middle ground among APV typologies. The techno-economic analysis identified single-axis systems as delivering the highest net present value (NPV) when paired with heat pump electrification. It also demonstrated that off-grid APV-biomethanation systems were economically unviable under all examined configurations, with negative NPV ranging from -6.27 to -8.33 M€. The fundamental constraint is battery storage cost, as achieving energy autonomy required storage capacities that inflated capital expenditure beyond recoverable levels. This finding establishes grid connection as a practical prerequisite for economically viable APV-biomethanation integration under current technology costs.

The life cycle assessment (LCA) independently confirmed that the interspace single-axis configuration achieved the lowest greenhouse gas emissions, ranging from 11 to 20 g CO_{2eq}/kWh, and outperformed other designs in eight additional impact categories. This convergence emerged from studies employing different methodologies, objectives, and system boundaries, suggesting that single-axis configurations genuinely balance energy yield, capital efficiency, and material consumption in ways that neither vertical nor dual-axis alternatives achieve.

Overhead APV systems enable machinery passage and flexible crop management, yet this functional advantage comes at quantifiable costs. The LCA revealed that overhead dual-axis configurations required 2.4 to 4.4 times more steel than interspace designs, translating directly into higher environmental burdens. Under land-constrained conditions, dual-axis systems require wider row spacing to avoid inter-row shading, which reduces the installable capacity within a given land area and consequently lowers total energy conversion and revenue. It should be noted that under scenarios with unlimited land availability or equal installed capacity across configurations, dual-axis systems would generate higher energy yields due to their superior solar tracking capability. These findings do not invalidate overhead configurations but establish that their deployment is justified where specific

agricultural operations demand elevated clearance, provided decision-makers account for the associated material intensity and land-use implications.

All APV configurations substantially outperformed grid electricity across nine of ten environmental impact categories, but mineral and metal resource consumption represents an unresolved challenge. APV systems exhibited 3.5 to 9.6 times higher mineral resource impacts than electricity grids, driven primarily by steel in mounting structures. This trade-off cannot be eliminated through configuration selection alone, as even the most material-efficient APV design remains more resource-intensive than grid electricity per kilowatt-hour. Addressing this limitation requires supply-chain interventions including increased recycled steel content, alternative structural materials, and end-of-life recovery systems.

The validation study revealed that commercial simulation platforms overestimated energy yields by 20.9 to 27.5% for the advanced dual-axis APV configuration examined. This finding has implications for techno-economic and environmental assessments that rely on simulated energy yields. While the UCSC platform demonstrated substantially better accuracy with deviations within 3.5%, the broader issue is that APV system assessments currently lack validated simulation tools for advanced configurations. Anti-tracking operation, which reduces yield by 59.8% under clear skies but only 17.8% under overcast conditions, cannot be modeled by any commercial platform. This capability gap constrains both research and commercial project development for crop-priority APV applications.

5.3 Scientific contribution

This thesis contributes three methodological advances to the field, which are summarized below.

- **Integrated optimization framework for APV-biomethane systems:** A transparent and reproducible optimization workflow is developed to compare APV typologies and heat-supply options under both grid-connected and off-grid configurations.
- **Evidence-based environmental benchmarking beyond climate change:** A consistent multi-category LCA comparison of advanced bifacial APV configurations is provided, clarifying when and why environmental rankings change across locations and impact categories, and supporting deployment decisions that avoid burden shifting.
- **Field-based validation for advanced APV operation:** An empirical cross-validation protocol is implemented for an overhead horizontal dual-axis APV system, quantifying model errors under FT and AT modes and identifying specific capability gaps in commercial tools related to tracking kinematics and near-shading representation.

5.4 Concluding remarks

Overall, APV systems can reconcile renewable energy expansion with agricultural land preservation, but configuration selection substantially affects outcomes. Single-axis tracking systems emerge from this research as offering a favorable balance across economic, environmental, and practical dimensions under land-constrained conditions. The mineral resource intensity of APV systems relative to grid electricity represents a persistent challenge that requires supply-chain interventions rather than design-level solutions alone. Commercial simulation tools require enhancement before they can reliably support investment decisions for advanced APV configurations and crop-priority operational modes. These findings provide a foundation for informed decision-making by stakeholders seeking to deploy APV technologies that genuinely serve both energy and agricultural objectives.

References

[1] Lowder SK, Skoet J, Raney T. The number, size, and distribution of farms, smallholder farms, and family farms worldwide. World Dev 2016;87:16–29.

[2] Dupraz C. Assessment of the ground coverage ratio of agrivoltaic systems as a proxy for potential crop productivity. Agrofor. Syst., 2023, p. 1–18.

[3] Bruno M, Gfüllner F, Berwind J. Enhancing agrivoltaic synergies through optimized tracking for apple orchards: A digital twin approach 2025.

[4] Fumey D, Chopard J, Lopez G, Persello S, Juillion P, Hitte V, et al. Dynamic agrivoltaics, climate protection for grapevine driven by artificial intelligence. 22nd GiESCO, 2023.

[5] Fiorentino G, Zucaro A, Cerbone A, Giocoli A, Motola V, Rinaldi C, et al. The contribution of biogas to the electricity supply chain: an Italian life cycle assessment database. Energies 2024;17:3264.

[6] EBA Statistical Report 2023. https://www.europeanbiogas.eu/eba-statistical-report-2023/ (Accessed 30 December 2025). n.d.

[7] Baccioli A, Antonelli M, Frigo S, Desideri U, Pasini G. Small scale bio-LNG plant: Comparison of different biogas upgrading techniques. Appl Energy 2018;217:328–35.

[8] Kiehbadroudinezhad M, Hosseinzadeh-Bandbafha H, Tajuddin SAFSA, Tabatabaei M, Aghbashlo M. A critical review of life cycle assessment of renewable agricultural systems. Sustain Energy Technol Assess 2025;73:104100.

[9] Abdalla MEB, Ayadi O, Al Omari A, Rinchi B, Al-Bakri JT. A pathway to food and energy security: Agrivoltaic potential in the MENA region. Energy Nexus 2026;21:100610. https://doi.org/10.1016/j.nexus.2025.100610.

[10] Jamil U, Pearce JM. Agrivoltaics as a systems innovation: Multi-dimensional benefits from global studies across climate, agriculture, energy, and ecosystems. Renew Sustain Energy Rev 2026;230:116721. https://doi.org/10.1016/j.rser.2026.116721.

[11] Bellone Y, Santangelo E, Assirelli A, Zainali S, Impollonia G, Croci M, et al. Agricultural mechanization in agrivoltaic systems: Challenges, adaptation, and possible advancements. Renew Sustain Energy Rev 2026;229:116661. https://doi.org/10.1016/j.rser.2025.116661.

[12] Mehta K, Jain R, Zörner W. Agrivoltaics Around the World: Potential, Technology, Crops and Policies to Address the Energy–Agriculture Nexus for Sustainable and Climate-Resilient Land Use. Energies 2025;18:6417. https://doi.org/10.3390/en18246417.

[13] Böhm J, De Witte T, Offermann F, Latacz-Lohmann U. Preserving agricultural land with agrivoltaic – But at what cost? An economic analysis of different agrivoltaic systems in Germany. Land Use Policy 2026;164:107966. https://doi.org/10.1016/j.landusepol.2026.107966.

[14] Sieborg MU, Engelbrecht N, Ottosen LDM, Kofoed MVW. Sunshine-to-fuel: Demonstration of coupled photovoltaic-driven biomethanation operation, process, and techno-economical evaluation. Energy Convers Manag 2024;299:117767.

[15] Su B, Wang H, Zhang X, He H, Zheng J. Using photovoltaic thermal technology to enhance biomethane generation via biogas upgrading in anaerobic digestion. Energy Convers Manag 2021;235:113965.

[16] Álvaro AG, Palomar CR, Torre RM, Redondo DH, Godos Crespo I. Hybridization of anaerobic digestion with solar energy: A solution for isolated livestock farms. Energy Convers Manag 2023;X, 20:100488.

[17] Temiz M, Sinbuathong N, Dincer I. Development and assessment of a new agrivoltaic-biogas energy system for sustainable communities. Int J Energy Res 2022;46:18663–75.

[18] Taramasso MA, Motaghi M, Casasso A. A techno-economic feasibility analysis of solutions to cover the thermal and electrical demands of anaerobic digesters. Renew Energy 2024;121485.

[19] Agostini A, Colauzzi M, Amaducci S. Innovative agrivoltaic systems to produce sustainable energy: An economic and environmental assessment. Appl Energy 2021;281:116102.

[20] Ravilla A, Shirkey G, Chen J, Jarchow M, Stary O, Celik I. Techno-economic and life cycle assessment of agrivoltaic system (AVS) designs. Sci Total Environ 2024;912:169274.

[21] Sponagel C, Weik J, Feuerbacher A, Bahrs E. Exploring the climate change mitigation potential and regional distribution of agrivoltaics with geodata-based farm economic modelling and life cycle assessment. J Environ Manage 2024;359:121021.

[22] Krexner T, Bauer A, Gronauer A, Mikovits C, Schmidt J, Kral I. Environmental life cycle assessment of a stilted and vertical bifacial crop-based agrivoltaic multi land-use system and comparison with a mono land-use of agricultural land. Renew Sustain Energy Rev 2024;196:114321.

[23] Grubbs EK, Gruss SM, Schull VZ, Gosney MJ, Mickelbart MV, Brouder S, et al. Optimized agrivoltaic tracking for nearly-full commodity crop and energy production. Renew Sustain Energy Rev 2024;191:114018.

[24] Willockx B, Lavaert C, Cappelle J. Performance evaluation of vertical bifacial and single-axis tracked agrivoltaic systems on arable land. Renew Energy 2023;217:119181.

[25] Alam H, Butt NZ. How does module tracking for agrivoltaics differ from standard photovoltaics? Food, energy, and technoeconomic implications. Renew Energy 2024;235:121151.

[26] Vernier J. A coupling method using CFD, radiative models and a surface model to simulate the micro-climate 2023.

[27] Bambokela JE, Belaid M, Muzenda E. Preliminary design of a biogas-solar PV hybrid minigrid system for off-grid agricultural communities 2020.

[28] Hao Y, Li W, Tian Z, Campana PE, Li H, Jin H, et al. Integration of concentrating PVs in anaerobic digestion for biomethane production. Appl Energy 2018;231:80–8.

[29] Calise F, Cappiello FL, Cimmino L, d'Accadia MD, Vicidomini M. Integration of photovoltaic panels and solar collectors into a plant producing biomethane for the transport sector: Dynamic simulation and case study. Heliyon 2023;9.

[30] Akarsu RT, Demir N. Techno-economic and environmental analysis of biogas-based hybrid renewable energy systems: A case study for a small-scale livestock farm. Process Saf Environ Prot 2024;191:1968–81.

[31] Murano R, Maisano N, Selvaggi R, Pappalardo G, Pecorino B. Critical Issues and Opportunities for Producing Biomethane in Italy. Energies 2021;14:2431.

[32] Bortoluzzi G, Gatti M, Sogni A, Consonni S. Biomethane production from agricultural resources in the Italian scenario: techno-economic analysis of water wash. Chem Eng Trans 2014;37.

[33] Carfora A, Pansini RV, Romano AA, Scandurra G. Renewable energy development and green public policies complementarities: The case of developed and developing countries. Renew Energy 2018;115:741–9.

[34] CIB - Consorzio Italiano Biogas. (2024). Biomethane feed-in tariff. https://www.consorziobiogas.it (Accessed 30 December 2025). n.d.

[35] Petrollese M, Cocco D. Techno-economic assessment of hybrid CSP-biogas power plants. Renew Energy 2020;155:420–31.

[36] ATTSU Group Company. https://www.attsu.com/en. (Accessed 30 December 2025). n.d.

[37] Bina SM, Fujii H, Tsuya S, Kosukegawa H. Comparative study of hybrid ground source heat pump in cooling and heating dominant climates. Energy Convers Manag 2022;252:115122.

[38] Viessmann Company. https://www.viessmann.ch/it/prodotti/pompa-di-calore/vitocal-350-g-pro.html. (Accessed 30 December 2025). n.d.

[39] Yang Z, Zhuo Y, Ercang L, Yuan Z. Travelling-wave thermoacoustic high-temperature heat pump for industrial waste heat recovery. Energy 2014;77:397–402.

[40] Bor DM, Ferreira CAI. Quick selection of industrial heat pump types including the impact of thermodynamic losses. Energy 2013;53:312–22.

[41] Ennemiri N, Berrada A, Emrani A, Abdelmajid J, El Mrabet R. Optimization of an off-grid PV/biogas/battery hybrid energy system for electrification: A case study in a commercial platform in Morocco. Energy Convers Manag 2024;X, 21:100508.

[42] Pöschl M, Ward S, Owende P. Evaluation of energy efficiency of various biogas production and utilization pathways. Appl Energy 2010;87:3305–21.

[43] TEDOM Group. https://www.tedom.com/en/. (Accessed 30 December 2025). n.d.

[44] Zainali S, Lu SM, Potenza E, Stridh B, Avelin A, Campana PE. 3D View Factor Power Output Modeling of Bifacial Fixed, Single, and Dual-Axis Agrivoltaic Systems. AgriVoltaics Conf. Proc., vol. 2, 2023.

[45] Lu SM, Zainali S, Sundström E, Nygren A, Stridh B, Avelin A, et al. Validation of Vertical Bifacial Agrivoltaic and Other Systems Modeling Effect of Dynamic Albedo on Irradiance and Power Output Estimations. AgriVoltaics Conf. Proc., vol. 2, 2023.

[46] Campana PE, Stridh B, Hörndahl T, Svensson SE, Zainali S, Lu SM, et al. Experimental results, integrated model validation, and economic aspects of agrivoltaic systems at northern latitudes. J Clean Prod 2024;437:140235.

[47] Maity R, Kumarasamy S, Razak AA, Minelli F. Solar energy analysis for agrivoltaic system design in tropical climates: A new integrated modeling framework. Energy 2026;344:139970. https://doi.org/10.1016/j.energy.2026.139970.

[48] Bellone Y, Croci M, Impollonia G, Zad AN, Colauzzi M, Campana PE, et al. Simulation-Based Decision Support for Agrivoltaic Systems. Appl Energy 2024;369:123490.

[49] Biavetti I, Karetsos S, Ceglar A, Toreti A, Panagos P. European meteorological data: contribution to research, development, and policy support. Second Int. Conf. Remote Sens. Geoinformation Environ., vol. RSCy2014) (Vol. 9229, SPIE; 2014, p. 31–9.

[50] Tong J, Xie L, Fang S, Yang W, Zhang K. Hourly solar irradiance forecasting based on encoder-decoder model using series decomposition and dynamic error compensation. Energy Convers Manag 2022;270:116049.

[51] Ibrahim IA, Khatib T. A novel hybrid model for hourly global solar radiation prediction using random forests technique and firefly algorithm. Energy Convers Manag 2017;138:413–25.

[52] Wang JJ, Jing YY, Zhang CF, Zhao JH. Review on multi-criteria decision analysis aid in sustainable energy decision-making. Renew Sustain Energy Rev 2009;13:2263–78.

[53] Ravi A, Sah B, Singh AR, Deng Y, He X, Kumar P, et al. A review of multi criteria decision making (MCDM) towards sustainable renewable energy development. Renew Sustain Energy Rev 2017;69:596–609.

[54] Salmeron JL, Vidal R, Mena A. Ranking fuzzy cognitive map based scenarios with TOPSIS. Expert Syst Appl 2012;39:2443–50.

[55] Cabral JB, Luczywo NA, Zanazzi JL. Scikit-Criteria: Colección de métodos de análisis multi-criterio integrado al stack científico de Python. XIV Simp. Argent. Investig. Oper., 2016.

[56] The PVSOL software, Version R8. (2024). Available at: https://pvsol.software/en/ (Accessed 30 December 2025). n.d.

[57] Ebaid MS, Qandil H, Hammad M. A unified approach for designing a photovoltaic solar system for the underground water pumping well-34 at Disi aquifer. Energy Convers Manag 2013;75:780–95.

[58] Urs RR, Sadiq M, Jaradat R, Mayyas A. Harvesting energy horizons: Bifacial PV and reversible fuel cells unite for sustainable building solutions. Int J Hydrog Energy 2024.

[59] Nikzad A, Chahartaghi M, Ahmadi MH. Technical, economic, and environmental modeling of solar water pump for irrigation of rice in Mazandaran province in Iran: A case study. J Clean Prod 2019;239:118007.

[60] Huawei Technologies Co., Ltd., https://solar.huawei.com//media/Solar/attachment/pdf/it/datasheet/LUNA2000-5-15-S0.pdf (Accessed 30 December 2025). n.d.

[61] Messenger RA, Ventre J. Photovoltaic Systems Engineering. CRC Press; 2010.

[62] Ali MS, Ali SU, Mian Qaisar S, Waqar A, Haroon F, Alzahrani A. Techno-economic analysis of hybrid renewable energy-based electricity supply to Gwadar, Pakistan. Sustainability 2022;14:16281.

[63] Calise F, Cappiello FL, Cimmino L, d'Accadia MD, Vicidomini M. Dynamic analysis and thermoeconomic optimization of a Power-to-Gas system driven by renewables. Energy Convers Manag 2024;313:118647.

[64] Micco S, Romano F, Jannelli E, Perna A, Minutillo M. Techno-economic analysis of a multi-energy system for the co-production of green hydrogen, renewable electricity, and heat. Int J Hydrog Energy 2023;48:31457–67.

[65] Reher T, Lavaert C, Willockx B, Huyghe Y, Bisschop J, Martens JA, et al. Potential of sugar beet (Beta vulgaris) and wheat (Triticum aestivum) production in vertical bifacial, tracked, or elevated agrivoltaic systems in Belgium. Appl Energy 2024;359:122679.

[66] Zidane TEK, Zainali S, Bellone Y, Guezgouz M, Khosravi A, Lu SM, et al. Economic evaluation of one-axis, vertical, and elevated agrivoltaic systems across Europe: a Monte Carlo Analysis. Appl Energy 2025;391:125826.

[67] Zainali S, Lu SM, Bellone Y, Campana PE. Optimisation of Agrivoltaic Systems within the Water-Energy-Food Nexus 2025.

[68] Noussan M, Negro V, Prussi M, Chiaramonti D. The potential role of biomethane for the decarbonization of transport: An analysis of 2030 scenarios in Italy. Appl Energy 2024;355:122322.

[69] Zad AN, Agostini A, Impollonia G, Zainali S, Croci M, Colauzzi M, et al. Life cycle assessment of various agrivoltaic systems across Europe. Sustain Prod Consum 2025;60:260–80.

[70] Weselek A, Ehmann A, Zikeli S, Lewandowski I, Schindele S, Högy P. Agrophotovoltaic systems: applications, challenges, and opportunities. A review. Agron Sustain Dev 2019;39:35.

[71] Dinesh H, Pearce JM. The potential of agrivoltaic systems. Renew Sustain Energy Rev 2016;54:299–308.

[72] Marrou H, Guilioni L, Dufour L, Dupraz C, Wery J. Microclimate under agrivoltaic systems: Is crop growth rate affected in the partial shade of solar panels? Agric For Meteorol 2013;177:117–32.

[73] Amaducci S, Yin X, Colauzzi M. Agrivoltaic systems to optimise land use for electric energy production. Appl Energy 2018;220:545–61.

[74] Wagner M, Lask J, Kiesel A, Lewandowski I, Weselek A, Högy P, et al. Agrivoltaics: The Environmental Impacts of Combining Food Crop Cultivation and Solar Energy Generation. Agronomy 2023;13:299.

[75] Busch C, Wydra K. Life cycle assessment of an agrivoltaic system with conventional potato production. J Renew Sustain Energy 2023;15.

[76] Leon A, Ishihara KN. Influence of allocation methods on the LC-CO2 emission of an agrivoltaic system. Resour Conserv Recycl 2018;138:110–7.

[77] Cheng H, Zhou X, Yang Y, Xu L, Ding Y, Yan T, et al. Environmental damages, cumulative exergy demand, and economic assessment of Panus giganteus farming with the application of solar technology. Sci Total Environ 2024;907:168020.

[78] Leon A, Ishihara KN. Assessment of new functional units for agrivoltaic systems. J Environ Manage 2018;226:493–8.

[79] Pascaris AS, Handler R, Schelly C, Pearce JM. Life cycle assessment of pasture-based agrivoltaic systems: Emissions and energy use of integrated rabbit production. Clean Responsible Consum 2021;3:100030.

[80] Handler R, Pearce JM. Greener sheep: Life cycle analysis of integrated sheep agrivoltaic systems. Clean Energy Syst 2022;3:100036.

[81] Zhang J, Wang T, Chang Y, Liu B. A sustainable development pattern integrating data centers and pasture-based agrivoltaic systems for ecologically fragile areas. Resour Conserv Recycl 2023;188:106684.

[82] Kumar NM, Chopra SS. Integrated techno-economic and life cycle assessment of shared circular business model based blockchain-enabled dynamic grapevoltaic farm for major grape growing states in India. Renew Energy 2023;209:365–81.

[83] Ravi S, Macknick J, Lobell D, Field C, Ganesan K, Jain R, et al. Colocation opportunities for large solar infrastructures and agriculture in drylands. Appl Energy 2016;165:383–92.

[84] Junedi MM, Ludin NA, Hamid NH, Kathleen PR, Hasila J, Affandi NA. Environmental and economic performance assessment of integrated conventional solar photovoltaic and agrophotovoltaic systems. Renew Sustain Energy Rev 2022;168:112799.

[85] Jouannais P, Marchand-Lasserre M, Douziech M, Pérez-López P. When is Agrivoltaism Environmentally Beneficial? A Consequential LCA and Scenario Discovery Approach. Environmental Science & Technology; 2025.

[86] Hersbach H, Bell B, Berrisford P, Hirahara S, Horányi A, Muñoz-Sabater J, et al. The ERA5 global reanalysis. Q J R Meteorol Soc 2020;146:1999–2049.

[87] Wilcox S, Marion W. User's manual for TMY3 data sets. Golden, CO: National Renewable Energy Laboratory; 2008.

[88] Kim S, Zirkelbach D, Künzel HM, Lee JH, Choi J. Development of test reference year using ISO 15927-4 and the influence of climatic parameters on building energy performance. Build Environ 2017;114:374–86.

[89] Riaz MH, Imran H, Alam H, Alam MA, Butt NZ. Crop-specific optimization of bifacial PV arrays for agrivoltaic food-energy production: The light-productivity-factor approach. IEEE J Photovolt 2022;12:572–80.

[90] Jia X, Zhou C, Tang Y, Wang W. Life cycle assessment on PERC solar modules. Sol Energy Mater Sol Cells 2021;227:111112.

[91] Nikzad A, Mehregan M. Techno-economic, and environmental evaluations of a novel cogeneration system based on solar energy and cryptocurrency mining. Sol Energy 2022;232:409–20.

[92] Johansson J. Albedo effect in APV (Agrivoltaics): Finding and implementing an albedo model for the APV site in Kärrbo 2023.

[93] Arthur P, Drahi E, Badosa J, Blanc P. Comprehensive Methodology applied to solar radiation prediction for dual use for vertical agrivoltaics system. EUPVSEC 41st Eur. Photovolt. Sol. Energy Conf., Page 8: 2024.

[94] Huawei Technologies Co., Ltd., Solar components producer. Available at: https://support.huawei.com/enterprise/en/doc/EDOC1100083285/eb33de84/technical-data/ (Accessed 30 December 2025). n.d.

[95] Zad, A.N., Agostini, A., Impollonia, G., Zainali, S., Croci, M., Colauzzi, M., Campana, P.E. and Amaducci, S., 2025. Life cycle assessment of various agrivoltaic systems across Europe. Sustainable Production and Consumption, 60, pp.260-280. https://ars.els-cdn.com/content/image/1-s2.0-S2352550925001964-mmc2.xlsx (Accessed 30 December 2025). n.d.

[96] Nia AS, Parashkoohi MG, Zamani DM, Afshari H. Optimization of energy use efficiency and environmental assessment in soybean and peanut farming using the imperialist competitive algorithm. Environ Sustain Indic 2024;100361.

[97] Searchinger T, Heimlich R, Houghton RA, Dong F, Elobeid A, Fabiosa J, et al. Use of US croplands for biofuels increases greenhouse gases through emissions from land-use change. Science 2008;319:1238–40.

[98] Agostini A, Battini F, Giuntoli J, Tabaglio V, Padella M, Baxter D, et al. Environmentally sustainable biogas? The key role of manure co-digestion with energy crops. Energies 2015;8:5234–65.

[99] Global economic model. GTAP. Available at: https://www.gtap.agecon.purdue.edu/models/landuse.asp (Accessed 30 December 2025). n.d.

[100] Global land use model. GLOBIOM. Available at: https://iiasa.ac.at/models-tools-data/globiom (Accessed 30 December 2025). n.d.

[101] Tekie S, Zainali S, Zidane TEK, Lu SM, Guezgouz M, Zhang J, et al. Unraveling the Crop Yield response under shading conditions through the deployment of a drought index: A meta-analysis 2025.

[102] Vicente-Serrano SM, Beguería S, López-Moreno JI. A Multi-scalar drought index sensitive to global warming: The Standardized Precipitation Evapotranspiration Index - SPEI. J Clim 2010;23:1696–718.

[103] Beguería S, Vicente-Serrano SM, Reig F, Latorre B. Standardized precipitation evapotranspiration index (SPEI) revisited: parameter fitting, evapotranspiration models, tools, datasets and drought monitoring. Int J Climatol 2014;34:3001–23.

[104] Ecoinvent, 2021. Ecoinvent v3.8. Available at: https://ecoinvent.org/the-ecoinvent-database/data-releases/ecoinvent-3-8/ (Accessed 30 December 2025). n.d.

[105] Steubing B, Wernet G, Reinhard J, Bauer C, Moreno-Ruiz E. The ecoinvent database version 3 (part II): analyzing LCA results and comparison to version 2. Int J Life Cycle Assess 2016;21:1269–81.

[106] Mason JE, Fthenakis VM, Hansen T, Kim HC. Energy payback and life-cycle CO2 emissions of the BOS in an optimized 3.5 MW PV installation. Prog Photovolt Res Appl 2006;14:179–90.

[107] Valmont Solar. https://www.valmontsolar.com/ (Accessed 30 December 2025). n.d.

[108] SentNet S.R.L. https://www.sentnet.it/ (Accessed 30 December 2025). n.d.

[109] Méndez L, Forniés E, Garrain D, Vázquez AP, Souto A, Vlasenko T. Upgraded metallurgical grade silicon and polysilicon for solar electricity production: a comparative life cycle assessment. Sci Total Environ 2021;789:147969.

[110] REM TEC S.R.L. http://www.remtec.energy/ (Accessed 30 December 2025). n.d.

[111] SimaPro, Software for life cycle analysis, Ver. 9.0, Pré consultants B.V. Available at: https://simapro.com/plans/ (Accessed 30 December 2025). n.d.

[112] Chavez DL, Azzaro-Pantel C, Montignac F, Ruby A. Integrating life cycle assessment in multi-objective optimization of green hydrogen systems: a review of literature and methodological challenges. Renew Sustain Energy Rev 2025;217:115689.

[113] Fazio S, Castellani V, Sala S, Schau E, Secchi M, Zampori L, et al. Supporting information to the characterisation factors of recommended EF Life Cycle Impact Assessment methods: new methods and differences with ILCD 2018.

[114] Weidema BP, Wesnæs MS. Data quality management for life cycle inventories—an example of using data quality indicators. J Clean Prod 1996;4:167–74.

[115] Magarelli A, Mazzeo A, Ferrara G. Fruit crop species with agrivoltaic systems: a critical review. Agronomy 2024;14:722.

[116] Graham M, Ates S, Melathopoulos AP, Moldenke AR, DeBano SJ, Best LR, et al. Solar photovoltaic panels in pastures reduce heat stress in cattle. Commun Earth Environ 2025;6:1–9.

[117] Kazem HA, Chaichan MT, Al-Waeli AHAH, Sopian K. Dual axis solar photovoltaic trackers: An in-depth review. Energy Sources Part Recovery Util Environ Eff 2024;46:15331–56.

[118] Lee C, SanChez G, Agrawal R, Bermel P. Simulation and Design Aspects of a Bifacial Single-Axis Tracker, to Enhance Co-Production of Crops and Power Output n.d.

[119] Barron-Gafford GA, Pavao-Zuckerman MA, Minor RL, Sutter LF, Barnett-Moreno I, Blackett DT, et al. Agrivoltaics provide mutual benefits across the food–energy–water nexus in drylands. Nat Sustain 2019;2:848–55.

[120] Lopez G, Juillion P, Hitte V, Lesniak V, Fumey D. Fruit discards due to several disorders and sunburn in 2022 and 2023 2024.

[121] Sturchio MA, Knapp AK. Evidence of photovoltaic aridity mitigation in semi-arid grasslands. Env Res Lett 2025;20:064047.

[122] Ganti V, Gruss SM, Cammarano D, Brouder SM, Bermel PA, Gitau MW, et al. Optimizing corn agrivoltaic farming through farm-scale experimentation and modeling 2024.

[123] Katsikogiannis A. Integration of Bifacial PV in Agrivoltaic Systems: A Synergistic Design Approach 2021:30.

[124] Tekie, Sultan, Sebastian Zainali, Silvia Ma Lu, Tekai Eddine Khalil Zidane, Arash Khosravi, K. Max Zhang, and Pietro Elia Campana. A Novel Operational Strategy to Maximize Crop and Electricity Production in Single Axis Agrivoltaic Systems Based on Light Response Curve and Daily Light Integral. n.d.

[125] Zad AN, Zainali S, Croci M, Guezgouz M, Impollonia G, Campana PE, et al. Techno-economic optimization of agrivoltaic-powered anaerobic digestion plant for biomethane production. Energy Convers Manag 2026;348:120791.

[126] HISUNAGE HSGDG655-132M12 datasheet. BLD Group; n.d.

[127] Growatt MAX 125KTL3-X LV Inverter Datasheet. Shenzhen Growatt New Energy Technology Co. Available at: https://growatt.tech/product/growatt-max-125-ktl3-lv-3-phase-industrial-inverter/ (Accessed 30 December 2025). n.d.

[128] DiOrio, N.A. and Deline, C.A. (2018). Bifacial simulation in SAM (No. NREL/PR-6A20-72360). National Renewable Energy Lab.(NREL), Golden, CO (United States). n.d.

[129] National Renewable Energy Laboratory. System Advisor Model (SAM). NREL. Available at: https://sam.nrel.gov/ (Accessed 30 December 2025). n.d.

[130] Institute of Solar Energy, Universidad Politécnica de Madrid. SISIFO - Photovoltaic System Simulator. Available at: https://www.ies.upm.es/sisifo/ (Accessed 30 December 2025). n.d.

[131] Kaleshwarwar A, Bahadure S. Validating the credibility of solar simulation tools using a real-world case study. Energy Build 2023;301:113697.

[132] Milosavljević DD, Kevkić TS, Jovanović SJ. Review and validation of photovoltaic solar simulation tools/software based on case study. Open Phys 2022;20:431–51.

[133] Habib S, Liu H, Tamoor M, Zaka MA, Jia Y, Hussien AG, et al. Technical modelling of solar photovoltaic water pumping system and evaluation of system performance and their socio-economic impact. Heliyon 2023;9.

[134] Meteorological measuring stations in Emilia-Romagna. Available at: https:// https://www.arpae.it/it (Accessed 30 December 2025). n.d.

[135] Wang L, Tang Y, Zhang S, Wang F, Wang J. Energy yield analysis of different bifacial PV (photovoltaic) technologies: TOPCon, HJT, PERC in Hainan. Sol Energy 2022;238:258–63.

[136] Holmgren WF, Hansen CW, Mikofski MA. pvlib python: A python package for modeling solar energy systems. J Open Source Softw 2018;3:884.

[137] Lorenzo E, Narvarte L, Muñoz J. Tracking and back-tracking. Prog Photovolt Res Appl 2011;19:747–53.

[138] Soto W, Klein SA, Beckman WA. Improvement and validation of a model for photovoltaic array performance. Sol Energy 2006;80:78-88,.

[139] Veberič D. Lambert W function for applications in physics. Comput Phys Commun 2012;183:2622–8.

[140] Photovoltaic system performance – Part 1: Monitoring, International Electrotechnical Commission. NSAI Standard; 2021.

[141] Ayala Pelaez S, Deline C. Bifacial PV systems energy yield modeling. Energy Procedia 2020;160:498–505.

[142] Antonanzas J, Osorio N, Escobar R, Urraca R, Martinez-de-Pison FJ, Antonanzas-Torres F. Review of photovoltaic power forecasting. Sol Energy 2016;136:78–111.

[143] Dolara A, Grimaccia F, Leva S, Mussetta M, Ogliari E. A physical hybrid artificial neural network for short term forecasting of PV plant power output. Energies 2015;8:1138–53.

[144] MathWorks. MATLAB (R2024b)-The Language of Technical Computing. MathWorks, Inc. Available at: https://www.mathworks.com/products/matlab.html (Accessed 30 December 2025). n.d.

[145] Arslan E, Küçük FA, Biçer Ç, Özsoy B. Determining energy, exergy and enviroeconomic analysis of stand-alone photovoltaic panel under harsh environment condition: Antarctica Horseshoe-Island cases. Renew Energy 2024;226:120440.

Acknowledgments

This journey has been one of the most transformative and memorable experiences of my life. It would have been impossible without the unwavering support, guidance, and encouragement of many incredible individuals.

Above all, I wish to express my deepest and most profound gratitude to my parents. Your unconditional love, endless belief in me, and countless sacrifices have been the foundation upon which this entire achievement rests. This thesis is as much a testament to your enduring support as it is to my own effort. Thank you for teaching me the value of perseverance and for being my anchors through every challenge.

I extend my sincere appreciation to my supervisor, Professor Stefano Amaducci, for his invaluable guidance. Thank you for always providing the timely, insightful advice and helpful suggestions that were critical for shaping my research skills and successfully developing this thesis. More than that, thank you for believing in the potential of this work and for being an extraordinary mentor throughout this entire journey.

My heartfelt thanks also go to my co-supervisor, Professor Pietro Elia Campana. Your technical expertise, encouraging perspectives, and steadfast support were crucial in navigating the complexities of multi-criteria optimization and assessment, significantly strengthening the quality and depth of my work.

I am grateful for the academic and institutional framework that supported my research. Thank you to the PhD in Agro-Food System (Agrisystem) for providing a stimulating and enriching intellectual environment.

This research was also made possible through financial support, and I wish to acknowledge the Portus project funded by the Romeo and Enrica Invernizzi Foundation for their generous contribution to my research activities.

Finally, a thank you to all my friends and colleagues, both within the Agro-Food System and beyond. Your collaboration and friendly support in gathering data and processing information made the rigorous demands of doctoral research feel lighter.

To everyone who inspired, encouraged, and helped me along this path, thank you from the bottom of my heart.

Short biography

Amirhossein Nik Zad was born on October 8, 1992, in Mahmoodabad, Iran. He completed his MSc degree in Energy Systems Engineering at Shahrood University of Technology in 2019. Following his Master's studies, Amirhossein developed a strong professional interest in photovoltaic energy, which led him to secure a fully funded PhD scholarship. He commenced his doctoral program in November 2022 at the Università Cattolica del Sacro Cuore in Piacenza, Italy, specializing in agrivoltaics (APV) systems. His PhD thesis comprises several critical research contributions. First, he developed a multi-objective genetic algorithm to simultaneously optimize economic performance and land utilization across distinct APV configurations integrated with anaerobic digestion plants. Second, he benchmarked various APV systems against conventional alternatives across multiple European climates to determine their environmental viability. Third, he conducted a comparative analysis of actual energy conversion by an advanced APV system against energy output predictions from commercial software and an in-house developed tool under real-world conditions, benchmarking the accuracy of these platforms through comprehensive error analysis. A significant achievement during his doctoral journey was his involvement as a key contributor to the Value4Farm Horizon Europe project, where he authored Deliverable 2.6 on optimizing small-scale APV systems for biogas farms and led high-impact publication. His research has gained international recognition, including poster presentations at the prestigious 6th AgriVoltaics World Conference in Freiburg, Germany in July 2025. Further deepening his specialization, he undertook a full-time research fellowship at Mälardalen University in Västerås, Sweden (September 2024-Janaury 2025). Demonstrating his professional commitment to the field, he serves as Associate Editor for the American Journal of Electrical Power and Energy Systems and has served as a journal reviewer since January 2022 for several respected Elsevier publications.

List of publications

Published journal papers:

- **Zad, A.N**., Zainali, S., Croci, M., Guezgouz, M., Impollonia, G., Campana, P.E. and Amaducci, S. (2026). Techno-economic optimization of agrivoltaic-powered anaerobic digestion plant for biomethane production. Energy Conversion and Management, 348, p.120791. https://doi.org/10.1016/j.enconman.2025.120791
- **Zad, A.N**., Agostini, A., Impollonia, G., Zainali, S., Croci, M., Colauzzi, M., Campana, P.E. and Amaducci, S. (2025). Life cycle assessment of various agrivoltaic systems across Europe. Sustainable Production and Consumption, 60, pp.260-280. https://doi.org/10.1016/j.spc.2025.10.003
- Bellone, Y., Croci, M., Impollonia, G., **Zad, A.N**., Colauzzi, M., Campana, P.E. and Amaducci, S. (2024). Simulation-based decision support for Agrivoltaic systems. Applied Energy, 369, p.123490. https://doi.org/10.1016/j.apenergy.2024.123490

Journal papers in review and in preparation:

- **Zad, A.N**., Zainali, S., Gavioli, V., Croci, M., Impollonia, G., Campana, P.E. and Amaducci, S. (202x) Comparative Analysis of Full Sun Tracking and Anti-Tracking Bifacial Dual-Axis Agrivoltaic Systems: Cross-Validation of Energy Conversion Using Commercial and In-House Simulation Platforms Under Real-World Conditions.
- Lu, S.M., Khosravi, A., Wang, X., Haworth, M., **Zad, A.N**., Bellone, Y. and Campana, P.E. (202x). Increasing land productivity with semi-transparent colored CdTe thin-film photovoltaics and broccoli cultivation in agrivoltaic systems.
- Khosravi, A., Zidane, T.E.K., Bellone, Y., **Zad, A.N**., Sortino, G., Guezgouz, M., Hörndahl, T., Lu, S.M., Zainali, S., Tekie, S., Avelin, A., Amaducci, S. and Campana, P.E. (202x). Evaluating Oat (Avena Sativa) Performance Under Vertical Agrivoltaic System in Sweden.
- Colauzzi, M., Sortino, G., Potenza, E., Bellone, Y., Impollonia, G., **Zad, A.N**., Croci, M. and Amaducci, S. (202x). Potato cultivation in Agrivoltaics systems in North Italy: A four-year case study to test the effect of different array setups on yield and tuber features.

PhD scientific activities

PhD exams of the doctoral school

- Applied Statistics
- Informatics Tools (Towards Big Data)
- Accounting Tools for Management
- Sustainability Management
- Climate Change
- English for Academic Purposes
- European Food Law and Policy
- Research Ethics and Epistemology
- Sustainable Crop Production
- Carbon farming & agricultural carbon credits
- Food Technologies and Sustainability
- Food Consumer Psychology
- Sustainable Animal Production

Courses

- Writing research paper and proposal
- Three-minute thesis
- Environmental Ethics and the Christian Proposal

Projects

Here is a list of the projects that I have participated during the PhD period:

Value4Farm: It is an EU Horizon Europe-funded initiative that aims to decarbonize the agricultural sector by integrating agrivoltaic and biogas technologies into sustainable value chains across Europe, with the ultimate goal of developing decision-support tools for farmers. As a contributor, my main role has involved authoring Deliverable D2.6 on optimizing small-scale agrivoltaic systems for biogas farms and leading high-impact publications, including a manuscript on the techno-economic optimization of agrivoltaic-powered anaerobic digestion and a published Life Cycle Assessment framework that supports the project's sustainability analysis objectives in Work Package 4.